Techniques for Denoising Brain Magnetic Resonance Images

by

Ashish Phophalia

201021014

A thesis submitted in the partial fulfillment of the requirements for the degree of

DOCTOR OF PHILOSOPHY

in

Information and Communication Technology

to

Dhirubhai Ambani Institute of Information and Communication Technology

Gandhinagar, India

January 2016

Declaration

This is to certify that

i) the thesis comprises my original work towards the degree of Doctor of Philosophy in Information and Communication Technology at DA-IICT and has not been submitted elsewhere for a degree.

ii) due acknowledgment has been made in the text to all other material used.

Signature of Student

Ashish Phophalia

Certificate

This is to certify that the thesis work entitled *Techniques for Denoising Brain Magnetic Resonance Images* has been carried out by *Ashish Phophalia (201021014)* for the degree of Doctor of Philosophy in Information and Communication Technology at this Institute under my supervision.

Thesis Supervisor

Prof. Suman K. Mitra

Acknowledgements

Before ending this journey of being PhD student at DAIICT, it will be incomplete without thanking numerous of people I met and will carry those memorable moments for the rest of my life. The first and foremost of them is my supervisor Prof. Suman K. Mitra who is currently serving as Dean of Academic Programs at DAIICT also. It was his belief that boosted the motivation to go forward for PhD degree after completion of my Master's degree with him. His vision, encouragement and belief towards me and my work led this journey to a satisfactory end but will carry forward this bonding throughout of my life. From academic point of view, I learned fundamentals of various courses including basic probability theory and statistical analysis to high level of pattern recognition and machine learning from him. Sharing the same office for last 2-3 years, I also learned many administrative fundamentals being in chair of Dean in the university. I admire him for his clear thinking process and understanding. It was my pleasure to share my phd problems along with financial and family issues during the course of this journey.

This thesis is shaped by comments and suggestions by my Research Progress Seminar Committee members: Prof. Manjunath V. Joshi, and Prof. Aditya Tatu, at DAIICT. It was a great pleasure to present parts of this thesis in every semester where this work was evaluated by Prof. Joshi's experience and Prof. Tatu's encouragement. They share two sides of a coin, where one emphasizes on publication in reputed conferences and journals the other envision this work in style of a movie with complete story from beginning to end. During this journey, I work closely with one of the most enthusiastic and aggressive researcher I have ever met, Prof. Ajit Rajwade who was there in DAIICT for one year and currently in Dept. of Computer Science & Engineering at Indian Institute of Technology, Bombay (IIT-B). It was my pleasure to discuss some statistical analysis of Rice distribution with Prof. Thatagatha Banerjee from Indian Institute of Management, Ahmedabad (IIM-A). This is also incomplete with thanking two reviewers Prof. Aboul Ella Hassanien, Professor, Cairo University,

Egypt and Dr. Pradipta Maji, Associate Professor, Machine Intelligence Unit, Indian Statistical Institute, Kolkata, India.

This work will be remain incomplete without thanking Gitam Shikkenawis viz. Gitam Brijesh Joshi & her parents for all possible support. She joined Prof. Mitra during her MTech Research at the same time when I came back to start my PhD with him. She also continued her PhD under the same umbrella. We had lots of discussions on research topics, lots of arguments in general with no meaning and outing for dinner and shopping. It was a great experience to work with other phd & master students where their nature and characteristics can be represented in N-dimensional space and may be orthogonal in some sense. I had great time with Milind and Shrishail (PhD) during stay in Hostel and silence maintained by Purvi (PhD) in the office during her initial year of phd. I enjoyed discussion with Paridhi (MTech 2010-12), Deshna (MTech 2011-13), Twinkle and Ravi (MTech 2012-14), Radhika, Hiral & Prashant (MTech 2013-15). Many a times it was fun in arguing with Deshna and Radhika also interaction with Bhavesh Sir (senior PhD to me) to some serious nodes (with all due respects) and discussion of Mukesh Goswami Sir (PhD student at DDIT, Gujarat). I would also like to thank my roommates in this journey Dushyant Sharma (M.Tech. 2010-12) and Mahipal Jadeja (PhD student 2013-). During these years, I also spent a semester at Marwadi Education Foundation campus as a faculty where I enjoyed a lot of time with Shiva (M.Tech Batchmate), Sandeep, Nikhil, Prakruti, Amit, Vishal, Gautam, Bindu Madhvan, R. R. Srikanth and Arti Kotak.

Staying at DAIICT for almost seven year is a great feeling and this place become happening place made by many BTech students I met here. Being a student member of IEEE, I shared approximately four events as a volunteer with Prof. Anil Roy whom I admire the most for his management and artistic envision. A vote of thanks to other faculties at DAIICT and staff members especially Mr. Prabhunath, Anuradha Ma'am, Deepa Ma'am, Mr. Mukesh for sharing some smiley moments.

This journey would never be accomplished with support of my parents Mr. Ashok Phophalia and Mrs. Anand Phophalia. Their wishes and sacrifices urged me to move

forward with quality completion of this journey. Hopefully, this moment will be joyous and cheering for them and recognition of their efforts. It is my brother Ankit Phophalia who took care of family and other responsibilities at home in my absence for all these years. I wish a great success to him in professional front to excel in the field of accounting and management. During this journey, I lost my grandfather who always supported me for studies which is one of the key factors for me to carry forward studies to higher academic grades. This journey would be incomplete without thanking my maternal grandparents and family who always wished best for me and supporting in best possible ways. This journey also brought new life long relations of Wife and in-laws. A special thanks to my wife Minkashi for joining this journey in the middle and moving along shoulder to shoulder till end. It was her to add a new dimension in this life with some ups and downs. In whole, I consider myself to lucky enough to have these wonderful people in my life.

Ashish Phophalia

Abstract

Advances in the computational science joined medical imaging domain to help humanity. It offers great support in clinical practices where automatic Computer Added Systems (CAD) help in identification and localization of abnormal tissues. In recent decades, a lot of research tuned non-invasive techniques have been devised to serve mankind. One of them is Magnetic Resonance Imaging (MRI) which provides structural information at higher resolution even in presence of bone structures in the body. Although it is free from ionizing ingredient, factors like electronic circuitry, patient movement etc. provoke some artifacts in imaging system considered as *noise*. One needs to get rid of these artifacts by means of software processing to enhance the performance of diagnostic process. This thesis is also an attempt to deal with noisy part of MRI and comply with preserving image structures such as boundary details and preventing over-smoothing. It has been observed that, in case of MR data, noise follows Rician distribution. As opposed to additive Gaussian noise, Rician noise is signal dependent in nature due to MR image acquisition process.

The thesis constitutes a relationship between MRI denoising and uncertainty model defined by Rough Set Theory (RST). RST already has shown some promising outcomes in image processing problems including segmentation, clustering whereas not much attention has been paid in image restoration task. The first part of the thesis proposes a novel method for object based segmentation and edge derivation given the noisy MR image. The edges are closed and continuous in nature and segmentation accuracy turns out to be better than well-known methods. The prior information is used as cues in various image denoising frameworks.

In Bilateral filter framework along with spatial and intensity cues, a new weighing factor is derived using prior segmentation and edge information. This further extends to non local framework where waiver in spatial relation conceded to access similar information from far of neighbors. Under non locality paradigm, a clustering based method is proposed which clubs together similar patches based on similarity criteria.

The proposed clustering method uniquely defines clusters of patches under multiple class set up. These clusters are then used to define the basis vectors using Principal Component Analysis (PCA) and Kernel Principal Component Analysis (KPCA) method followed by hard thresholding shrinkage procedure. Afterwards, multiple estimations of a pixel are averaged by number of estimations. In total, number of PCA or KPCA operations are far less than other contemporary methods which repeat the same process over chunks of patches in the image space.

The concept is then extended for 3D MRI data. The 3D imaging provides better view of objects from three directions as compared to 2D imaging where only one face of object can be viewed. It involves a complex relationship as compared to 2D imaging and hence is computationally expensive. But it also includes more information which helps in visualizing the object, its shape, boundary etc. similar to real world phenomenon. We extended the segmentation and edge derivation mechanism to 3D data in last part of the thesis. Clustering process is also extended by converting each voxel to one dimensional vector. This part explores various kernels over Rician noise distributed MR data. The results are promising in terms of structure measures even with some simple kernels.

Contents

List of Figures

List of Tables

Chapter 1

Introduction

Non-invasive imaging technique has been great help for medical practitioners for many decades. Starting from X-Ray imaging, the technique of medical imaging has traveled a long way and is constantly being extremely helpful for diagnosis. With the introduction of digital techniques, medical imaging got its strength in recent years.

The science of medical imaging has matured a lot in last few decades. More sophisticated machines and non-invasive techniques have made medical imaging popular and have thereby made the diagnosis more accurate. However, the main premise of accurate diagnosis is noise free images which are still elusive. Parallel research on removing artifacts/noise arising out of hardware, software and physical problems are going on. The present thesis is an attempt in this direction. In particular, techniques to estimate original data from its noisy form are presented for various noise models. The type of medical image considered is Magnetic Resonance Imaging (MRI) of brain tissues.

1.1 Overview of MRI

Magnetic Resonance Imaging (MRI) is one of the most popular clinical imaging methods developed alongside Computer Tomography (CT) and X-Rays Technology. It is an ionization and radiation free modality, hence is a non-invasive technique and safer

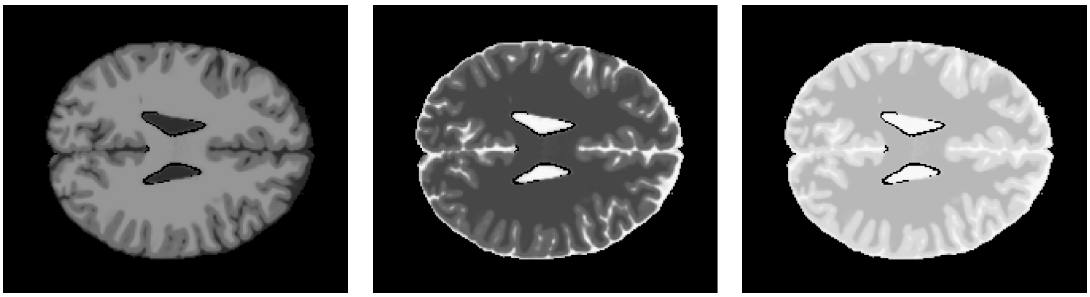

(a) T1 (b) T2 (c) PD

Figure 1.1: Sample images from Phantom BrainWeb Database [1]

than CT, X-Ray and other techniques. It also provides a better soft tissue contrast and image resolution for diagnostic purpose [3], [4]. The MRI modality built upon phenomenon of Nuclear Magnetic Resonance (NMR), was discovered by F. Bloch and E. Purcell independently in 1946 (both awarded Nobel prizes in 1952). Further investigation of NMR phenomena led it to be useful for human society in notable works by Richard Ernst, Paul C. Lauterbur and Sir Peter Mansfield who won the Nobel prize in 1991, 2003 and 2003 respectively.

The principle of NMR involves quantum and classical mechanics, which involve processing of protons (present in human body) under external Magnetic field. The crux of MRI modality is utilization of abundance containment of hydrogen nucleus present in human body in the form of water. The protons of H-atoms are aligned by the external field. Under a radio frequency (RF) pulse, protons release their energy generating an electromagnetic signal that gets recorded by receiver coils of MRI scanners. These electromagnetic signals get encoded in phase and frequency components. The Inverse Fourier transform of raw data generates image slice either 2 or 3 dimensional, also known as *k-space*. The reconstruction process from raw signal to image space, provides an added choice to generate any particular slice in 2D form or complete volumetric (3D) representation [5], [6]. MRI offers various modalities, in addition, namely *T1*, *T2*, *PD* (Proton Density) modality, shown in Figure 1.1.

Although a versatile technique, the quality of image is often affected during image acquisition process. The artifacts can mainly be classified as:

- Hardware Related: such as power supply instability, thermal noise etc.
- Software Related: such as error in decoding pulse sequence, intensity inhomogeneity etc.
- Patient Related: such as body movement, holding breath for a long time, blood flow etc.
- Physics Related: such as magnetic susceptibility, Gibbs ringing artifacts etc.

Many of the artifacts mentioned above are taken care of by MR scanner available. Some noise/artifacts still remain in the scan which needed to be removed. Otherwise, it may affect post-processing step which involves tissue identification, tissue segmentation and other diagnostic decisions.

In the reconstruction step, there is always an *uncertainty* involved due to sampling of Fourier domain to spatial domain, interpolation techniques used etc. This uncertainty can be defined as whether a spatial location is representing an actual tissue information of the subject or a true signal is may be affected by encoding scheme or effect of neighborhood and so on. This uncertainty leads to some undesirable visual effects, commonly referred as *noisy image*, which are needed to be overcome by some software/mathematical modeling (referred as *Image Denoising Problem*). Here, Figure 1.2 shows two real sample images of different subjects (human) from benchmark databases [7], [8] where noise is clearly visible. The image denoising problem is in fact an *inverse problem* which tries to reconstruct a true noise-free image [9], hence, can ease the image segmentation, disease identification etc.

The acquisition process of medical images is sensitive to noise or undesired signals. Since noise is an inherent part of MRI data, denoising becomes a crucial ingredient of medical image analysis process. Hence, there are two sets of problems: (a) estimation and analysis of noise model/parameter and other artifacts such as intensity inhomogeneity, bias correction etc. and (b) construction of adaptive models for denoising purpose. However, these can be considered independent problems or one can use the

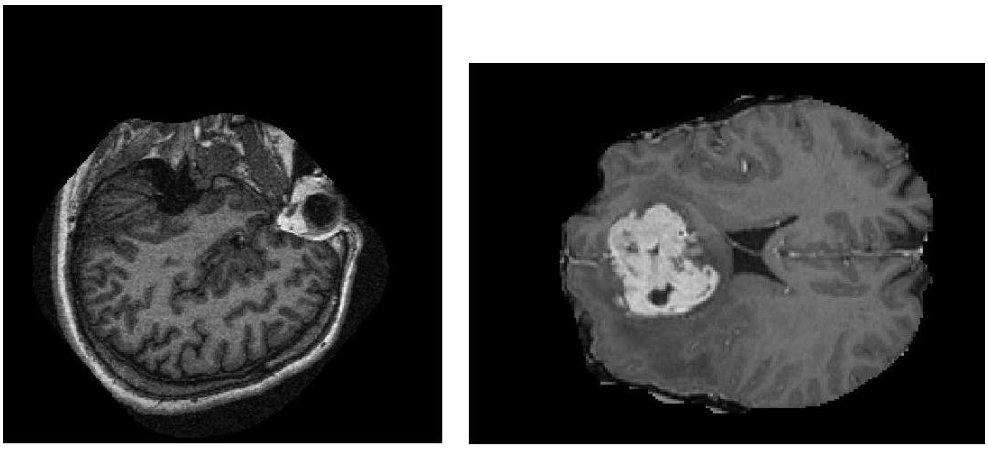

(a) OASIS database [7] (b) BRATS database [8]

Figure 1.2: Sample images from Real Databases

first one as guided input for the other. An inaccurate noise model may lead to doubt on reliability of denoising method. Traditionally, Gaussian model is preferred at high SNR locations in MRI [10]. A lot of efforts have been put to build a statistical noise model in MRI [10], [11], [12], [13]. Similarly, efforts have been made to estimate parameters of models in [2], [14], [15], [16].

On the other side, to develop denoising methods according to noise model in MRI is highly sought. In this regard, many conventional methods have been modified accordingly to adjust the nature of MRI data [17], [18], [19], [20]. However, one needs to take care of the tissue information and boundary information in image and keep them intact at the end of denoising process. In fact, Cerebrospinal Fluid (CSF), Gray Matter (GM) and White Matter (WM) play significant role in differentiating healthy brain from an abnormal one and also in clinical examinations [21]. So, even a small change in it may produce a wrong clinical decision. Hence, any preprocessing part must preserve the structure and properties of tissue as in the human subject. A large review on denoising methods in MRI can be found in [22].

1.2 Motivation

It is already stated that noise from different sources and for different conditions accumulate in MR images. Hence, the main motivation of this work is to get MR images which are noise free by pre-processing techniques before going into image analysis such as tissue segmentation. Noise most naturally affects boundaries of different tissues, thereby making it most difficult to identify proper edges. Another motivation of the thesis, rather than first motivation is to get edges as proper as possible from the noisy image.

Moreover, study revealed that the noise model present in MR images is very different from that of natural images. This happens due to several unique sources of noise generation and their combination. Thus, it is quite obvious that the technique used in natural image denoising may not work properly for medical images. Another motivation was to investigate such noise and explore the technique of removal of noise.

In MRI data, many edge detection methods failed and were not able to capture all the edges [23]. The edges, that we are looking for, give rise to object boundaries which must be closed in nature. The purpose of closed boundaries is to govern denoising process near the boundary regions where two different tissues may interact. Otherwise, denoising of one type of tissues may affect/disturb another type of tissues at boundary. However, most of the methods proposed earlier [24] [25], fail to get such closed boundaries while finding the edges.

Another significant difference (between natural images and medical images) lies in the noise realization. Commonly, noise in natural images is considered as additive and white in nature, defined as $Y = X + \eta$, where X is the actual signal and η is the error component or noise inducted in the acquisition process. Here, noise occurrence has been assumed to be independent and identically distributed (IID) noise. The Rician noise was built from white Gaussian noise in the complex domain, defined below

$$Y = \sqrt{(X + \eta_1)^2 + (\eta_2)^2} \tag{1.1}$$

where X is the noise free image, $\eta_1 \sim N(0, \sigma_n)$, $\eta_2 \sim N(0, \sigma_n)$ and σ_n is the standard deviation of the added white Gaussian noise. The signal dependency behavior makes it difficult to implement many denoising methods in straight forward manner. However, some methods are acquainted with Variance Stabilization Techniques (VST) for rician data, proposed in [2]. In addition, MRI denoising with Rician noise needs to have bias correction module [20]. However, some methods also suggest for bias correction in [26], [27], [28], [29].

Disturbances or *noise* induced in acquisition process lower down the quality of the signal. Hence, it is desirable to have denoising methods suitable for Rician kind of distribution while sustaining the integrity of the image scan. Noise brings uncertainty in data and changes image intensity abruptly. Hence, it is difficult to find the amount of change at each location in the MRI. One can only estimate/approximate the possibility of true value at each location using other information from data.

A keen observation about MRI brain images is that they are symmetrical many a times, hence one can use this kind of structural property in denoising process (also evident in Figure 1.1 and 1.2). This property can be useful in patch based processing non locally. In recent years, image denoising literature has dealt in patch based denoising where idea is to get the similar patches with in the image space. However, finding similar patches for each patch is tedious and time consuming. Hence, such methods are restricted to find similarity with a given local neighborhood of the underlying patch.

1.3 Scope and accomplishments of the thesis

The main scope of this thesis is to handle the uncertainty due to noise present in MR image and make it as clean as possible. The clean image is expected to lead towards robust diagnosis. The noise present in the image is assumed to be an uncertainty model as no prior information is available to decide whether a pixel of the image is noisy or non-noisy. Emphasis is given to deal this uncertainty through soft computing

approach. Rough Set Theory (RST) is a strong and well accepted component of soft computing. RST provides a framework that can handle improper/incomplete information and there by supports the decision makers to make more accurate conclusion.

Rough Set Theory was proposed by Z. Pawlak in 1982 to handle the uncertainity in the data [30]. The applicability of RST for many decision making system has been studied for last two decades. The applicability of RST for medical image analysis has also been studied. Some notable works can be found in [31], [32], [33]. This thesis explores applicability of RST for medical image denoising problem. So far, almost no attempt has been made towards this. The first work reported was in 2008 [34], where the use of RST for medical image denoising was in nascent stage. This thesis is an attempt to strengthen the applicability of RST in medical image denoising field. However, the scope is restricted to brain MR images. Chapter-wise major accomplishments of the thesis are listed down:

(1) A Rough Set based generalized multi-class thresholding mechanism is defined by maximizing rough entropy. Based on this, Rough Class Label (RCL) and Rough Edge Map (REM) are defined. The REM is closed and continuous in nature which is a unique feature. Both RCM and REL accelerate denoising process.

(2) Under Bilateral Filter (BF) framework [35], different treatments are adopted for homogeneous and heterogeneous regions present in the image. This filter mainly consists of spatial and photometric similarity. By adopting varying weights for these two similarity measures, homogeneous and heterogeneous regions are catered in different ways. Along with two existing components of BF, a third component is derived using RCL and REM to enhance the performance.

(3) Recent advancements suggested in the field of image denoising are mostly patch based where the denoising task is carried out by aligning self-similar patches. The basic framework is known as Non Local Self Similar (NLSS). Due to the computational complexity, the search for similar patches is restricted, though ideally it could be anywhere within the image support. Thus the current state

of the art can be looked upon as a restriction on the NLSS framework. This framework has also been applied on transformed domain images. PCA is the most popular way to construct transformed domain images. RST based approaches for aligning all the self similar patches within the image support are proposed. This new alignment approach has also been applied on transformed domain image.

(4) Recent studies of MR images reveal that noise present is Rician in nature rather than Gaussian [11]. Naturally, it is expected that PCA based method may not be suitable under Rician noise. A Kernel Principal Component Analysis (KPCA, [36]) based method has been proposed for Rician noise removal. This also incorporates RST based alignment of self similar patches.

(5) A common way to analysis 3D volumetric MR image is slicing it to 2D image. Recently with the help of available computational power, researchers are analyzing 3D data directly. Keeping this in mind, RCL and REM, as proposed above, are extended for 3D volumetric data. Assuming Rician noise, a structure preserving KPCA based method is presented for 3D MRI data. Experiments are carried out with varying kernels.

1.4 Organization of thesis

This work is on establishing a relevance of rough set theory in context of medical image denoising problem. The work is built upon the proposed framework for rough class labels (RCL) and rough edge map (REM) generation method. These information are further utilized in some of the well-known image denoising framework in the context of MR images. RCL and REM are used as a regularization term in bilateral filter whereas patch based RCM and REM are used in non local means and principal component analysis based methodologies. This work proposed a unique notion of clustering of image patches which is used for denoising and is comparable to state-of-the-art methods. To explore structure of image patches in higher dimensional space,

a kernel principal component analysis based method is designed. The same concept is extended for 3D patches to work on 3D MR image denoising. Brief overviews of chapters are as under.

We have developed a generalized notion of Rough Class Label (RCL) and Rough Edge Map (REM) subjected to rough entropy criteria in Chapter 2. The proposed approach defines class in terms of object(s) of interest in the image and their combined continuous closed boundary. The closed boundary works as a regularizing term in the denoising process. The class information helps the denoising process based on similarity between the underlying pixel/location in the image. The proposed method of edge map is found to be superior to some of the well-established methods in the field of image processing and computer vision.

Bilateral Filter is considered as the first method in modern image denoising literature. The method uses spatial and photometric similarity between the pixels for denoising. The proposed method, in Chapter 3, adds one more weighing component of similarity in conventional bilateral filter using the REM and RCL information. The added information is found to be suitable in terms of denoising performance in comparison to methods from the class of bilateral filters.

The next revolutionary idea in denoising is the notion of *Non-Local Self Similarity*. In Chapter 4, we propose a more principled approach to explore self similarity within the image space. The proposed approach makes cluster of patches according to REM and RCL information which are further utilized in image denoising. The strategy performed superior than many of the existing methods. The current method can be considered as non-local in *true sense* where whole image space is explored.

The Principal Component Analysis (PCA) is one of the well-known nonparametric methods and has been explored in image denoising problem. However, PCA inherently assumes data to be Gaussian in Nature. The applicability of PCA in MRI images denoising is not advocated as nature of noise is not Gaussian. To deal with Rician noise of MRI images, a manifold based method using Kernel Principal Component Analysis has been explored in Chapter 5. The proposed method transforms

data to feature space where denoising takes place and noise free data (ideally) is re-projected back to image space. Experimentally, the performance of rough set with KPCA method is found to be comparable with state-of-the-art methods under Rician noise model of MRI.

The MRI generation process is flexible in formation of 3D and 2D images. The 3D data provides insight into inter-slice and intra-slice relationship between tissues. Currently, a lot of attention is devoted for processing 3D in real-time scenario. A 3D version of RCL and REM has been proposed in search of similar 3D patches for denoising. A structure preserving method is proposed in Chapter 6 in comparison to state-of-the-art method. This work also explores various kernels for better performance.

This work is concluded in Chapter 7 with some of the possible directions of future work.

Chapter 2

Rough Set in Image Processing

Granular information processing added a new dimension to information processing under Soft Computing umbrella. A *Granule* is defined as a collection of few information units forming larger ones and *Granulation* operation is decomposition of universe into parts [37]. The term *Granular Computing* (GrC) is intended to deal with uncertainty, partial truth, impreciseness under the granule space [38]. Granules at the lowest level are composed of atomic particle of the universe of discourse. This composition could be defined on spatial neighborhood, indistinguishable property, similarity function, cohesion etc. between atomic particles. The soft computing approaches such as Fuzzy Logic, Rough Set, Neural Network etc. try to model vagueness and uncertainty under GrC framework.

2.1 Background Study on Rough Set

Rough Sets provide a unique approach to knowledge discovery and approximation of sets using granular information. It provides structures for overlapping boundary, given domain knowledge. Rough set methods have been applied as a component of hybrid solutions in machine learning and data mining [39]. They have been found to be particularly useful for rule induction and feature selection (semantics-preserving dimensionality reduction). Rough set-based data analysis methods have been success-

fully applied in bio-informatics [40], economics and finance [41], medical imaging [42], multimedia [43], web mining [44], signal and image processing [45], decision theoretic analysis [46], software engineering [47], robotics [48], and semiconductor engineering [49] etc.

2.1.1 Soft Computing Siblings

The Rough Set Theory (RST) was proposed by Z. Pawlak in 1982 [30]. RST along with Fuzzy Logic [50] intended to deal vagueness. In Fuzzy Logic, individual elements are defined in terms of membership function for belonging to a particular set or object. In contrast, RST induces notion of approximation space [51]. Using a granular representation, RST has access to look at subset of object as one unit instead of dealing with individuals. This in turn gives more insight to nature of elements in terms of similarity measures. Recently, Near Set was proposed in [52] to focus on the discovery of sets having matching description that does not require a consideration of approximation boundaries. However, RST and Near set are considered as two sides of the same coin [31]. RST and Fuzzy Sets are claimed to be two different approaches in [53], where as in [54] it has been proved that rough sets are fuzzy sets but converse is not true. Also, some combinations of RST and fuzzy sets were proposed in the past as Rough Fuzzy Set and Fuzzy Rough Set [55], [56].

2.1.2 Rough Set and its extension to Image Processing

Rough set concept can be defined quite generally by means of topological operations, interior and closure, called *approximations* [30]. Given a set of objects U called the universe and an indispensability relation $R \subseteq U \times U$, representing our lack of knowledge about elements of U. Assume that R is an equivalence relation. Let X be a subset of U. Now characterize the set X with respect to R. To this end we will need the basic concepts of rough set theory given below.

- The lower approximation of a set X with respect to R is the set of all objects,

which can be for *certain* classified as X with respect to R (are *certainly* X with respect to R).

- The upper approximation of a set X with respect to R is the set of all objects which can be *possibly* classified as X with respect to R (are *possibly* X in view of R).

- The boundary region of a set X with respect to R is the set of all objects, which can be classified neither as X nor as $not - X$ with respect to R.

Now, set X would have following two possibilities:

- Set X is crisp (exact with respect to R), if the boundary region of X is empty.

- Set X is rough (inexact with respect to R), if the boundary region of X is nonempty.

The equivalence class of R determined by element x is denoted by $R(x)$. The indispensability relation in certain sense describes lack of knowledge about the universe. Equivalence classes formed by indispensability relation, called *granules* generated by R, represent elementary portion of knowledge perceived due to R. Thus in view of the indispensability relation, in general, it allows to observe individual objects but forced to reason only about the accessible granules of knowledge. Formal definitions of approximations and the boundary region are as follows:

- R-lower approximation of X

$$\underline{R}(x) = \bigcup_{x \in U} R(x) : R(x) \subseteq X \tag{2.1}$$

- R-upper approximation of X

$$\overline{R}(x) = \bigcup_{x \in U} R(x) : R(x) \cap X \neq \phi \tag{2.2}$$

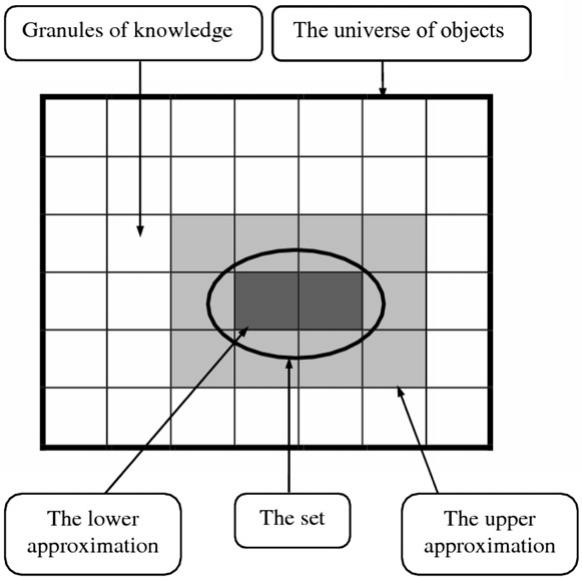

Figure 2.1: Image granules with upper and lower approximation of an object as conceptualized in Rough Set Theory

- R-boundary region of X

$$RN_R(X) = \overline{R}(X) - \underline{R}(X) \tag{2.3}$$

The lower approximation of a set is union of all granules which are entirely included in the set; the upper approximation is union of all granules which have non-empty intersection with the set; the boundary region of set is the difference between the upper and the lower approximation. The figurative description is given in Figure 2.1.

Extension to Image Processing

RST incorporates the notion of *granules* (group of neighboring pixels in case of image). As suggested in [57], the image space, Ω can be partitioned in overlapping/ non-overlapping granules (G_i) of size $m \times n$ pixels, to derive more information under given attribute vector (Θ) for each object (C^k, k^{th} object) present in the image. Under RST, each object/class with given attribute is represented in terms of lower approximation ($\underline{C}^k_\Theta$) and upper approximation ($\overline{C}^k_\Theta$) separately. The $\underline{C}^k_\Theta$ consists of

certainly classified granules which are part of object C^k under attribute Θ. The $\overline{C}^k_\Theta$ constructed by *possible* granules of that class defined by attribute Θ including $\underline{C}^k_\Theta$. The set difference of both approximations provide *boundary set* of the object. This establishes an equivalence relationship among the data present in any approximation given the attribute(s). In this work, pixel intensity is considered as an attribute to distinguish objects present in the image. Each object in the image assumed to be confined in intensity range. This range, as intensity thresholds, is obtained from image histogram. Here, thresholds obtained from histogram serves as feature and an object C^k is confined within two intensity thresholds given by $[\Theta_{k-1}, \Theta_k]$. Mathematically, lower and upper approximation of object C^k with given attribute Θ can be defined as follows:

$$\underline{C}^k_\Theta = \left\{ \bigcup_i G_i | \Theta_{k-1} \leq P_j < \Theta_k, \forall j = 1, 2, ..., mn \ \ and \ \ pixel \ \ P_j \in G_i \ \ granule \right\} \quad (2.4)$$

$$\overline{C}^k_\Theta = \left\{ \bigcup_i G_i | \Theta_{k-1} \leq P_j < \Theta_k, \exists j = 1, 2, ..., mn \ \ and \ \ pixel \ \ P_j \in G_i \ \ granule \right\} \quad (2.5)$$

For given attribute(s), a granule can be classified in lower or upper approximation of an object. The attribute considered here is the intensity values at each location in the image space. The objects present in the image are categorized in intensity range by optimizing noisy image histogram. The class label can be assigned by comparing intensity value at each location against the intensity ranges of all the objects. Similarly, a granule (set of adjacent pixels) is assigned to an object's lower approximation (and upper also) if all the pixels fall in its intensity range. If some pixels of the granule fall in the intensity range then granule will be considered in upper approximation (not part of lower approximation). If none of the pixel in the granule follows intensity range then it can be considered as background for particular object. The union of difference of both the approximations of all objects will generate pixels which are very near to possible edges in the image.

2.1.3 Applications of RST in Image Processing & Pattern Recognition

RST have been applied to handle various challenges in the field of image processing and medical imaging. It has been applied across various problems from segmentation to clustering, Feature reduction to Information theoretic analysis of various imaging modalities including Magnetic Resonance Imaging (MRI), CT, Remote Sensing Imaging, Fingerprint Imaging, Face Images etc. A recent review of RST in above mentioned domains can be found in [31], [32]. RST has been explored on Face Recognition problem in [58], brain tumor segmentation and processing in [59], [60]. RST based entropy minimization method has been applied in Remote sensing and character images in [57] whereas region of interest has been extracted from medical images in [61]. The partial volume effect is dealt by RST in [62], cancer detection is attempted in [63] and some other implementations have been reported in [64], [65], [66], [67], [68], [69], [70], [71].

2.2 Proposed Class Label & Edge Map

The major contribution of this work is to provide more information from noisy image to the denoising framework to boost up the performance. The edge information can be used to stop across the boundaries. But the presence of noise makes it more difficult to get actual edges, hence makes it an ill-posed problem [57]. This prompted the present work to select rough set theory to get imprecise edge information that is expected to include actual edges. The granule information processing of Rough Set Theory (RST) helps to visualize the possible presence of edge or heterogeneity in the granules. Granules are very small image blocks of size 2×1, 1×2 or 2×2 etc. The RST based approach, with the help of granules, provides partitions in the image to create lower and upper approximations of the objects. Note that, lower approximation set will be contained completely in upper approximation set. The difference of both approximations provides a possible edge region for a particular object or class present

in the image. Here, in this work, we considered four major class/objects namely, CSF, White matter, Gray matter and Background in the brain MR images. For denoising task, as a regularization term, the Rough Edge Map (REM) of the image and Rough Class Labels (RCL) of each pixel are obtained. The procedure for obtaining REM and RCL are presented in next two subsections followed by design of the proposed filter.

2.2.1 Rough Class Labels

Objective of this step is to assign a class label to each individual pixel. However, presence of noise makes this task hard. It is even harder as noise level increases. Finding a suitable threshold from the histogram of the image is a common practice to discriminate objects and thereby assigning class labels to the pixels. But, histogram of noisy image may not lead to precise threshold for object segmentation. This imprecise threshold in turn will define imprecise object boundary that could affect the performance of denoising Filter. RST, being known for handling impreciseness, is expected to give rise to a threshold that could boost up the performance of denoising Filter.

The impreciseness is avoided as far as possible by optimizing Rough Entropy to find a threshold as precise as possible. Now onwards, this threshold will be referred as Rough Entropy Threshold (RE_T). Originally, RE_T was proposed for a two class problem [57], known as binarization. Initial approximate value of a threshold (valley in the histogram) is obtained by using a window based method from the histogram. This value is then refined by optimizing Rough Entropy criteria, defined as [57]:

$$RE_T = -\frac{1}{2}\left[R_{O_T} log_e\left(\frac{R_{O_T}}{e}\right) + R_{B_T} log_e\left(\frac{R_{B_T}}{e}\right)\right] \tag{2.6}$$

where $R_{O_T} = 1 - \left|\overline{O}_T\right| / \left|\underline{O}_T\right|$ and $R_{B_T} = 1 - \left|\overline{B}_T\right| / \left|\underline{B}_T\right|$ ($\left|\overline{S}\right|$ and $\left|\underline{S}\right|$ are cardinality of lower and upper approximation of set S respectively) are roughness of object of interest (O_T) and background (B_T) respectively.

In the present context, we are using MR images (noisy) having more than two classes. The above defined RE_T for two class problem is applied in successive manner to get thresholds for multi-modal histogram. The threshold of an object is obtained by considering this current object as one class and all other objects as another class (background). The image thus binarized depicts only one object. After getting the threshold, each pixel is assigned a single bit binary symbol 0 or 1 depending on whether it is below threshold or above threshold respectively. The procedure is repeated with respect to all objects. So in case there are N objects, $N-1$ thresholds are obtained and consequently at the end, each pixel will get a binary code of length N. It is expected that, out of 2^N possible binary codes, there only N different binary codes will be assigned to all pixels. Pixels having same binary code belong to the same class. By this way, class labels are assigned to each pixel. A figurative explanation is shown in Figure 2.2.

The entire procedure is summarized below

a. Estimate approximate thresholds from the noisy image histogram using parzen window approach.

b. Optimize each threshold separately using rough entropy criteria under GrC framework (Eq. 2.6).

c. Binarize the image with respect to each optimized threshold. For each threshold, assign 1 if pixel value is greater or equal to the threshold, 0 otherwise.

d. Combine assigned symbols (1 or 0) of each pixel for all thresholds. This will lead to representing each pixel by a binary string of length K, if there are $K-1$ thresholds.

e. Classify all binary strings and there by pixels. Strings having same symbol at same position will be classified as same class.

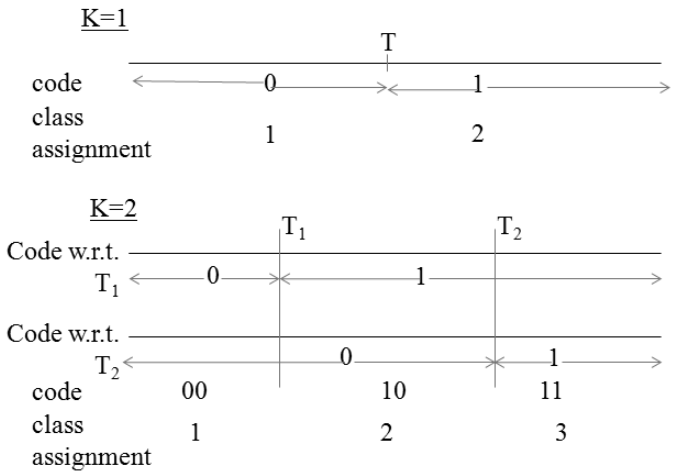

Figure 2.2: Code and Class assignment for different number of thresholds. Here K is number of thresholds.

2.2.2 Rough Edge Map

The size of granules is an important factor for finding Rough Edge Map (REM). For deriving edge information, a heterogeneous granule is considered as having a possible edge location. In this work, the granule size is kept as 2×2. This leads to a situation where some granule will not be counted entirely in lower approximation of an object. All such granules will be considered as boundary for an object and union of all object boundaries will give a Rough Edge Map of the image.

The problem now turns to find those granules which are possibly on the boundary of an object. This can be done by considering each optimized threshold separately. First, binarize the image corresponding to each optimized threshold. A granule will be called *homogeneous*, if all the pixels of the granule are either below threshold or above it. Otherwise, it will be *heterogeneous* in nature, which in-fact, will form the edge map of the image.

2.3 Experimental Results

2.3.1 Overview on Edge extraction Methods

An abrupt change in image intensity is considered as presence of an edge or boundary between two different objects. This provokes researchers to adopt an edge detection method to find boundaries of objects. However, most of the edge detectors may not give rise to close curves and hence fail to build complete object boundaries. This motivated researcher to explore mechanism that can evolve near perfect object boundaries (closed curves). Region Growing (RG) and Active Contour (AC) [72] based methods are some such techniques. Moreover, edge detector based object boundary evolution could be sensitive to the presence of noise with a few exceptions ([73], [24]). Region Growing based methods are also susceptible to noise. On the other hand, AC based methods could survive against noise at least up to certain extent. Both RG and AC methods are highly dependent on initialization. Though many modification of AC method are available [74], [75], still a more robust object boundary detection method is high demand, especially in the field of medical images.

Snake Model [72] is the basis of AC based methods. Various attempts have been made to make this model more robust against noise and other artifacts [74], [75]. A milestone achievement in this area was proposed by Chan and Vese [75]. Till time, Snake models worked under binary assumption where object boundaries used to evolve by segmenting Foreground and Background. A Multiphase Snake model was first proposed in [25], to generalize the notion of detecting multiple object boundaries. This method deals with partitioning image into 2^N objects considering N level sets. This restricts its usage for images where number of objects is not power of 2.

The Active Contour Models (Snake Models) are energy minimizing spline curves to derive object boundary in the image. The energy minimization depends totally on object shape, location and initialization of the contour. ACMs do not solve the entire problem of finding contour in the images [76]. The weighted combination of internal and external image forces forms an energy-minimization functional in the

Snake model. The internal force depends on shape of the snake while external force is dependent on image features such as edges, lines etc. In mathematical form, it can be written as

$$\psi^*_{snake} = \int_0^1 \psi_{snake}\mathbf{c}(s)ds \tag{2.7}$$

where $\mathbf{c}$(s) is parametric representation of the contour. Using Calculus of Variation, the Euler-Lagrange condition states that the spline $\mathbf{c}$(s) which minimizes ψ^*_{snake} must satisfy

$$\frac{d}{ds}\psi_{\mathbf{c}_s} - \psi_{\mathbf{c}} = 0 \tag{2.8}$$

where $\psi_{\mathbf{c}_s}$ is the partial derivative of ψ with respect to $\frac{d\mathbf{c}}{ds}$ and $\psi_{\mathbf{c}}$ is the partial derivative of ψ with respect to $\mathbf{c}$.

The Chan-Vese (CV) method works on bi-model image assuming image space, Ω, to be part of either object or background. The CV model is defined as follows:

$$\begin{aligned}\psi(\mathbf{c}, \mu_1, \mu_2) = \lambda_1 \int_{inside(\mathbf{c})} |I(x,y) - \mu_1|^2 \, dxdy + \\ \lambda_2 \int_{outside(\mathbf{c})} |I(x,y) - \mu_2|^2 \, dxdy, (x,y) \in \Omega\end{aligned} \tag{2.9}$$

where I(x,y) is intensity value at location (x,y), μ_1, μ_2 are two constants which are average intensities inside and outside the contour respectively. The Multiphase Chan-Vese (MCV) Method, proposed in [25], uses multiple level sets to partition the image space. The space can be divided into objects and background with respect to each level set used. Hence, the combination of N level sets will partition the space into 2^N non-overlapping segments. This method does not require the computation on Euler-Lagrange's equation. But it suffers from initialization of multiple contours and one cannot find desired segmentation if the number of objects is not exponent of 2.

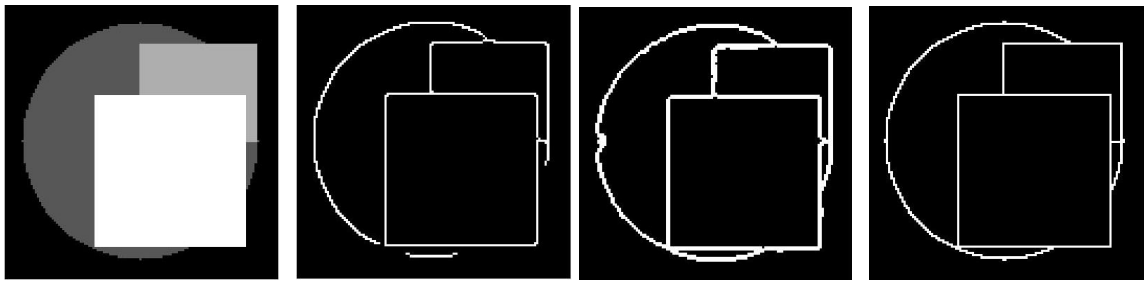

(a) (b) (c) (d)

Figure 2.3: (a) Synthetic Image, (b) Canny Edge Detector, (c) Multiphase Chan-Vese Method and (d) Proposed Method

2.3.2 Simulation Results

The experiments are performed on synthetic image having four objects including background and Magnetic Resonance Human Brain Phantom Images [1]. These images contain four objects naturally. A synthetic image of size 128×128 with four objects of different intensity level is shown in Figure 2.3(a). The results of Canny edge detector, Multiphase Chan-Vese (MCV) Method [25] and proposed method are Figures 2.3(b)-2.3(d) respectively. Canny edge detector is unable to extract continuous boundary, whereas MCV and RST based methods retain the close boundaries of objects. The Gaussian noise of zero mean and standard deviation 15 is added in image shown in Figure 2.4(a). The results are shown in Figure 2.4. Again, Canny edge detector generates spurious edges and is not able to extract close boundary curve. MCV method and proposed method retain the closed object boundaries. However, the result of RST based method seems to be better as to retain very thin boundaries as desired.

Another experiment is performed on MR brain image obtained from Brain Web Dataset [1]. The specifications are as follows: Modality= T1, Protocol=ICBM, RF=20%. The presented work considered 4 classes in the image slice, namely Cerebrospinal Fluid (CSF), Gray Matter (GM), White Matter (WM) and Background. The results for object boundary detection and hence segmentation are shown in Figure 2.5. The Figure 2.5a is noise free slice 100 image whereas Gaussian noise of zero

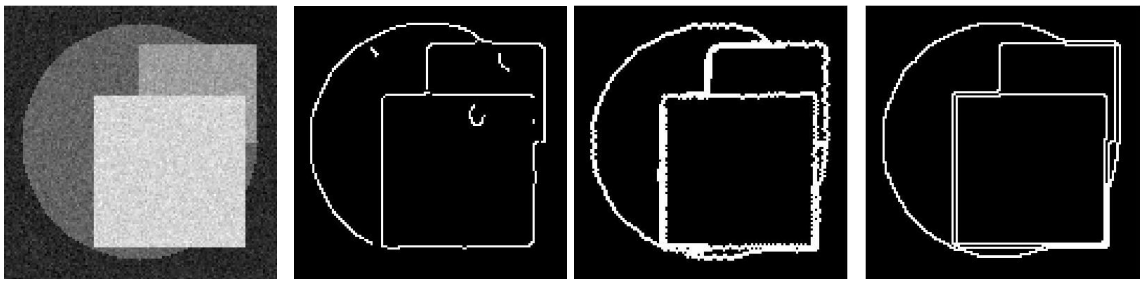

(a) (b) (c) (d)

Figure 2.4: (a) Noisy Image with $N(0, 15)$, (b) Canny Edge Detector, (c) Multiphase Chan-Vese Method and (d) Proposed Method

mean and standard deviation 15 is added which is shown in Figure 2.5b. Figure 2.5c shows output of canny edge detector. The edges do not build object boundaries as those are disconnected. Figure 2.5d shows output of MCV method after 500 iterations while Figure 2.5e is output of proposed method. Figure 2.5f is ground truth segmentation of Figure 2.5a. The results of MCV method and proposed method is shown in Figure 2.5g and 2.5h respectively. The segmentation accuracy of MCV method was found to be 68.84% whereas it is 91.87% in proposed method. Note that these statistics are obtained while comparing with ground truth.

The current state-of-the-art research on image denoising, inpainting suggest patch based approach. For each candidate patch, the task is to find all similar patches within image boundary. So naturally if a patch is within an object, its similar patches are expected to be within that object itself. Similarly, if a patch is on the boundary of two objects, similar patches would be on boundary too. Accurate object boundary detection followed by segmentation could expedite search for similar patches. However, performance depends on the accuracy of detecting object boundary. With this notion in mind, we selected a patch and find its similar patches from the segmented image preceded by MCV and RST method. Figure 2.6 shows experiment of finding similar patches for a given patch. Figure 2.6a and 2.6b show patch location in image and zoomed version respectively. Note that this patch is inside the circle drawn. Figure 2.6c shows the similar patches found in the ground truth segmentation. Figure 2.6d

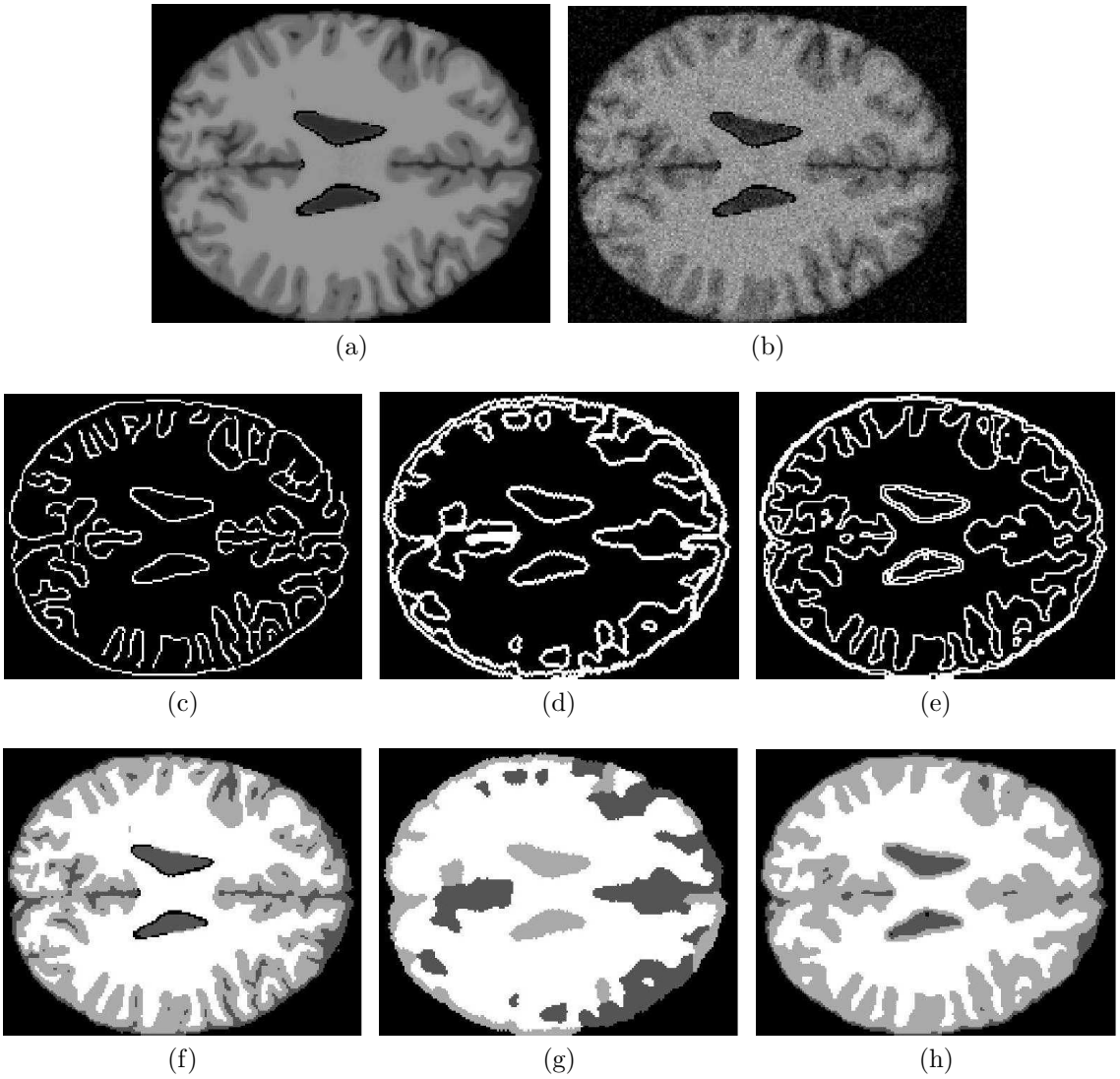

Figure 2.5: (a) Noise free MR Image, (b) Noisy MR Image, (c) Canny edge detection on noisy image (d) Boundary extraction from MCV method, (e) Boundary extraction from proposed RST based method, (f) Ground Truth segmentation of noise free MR image (a), (g) Segmentation from MCV method, accuracy = 68.84% and (h) Segmentation from proposed method, accuracy = 91.87%.

is similar patches obtained from MCV segmentation whereas Figure 2.6e is similar patches identified by proposed method. From ground truth segmentation, there are 5285 patches are found. In case of MCV method, 8738 similar patches are found, out of which only 5132 patches are matching with ground truth patches (matching ratio = 58.73%). From proposed method, 5291 patches are detected to be similar patches and out of which 4936 patches are matching with ground truth patches (matching ratio = 93%). Hence, proposed method can explore more similar patches from object boundaries in comparison to MCV method.

2.4 Conclusion

Rough set has capacity to handle the uncertainty present in the data. This characteristic of RST makes it a suitable candidate to obtain Edge and Class information from the noisy image. The edge information and class information in-turn boost up the performance of further diagnostic process. The obtained edge map is found to be continuous and closed and is capable of defining object boundaries even in noisy situations. It appeared to be defining object boundaries in a better way compared to a couple of existing methodologies such as Canny Edge Detector and Active Contour methods.

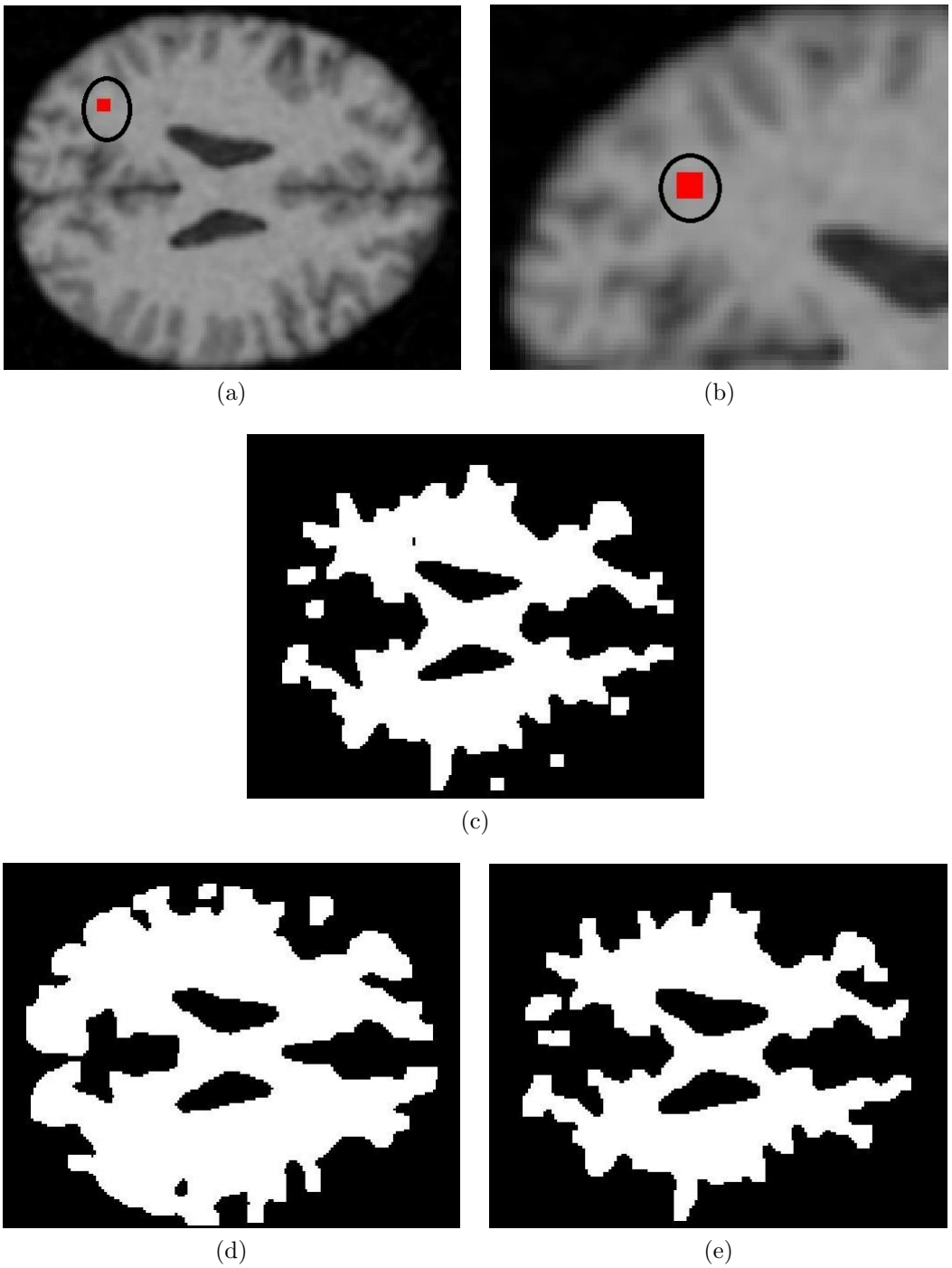

(a) (b)

(c)

(d) (e)

Figure 2.6: (a) A patch (5x5) is shown at location (39,39), (b) Zoomed part of patch location, (c) Similar patches available in Ground Truth segmentation, (d) Similar patches obtained from MCV method and (e) Similar patches obtained from proposed method. 58.73% and 93% patch matches are observed with MCV method and Proposed method given ground truth patches shown in (c) respectively.

Chapter 3

Image Denoising in Early Age

Initial work in the domain of denoising includes Mean and Median filters, Isotropic filter, Anisotropic filter [77], [17], [78], robust statistics [79], [80]. Furthermore, non-iterative and more edge preserving Bilateral filter, proposed in [35], revolutionized notion of denoising. The origin of it has been shown from Anisotropic diffusion methods under Bayesian approach in [81]. Bilateral Filter uses two filters simultaneously, one on spatial location and another on intensity values. Since its inception, there have been many modifications of bilateral filter as suggested in [82], [83], [84], [85], [86]. However, its constant time version, in terms of computational complexity, have been proposed recently in [87], [88]. It is even extended to Trilateral filters [89], [90] and for medical images in [91]. The third filter which is used simultaneously with bilateral filters, is designed in various ways. One can conclude that more information could lead to better performance. In the present chapter, the filter proposed is trilateral by nature. The third component of the filter is based on edge information and neighborhood information. Various edge detectors, such as Canny [24] or segmentation methods and gradient based methods such as Active Contour Methods [72],[75], could be utilized for obtaining edge details. However, we are looking for edges that give rise to object boundaries, which are closed in nature. Most of the above mentioned methods fail to get such closed boundaries while finding the edges. Moreover, the method such as Active Contour fails to get object boundaries where number of

objects is not in power of two. The details of these are available in Chapter 2. The current work includes Rough Set, [30], based methodology to find object boundaries which are closed and continuous. As we mentioned, the third component of filter also depends on neighborhood information, each image pixel is labeled as one of the objects/classes present in the image. This class information (class label) is obtained through the Rough set based mechanism [Chapter 2]. The edge map and class labels are obtained simultaneously. There are few methods available which use pair of images to denoise under bilateral framework, named Cross Bilateral Filter and Dual Bilateral Filter. (Refer to [92] for more details). Now, very briefly, we will discuss bilateral filter and related work before describing our proposed filter.

3.1 Related Work

The Bilateral Filter (BF) inherently defines spatial and range (photometric) filter to denoise an image according to spatial domain and intensity domain respectively [35]. The final filter uses the product of weights of both the filters for a neighboring pixel. Mathematically, BF can be defined as

$$\Delta(i,j) = \psi(i,j)\zeta(i,j) \tag{3.1}$$

where ψ and ζ are monotonically decreasing non-negative functions for spatial and intensity closeness, i is the center pixel location and location j is in neighborhood of i, i.e. $j \in N(i)$, within window $w \times w$. In general, both functions are assumed to be Gaussian in nature and controlled by their parameters, σ_ψ and σ_ζ respectively. These functions are defined as

$$\psi(i,j) = G_{\sigma_\psi}(\|i-j\|) \tag{3.2}$$

$$\zeta(i,j) = G_{\sigma_\zeta}(\|Y(i)-Y(j)\|) \tag{3.3}$$

where $Y(i)$ represent intensity at location i. The denoised pixel intensity $\widehat{Y}(i)$ at the location i is given by

$$\widehat{Y}(i) = \frac{\sum_{j \in N(i)} \Delta(i,j) Y(j)}{\sum_{j \in N(i)} \Delta(i,j)} \tag{3.4}$$

The Scaled Bilateral Filter proposed in [83], is one of the state-of-the-art approach proposed on conventional BF framework. The key idea behind this is consider the closeness in the scale-space domain where noise will get suppressed by some amount. In this approach, input is first convolved with a Gaussian kernel of suitable size. In its intensity filter, the difference is considered between scaled version of input image at location p with input image at location q. But this blurring may lead to a loss of edge information. The selection of appropriate scale for comparison purpose was not suggested. The spatial filter is kept same. The intensity filter, ζ, is defined as follows:

$$\zeta(p,q) = G_{\sigma_\zeta}\left(\|I_G(p) - I(q)\|\right) \tag{3.5}$$

$$I_G(p) = \sum_{q \in N(p)} G_{scale}\left(\|p-q\|\right) I(q) \tag{3.6}$$

Here, I_G is the scaled version of input image I, p and q are positions in the image and $N(p)$ is the neighborhood considered around position p.

A Wavelet based Bilateral Filter has been proposed in multi-resolution framework [86]. An input image is decomposed into its approximation (LL band) and detail sub-bands (LH, HL, HH bands) through wavelet decomposition at two levels using 'db8' filter. The BF is applied on approximation sub-band at both level and wavelet thresholding is applied on detail sub-bands. The denoised image is reconstructed using filtered approximation band and detail sub-bands (after applying thresholding on coefficients) at both the level using inverse wavelet transformation. The structure and behavior of conventional Bilateral Filter [35] remains intact (refer to eq. (1)), however, it is applied at various level of wavelet pyramid structure. More details can be found in [86].

In BF, a pixel is estimated using weighted average of pixels in the given neigh-

borhood space as discussed above. The extreme case of it can be defined if the neighborhood window is assumed to be equal to given image space for each pixel. This philosophy leads to the concept of Non Local Means [93] approach designed for image denoising. Non-Local similarity focuses on the range filter by leveraging the effect of spatial filter in predefined neighborhood. In other words, it inherently assumes complete image space and estimation is based on weighted average of range kernel function. Chapter 4 will provide more in-depth details.

3.2 Design of Proposed Filter

The proposed filter introduces a term which boosts up the impact of spatial closeness and intensity closeness. The introduced term is adaptive in nature and derived from Rough Edge Map and Rough Class Labels obtained from noisy image. The spatial filter in the conventional approach does not consider presence of edge in the image. Similarly, range filter is simply governed by parameters of functional form like decay parameter if function is assumed to be Gaussian. This leads to include more information about edges and homogeneous region of the image.

The third term $\rho(i,j) \in [0,1]$ is defined for each pixel of the image conditioned on REM information around pixel (x,y) and RCL information at location (i,j) (Here, (x,y) is the current pixel location in the image space and (i,j) location is in the predefined neighborhood of (x,y) location). Both the information utilizes the uncertainty or roughness of the image due to presence of noise. In this proposal, a fuzzy notion is adopted to derive the value of ρ for each pixel depending on both the information. Here, the value of ρ is categorized in three notions, namely small (ρ_s), moderate (ρ_m) and high (ρ_h) based on impact of both the information for each pixel. The restriction of ρ is defined as follows

a. $\rho_h(i,j) \in [0, 0.4]$

b. $\rho_m(i,j) \in (0.4, 0.7]$

c. $\rho_s(i,j) \in (0.7, 1]$

So far, the ranges of small, medium and large values of ρ are fixed intuitively by looking at its impact on the filter. However, a sigmoidal type of function could be used. The third weight (ρ) is expected to either boost up or lower down the effect of other two weights in conventional bilateral filter. The neighbors of a pixel are defined by considering $w \times w$ window centered at each pixel. The pseudo assignment is as follows:

1. if $REM(i,j) == 1$
2. if $class(i,j) == class(x,y)$
3. $\rho(i,j) = \rho_m$;
4. $else$
5. $\rho(i,j) = \rho_s$;
6. end
7. $else$
8. $if class(i,j) == class(x,y)$
9. $if REM(x,y) == 1$
10. $\rho(i,j) = \rho_m$;
11. $else$
12. $\rho(i,j) = \rho_h$;
13. end
14. $else$
15. $if REM(x,y) == 1$

16. $\rho(i,j) = \rho_s$;

17. *else*

18. $\rho(i,j) = \rho_s$; (This should not occur)

19. *end*

20. *end*

21. *end*

The proposed filter is designed as follows

$$\Delta'(i,j) = \rho(i,j)(\psi(i,j)\zeta(i,j)) \tag{3.7}$$

The first condition (1) emphasizes that whether neighbor pixel is near to an edge or not. The granule processing will give a thick edge which will also consider pixels near to actual edges. Conditions $(1) - (6)$ reveal that the edge may pass through neighbor pixel and both are from same class, so current pixel is also near to an edge hence assign moderate weight to preserve that edge. Otherwise both the pixel belongs to different classes and hence assigns small weight so that it will have less impact.

If an edge is not passing through neighbor pixel then check whether they belong to same class or not in condition (8). If both are from same class and edge is passing from center pixel (condition (9)) then assign moderate weight to preserve that edge, otherwise (condition (11)), they both belong to homogeneous area and have high dependency on each other so assign high weight to increase the impact.

If both pixel and its neighbor do not belong to same class (condition (14)) and center pixel is an edge pixel (condition (15)) then both belong to different classes and edge is passing in between these two, so assign high weight. The condition (17) should not occur ideally (but this case has been observed in experiments), so assign high weight to have less impact on the current pixel.

3.3 Computational Complexity

In this subsection, we evaluate the computational complexity of the method proposed along with some other methods which are used for comparison. All the methods based on bilateral filter are window based method, in other words, methods are restricted in sufficient large window around current pixel for estimating its true value. Let S be the predefined size of the neighborhood such as $3 \times 3, 5 \times 5$ etc. and N be the total number pixel of the image. Here, we assume that S involves in the computation of spatial and range filters as defined in Section 3.1. Being a point-wise processing method, for each pixel computation of both filters need to be performed. Hence the complexity of Bilateral filter [35] can be defined as $O(NS)$ [92]. In extreme case (worst case complexity), S can be extended to image space which makes complexity in order of $O(N^2)$.

In case of Scaled Bilateral filter [83], first scaled version of input image is computed using Gaussian function with filter size K and range filter is based on difference between scaled image and input image for each pixel. Hence, the complexity can be defined as $O(N(S + K))$. The Multi-Resolution Bilateral filter [86] is based only bilateral filter with additional two level wavelet decomposition. The method deploys bilateral filter three times at various stages (Refer to schema provided in [86]). Hence, computationally it can be defined in terms of $O(3NS + W)$, where W denotes the computation required for two level decomposition and reconstruction.

The proposed method first computes Class information and Edge information based on three optimized thresholds (see subsections 3.1 and 3.2). Note that, in the current context, as we know there are four classes possible, hence the number of thresholds are fixed to three. Let us consider, T_{avg} number of intensity values are considered to find each optimized threshold. So the complexity of this task would be $O(N * T_{avg})$. Now while designing the filter, an additional step is proposed along with the conventional bilateral filter. This additional step assigns weight to each pixel by comparing class information and edge information. Hence, the overall computational

Table 3.1: Computational complexity for methods used in this work

Approach	Complexity
Bilateral Filter [35]	$O(NS)$
Multi Resolution Bilateral Filter [86]	$O(3NS + W)$
Scaled Bilateral Filter [83]	$O(N(S + K))$
Proposed Filter	$O(N(S + C + T_{avg})$

complexity becomes $O(N(S + C) + N * T_{avg})$, where C denotes the time to compute weights. In extreme case, if S and C are extended to image space, then complexity turns out to be $O(N^2)$ which is same as Bilateral filter. Thus, it could be concluded that the proposed method does not carry high computational cost.

3.4 Experimental Results

The work has been carried out on $2D$ monochrome human brain MR images. The experiments were performed on one simulated dataset downloaded from Brain Web [1] and two real data sets namely, Open Access Series of Imaging Studies (OASIS, [7]) and Brain Tumor Segmentation challenge data from MICCAI 2012 confernce (BRATS, [8]). The experimental setup considers two noise models, Gaussian and Rician in nature on Brain Web data. The method of addition of Rician noise is as presented in [94]. To evaluate performance of denoising algorithm, four evaluation measures are used. The measures consist of Peak Signal to Noise Ration (PSNR), Root Mean Square Error (RMSE), Structure SIMilarity (SSIM) Index proposed in [95] and Feature SIMilarity (FSIM) Index proposed in [96]. Note that these performance measures are wisely used to validate denoising algorithms. In the real databases, noise is assumed to be Rician in nature. The parameters of all methods are mentioned in the table 3.2. All the experiments were performed in MATLAB 2012(b) environment on Lenovo Z580 with Intel core i7 Windows7 laptop. The next subsection briefly describe the evaluation measure in more detail followed by experimental set up and results on all the data sets.

Table 3.2: Parameter values for methods used in this work

Approach	# of parameters	Parameter value
Bilateral Filter [35]	2	$\sigma_\psi = 5$ and $\sigma_\zeta = 0.01$
Multi Resolution Bilateral Filter [86]	3	$\sigma_\psi = 5$, $L = 2$ σ_ζ = estimated from input image
Scaled Bilateral Filter [83]	3	$scale = 0.5$, $\sigma_\psi = 5$ and $\sigma_\zeta = 0.01$
Proposed Filter	3	$\sigma_\psi = 5$ and $\sigma_\zeta = 0.01$ $\rho = adaptive$

3.4.1 Evaluation Measures

The evaluation measures used are defined as follows: Let I be *noise-free* image of size $M \times N$ and $\hat{(I)}$ be is its noise-free approximation.

- Root Mean Square Ratio (RMSE)

$$MeanSquareError(MSE) = \frac{1}{MN}\sum_{i=1}^{M}\sum_{j=1}^{N}\left(I(i,j) - \hat{I}(i,j)\right)$$

$$RMSE = \sqrt{MSE} \tag{3.8}$$

- Peak-Signal-to-Noise Ratio (PSNR)

$$PSNR = 10log_{10}\left(\frac{L^2}{MSE}\right) \tag{3.9}$$

  where L is maximum intensity level present in the image I and MSE is same as defined above.

- Structural Similarity Index (SSIM) [95]

$$SSIM(x,y) = \frac{(2\mu_x\mu_y + \epsilon_1)(2\sigma_{xy} + \epsilon_2)}{(\mu_x^2 + \mu_y^2 + \epsilon_1)(\sigma_x^2 + \sigma_y^2 + \epsilon_2)}$$

$$MSSIM = \frac{1}{M}\sum_{j=1}^{M} SSIM(x_j, y_j) \tag{3.10}$$

where ϵ_1, ϵ_2 ensure stability when either $(\mu_x^2 + \mu_y^2)$ or $(\sigma_x^2 + \sigma_y^2)$ us close to zero. The SSIM is defined over a local window centered at (x, y) and average over such windows gives a single measure for entire image, named as Mean SSIM (MSSIM).

- Feature Similarity Index (FSIM) [96]

$$FSIM = \frac{\sum_{x\in\Omega} S_L(x) PC_m(x)}{\sum_{x\in\Omega} PC_m(x)} \tag{3.11}$$

where Ω defines entire image spatial domain. The similarity measure $S_L(x)$ is defined as product of similarity function on Phase Congruency (PC) and similarity function of Gradient Magnitude (GM) (i.e. $S_L(x) = S_{PC}(x).S_G(x)$). The functions $S_{PC}(x)$ and $S_G(x)$ are as follows:

$$S_{PC}(x) = \frac{2PC_1(x).PC_2(x) + \epsilon_1}{PC_1^2(x) + PC_2^2(x) + \epsilon_1} \quad \& \quad S_G(x) = \frac{2G_1(x).G_2(x) + \epsilon_2}{G_1^2(x) + G_2^2(x) + \epsilon_2} \tag{3.12}$$

where ϵ_1, ϵ_2 ensure stability of above functions.

3.4.2 Simulation Results

Results on Brain Web Database

The implementation of algorithm on phantom data provides an insight of the algorithm and ability to compare the results with available ground truth data. The Brain Web database consists of phantom volumetric data with their ground truth details. The other specifications are: size = $181 \times 217 \times 181$, modality = $T_1\&T_2$, protocol = $ICBM$, RF= 0% and noise = 0%. The 2D slices are extracted from 3D volume data of size 140×176 after removing unnecessary background area and normalized in the range $[0, 1]$.

The experiments are performed with different noise levels by adding **Gaussian noise** and **Rician noise** in the data (Rician noise model and its properties are

discussed in detail in Chapter 5). The addition of noise is done as suggested in [94]. In case of Rician noise, the bias removal ($= 2\sigma^2$, where σ is noise standard deviation) is also done as suggested in [20]. The results of both noise models at with different noise levels are shown in tables. Table 3.3 and 3.4 show results on Gaussian noise distribution over T1 and T2 images. In most of the cases, proposed method clearly outperforms than other methods. Table 3.5 and 3.6 show results on Rician noise distribution over both the modalities. In all the cases, NLM filter clearly outperforms others in the class of Bilateral filters. However, proposed method performed better than other methods in Bilateral category. The experiments were performed on 50 slices of both the modalities on Gaussian noise and Rician noise. The results of PSNR and SSIM values are shown in Figure 3.1 and 3.2 where one can observe the superior performance among bilateral filters (Note, we have shown results on bilateral class of filters only). The Figures 3.3 and 3.4 show the denoised images with various methods on slice 100 of T1 modality under Gaussian noise and Rician noise respectively.

Table 3.3: Performance comparison of proposed denoising filter with other approaches on various quantitative measures under **Gaussian Noise** assumption on **T1** images of Brain Web database

Noise		Slice 70				Slice 100			
SD	Methods	PSNR	RMSE	MSSIM	FSIM	PSNR	RMSE	MSSIM	FSIM
3	Noisy Image	39	8.18	0.9472	0.9752	39.18	7.85	0.9345	0.973
	Bilateral	40.23	6.17	0.9644	0.9866	40.81	5.39	0.9612	0.9869
	Multi Resolution Bilateral	35.19	19.68	0.9275	0.9566	37.57	11.37	0.9533	0.9769
	Scaled Bilateral	40.09	6.37	0.9661	0.9903	40.32	6.03	0.9637	0.9906
	Proposed Method	40.6	5.66	0.9686	0.9898	41.35	4.75	0.9676	0.9907
5	Noisy Image	34.57	22.72	0.8776	0.9409	34.75	21.8	0.8541	0.9358
	Bilateral	35.25	19.27	0.898	0.9546	35.64	17.75	0.8835	0.9522
	Multi Resolution Bilateral	33.04	32.28	0.8840	0.9372	34.39	23.68	0.9058	0.9610
	Scaled Bilateral	35.78	17.15	0.9099	0.9683	36.14	15.81	0.9017	0.9676
	Proposed Method	36.53	14.44	0.9293	0.9772	37.36	11.95	0.9288	0.9793
7	Noisy Image	31.64	44.54	0.8028	0.9025	31.82	42.74	0.7735	0.8974
	Bilateral	32.07	40.35	0.8191	0.914	32.33	38	0.7951	0.9081
	Multi Resolution Bilateral	31.28	48.42	0.8391	0.9144	32.12	39.90	0.8577	0.9406
	Scaled Bilateral	32.69	34.96	0.8387	0.9342	33.06	32.15	0.8243	0.9317
	Proposed Method	33.58	28.5	0.8734	0.9547	34.2	24.72	0.8648	0.953
10	Noisy Image	28.55	90.89	0.6971	0.8458	28.72	87.22	0.6679	0.8352
	Bilateral	28.77	86.34	0.7068	0.8534	28.98	82.83	0.6795	0.8439
	Multi Resolution Bilateral	29.3	76.41	0.7783	0.8787	29.88	66.86	0.7954	0.9086
	Scaled Bilateral	29.45	73.79	0.7323	0.8779	29.74	69.08	0.712	0.8706
	Proposed Method	31.13	50.15	0.8156	0.936	31.67	44.26	0.8171	0.9433
15	Noisy Image	25.02	204.45	0.5524	0.7635	25.2	196.21	0.5323	0.7504
	Bilateral	25.13	199.67	0.5566	0.7673	25.31	191.34	0.5367	0.7545
	Multi Resolution Bilateral	27.19	124.24	0.7051	0.8321	27.86	106.4155	0.7290	0.8709
	Scaled Bilateral	25.86	168.82	0.5831	0.7927	26.09	160.05	0.5649	0.7807
	Proposed Method	27	129.88	0.64	0.8477	27.54	114.49	0.6481	0.8612

Table 3.4: Performance comparison of proposed denoising filter with other approaches on various quantitative measures under **Gaussian Noise** assumption on **T2** images of Brain Web database

Noise		Slice 70				Slice 100			
SD	Methods	PSNR	RMSE	MSSIM	FSIM	PSNR	RMSE	MSSIM	FSIM
3	Noisy Image	39	8.17	0.949	0.9793	39.18	7.85	0.9372	0.9769
	Bilateral	40.14	6.25	0.9663	0.9887	40.79	5.42	0.9638	0.9892
	Multi Resolution Bilateral	30.89	52.94	0.8795	0.9121	33.14	31.54	0.9330	0.9492
	Scaled Bilateral	39.08	8.04	0.9682	0.9913	38.75	8.67	0.9668	0.9923
	Proposed Method	40.5	5.79	0.9705	0.991	41.25	4.88	0.9697	0.9921
7	Noisy Image	31.67	44.22	0.8124	0.92	31.85	42.5	0.7852	0.9101
	Bilateral	32.08	40.31	0.8281	0.9292	32.33	38.02	0.8059	0.9219
	Multi Resolution Bilateral	28.09	100.9823	0.8106	0.8784	29.57	71.73	0.8503	0.9185
	Scaled Bilateral	32.55	36.13	0.8492	0.947	32.8	34.15	0.8368	0.9452
	Proposed Method	33.3	30.4	0.8705	0.9575	33.81	27.04	0.8652	0.957
10	Noisy Image	28.6	89.81	0.7166	0.8745	28.76	86.48	0.6893	0.86
	Bilateral	28.82	85.33	0.7259	0.8808	29.01	81.66	0.7002	0.8675
	Multi Resolution Bilateral	26.47	146.58	0.7701	0.8582	27.67	111.26	0.8030	0.8969
	Scaled Bilateral	29.43	74.2	0.7517	0.9028	29.68	70.02	0.7328	0.8957
	Proposed Method	31.01	51.59	0.8411	0.9299	30.98	51.96	0.8067	0.9393
15	Noisy Image	25.1	200.95	0.5917	0.8094	25.26	193.86	0.5722	0.79
	Bilateral	25.21	196.08	0.5958	0.8127	25.37	188.86	0.5765	0.7935
	Multi Resolution Bilateral	24.28	242.7605	0.7129	0.8252	25.0257	204.42	0.7356	0.8550
	Scaled Bilateral	25.86	168.62	0.6203	0.8342	26.07	160.54	0.6024	0.8192
	Proposed Method	28.48	92.25	0.7604	0.9078	28.69	87.85	0.7405	0.9057
20	Noisy Image	22.62	355.37	0.5015	0.7565	22.77	343.43	0.49	0.7338
	Bilateral	22.69	350.31	0.5037	0.7584	22.84	338.31	0.4919	0.756
	Multi Resolution Bilateral	22.56	360.91	0.6627	0.7899	23.17	313.07	0.6843	0.8159
	Scaled Bilateral	23.42	295.54	0.5264	0.7794	23.58	285.04	0.5137	0.7580
	Proposed Method	25.59	179.47	0.6313	0.8526	25.78	171.65	0.6114	0.8393
25	Noisy Image	20.71	552.55	0.4343	0.712	20.85	534.03	0.4285	0.688
	Bilateral	20.75	547.7	0.4354	0.7133	20.9	529.16	0.4296	0.6892
	Multi Resolution Bilateral	21.3	482.08	0.6227	0.7585	21.7321	436.39	0.6415	0.7796
	Scaled Bilateral	21.53	457	0.4556	0.7336	21.69	440.93	0.4481	0.7091
	Proposed Method	22.87	335.54	0.5149	0.7876	22.88	335.4	0.4957	0.7661

Table 3.5: Performance comparison of proposed denoising filter with other approaches on various quantitative measures under **Rician Noise** assumption on **T1** images of Brain Web database

Noise		Slice 70				Slice 100			
SD	Methods	PSNR	RMSE	MSSIM	FSIM	PSNR	RMSE	MSSIM	FSIM
3	Noisy Image	37.83	10.71	0.9068	0.973	37.55	11.43	0.8712	0.97
	Bilateral	40.23	6.17	0.9707	0.9861	40.83	5.37	0.9718	0.9862
	Multi Resolution Bilateral	35.1	20.1	0.9395	0.9549	37.32	12.06	0.9730	0.9744
	Scaled Bilateral	40.2	6.21	0.9794	0.9902	40.44	5.87	0.9854	0.9904
	Proposed Method	40.69	5.55	0.979	0.9896	41.56	4.54	0.9845	0.9906
5	Noisy Image	33.4	29.75	0.8384	0.9358	33.11	31.74	0.7937	0.93
	Bilateral	35.15	19.86	0.8992	0.9517	35.46	18.48	0.8867	0.949
	Multi Resolution Bilateral	32.89	33.41	0.9100	0.9334	33.89	26.52	0.9467	0.9538
	Scaled Bilateral	35.83	16.98	0.931	0.9667	36.21	15.58	0.9368	0.9658
	Proposed Method	36.66	14.02	0.9538	0.9769	37.57	11.38	0.9683	0.9789
7	Noisy Image	30.47	58.29	0.7705	0.8942	30.19	62.2	0.7248	0.8838
	Bilateral	31.87	42.27	0.8144	0.9084	32.07	40.39	0.7892	0.9019
	Multi Resolution Bilateral	30.92	52.67	0.8713	0.9037	31.67	44.27	0.9164	0.9284
	Scaled Bilateral	32.64	35.43	0.8551	0.9297	32.99	32.7	0.8521	0.9259
	Proposed Method	33.58	28.47	0.9007	0.9523	34.2	24.31	0.9107	0.9508
10	Noisy Image	27.38	118.87	0.6733	0.8336	27.1	126.89	0.6332	0.8193
	Bilateral	28.48	92.17	0.6986	0.8439	28.63	89.22	0.67	0.8337
	Multi Resolution Bilateral	29.09	80.25	0.8233	0.8664	29.81	67.88	0.8781	0.8959
	Scaled Bilateral	29.27	76.88	0.7364	0.8686	29.52	72.61	0.7201	0.81
	Proposed Method	31.22	49.06	0.8613	0.9349	31.81	42.8	0.8991	0.9418
15	Noisy Image	23.87	266.81	0.5358	0.7467	23.58	285.02	0.5089	0.7285
	Bilateral	24.7	220.34	0.545	0.7518	24.83	213.77	0.5239	0.7386
	Multi Resolution Bilateral	27.07	127.77	0.7577	0.8182	27.71	110.23	0.8202	0.8523
	Scaled Bilateral	25.5	183.17	0.5763	0.7775	25.69	175.35	0.5585	0.7641
	Proposed Method	26.72	138.47	0.6579	0.8365	27.27	121.91	0.6964	0.8476

(a) Legends

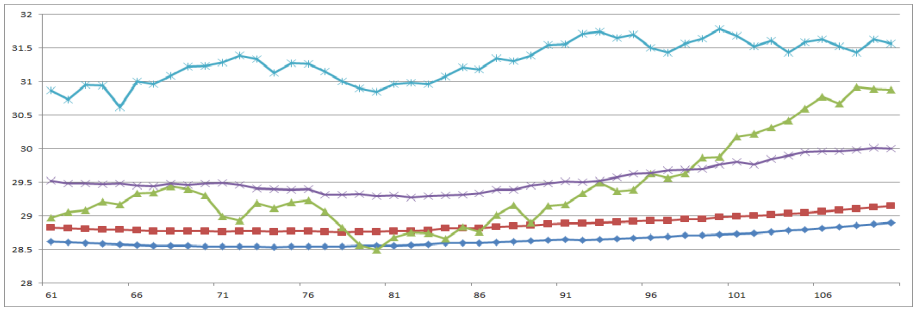

(b) PSNR comparison with Gaussian noise

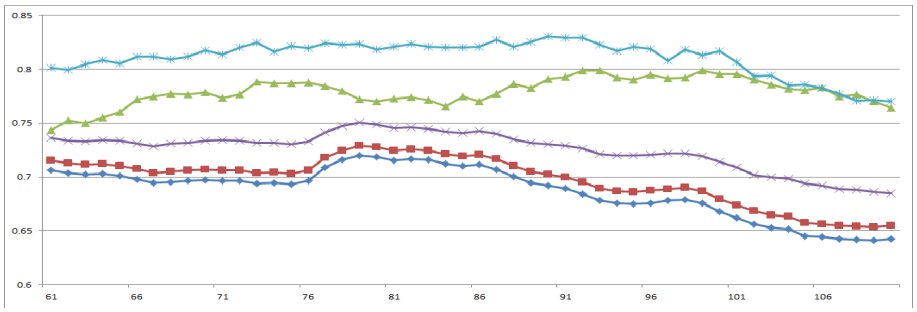

(c) SSIM comparison with Gaussian noise

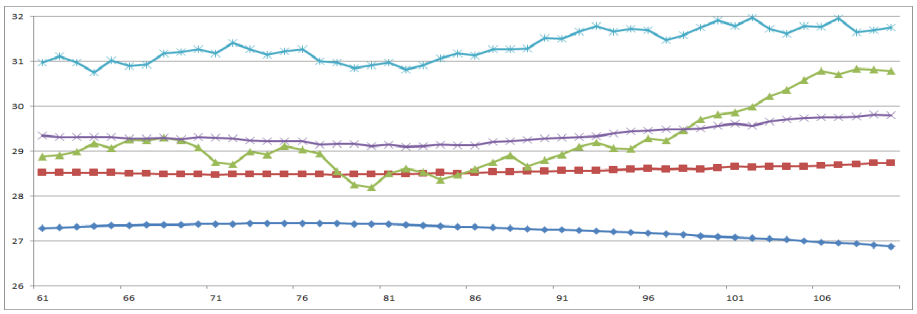

(d) PSNR comparison with Rician noise

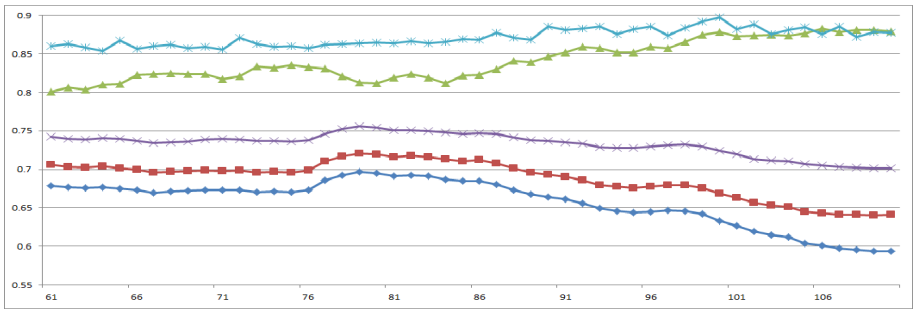

(e) SSIM comparison with Rician noise

Figure 3.1: Graphs for PSNR & SSIM comparison of T1 images with Gaussian noise and Rician noise for noise level 10.

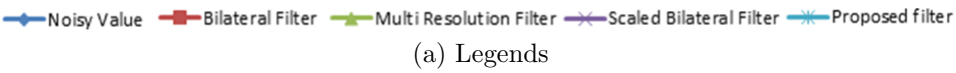

(a) Legends

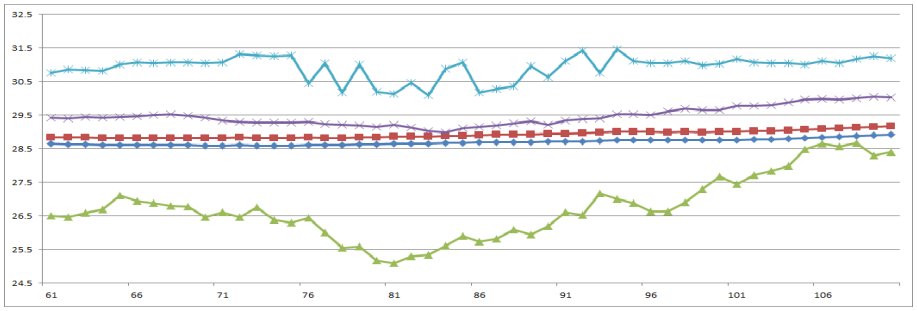

(b) PSNR comparison with Gaussian noise

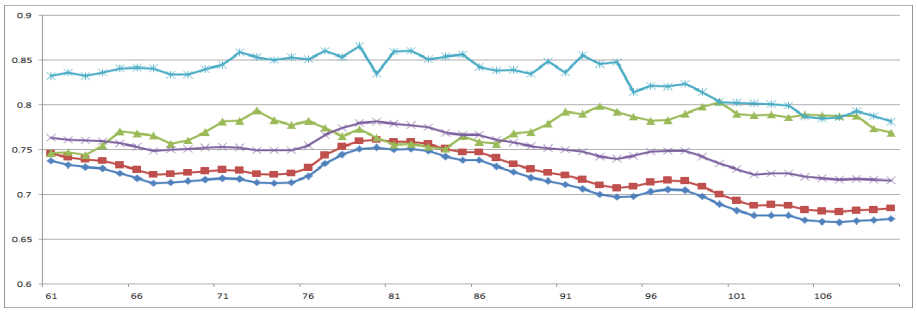

(c) SSIM comparison with Gaussian noise

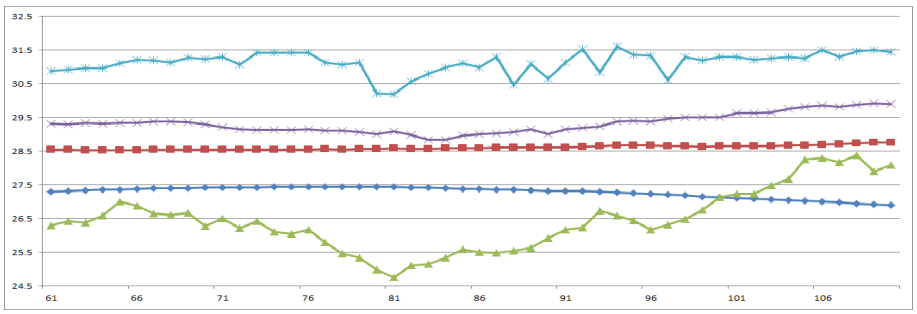

(d) PSNR comparison with Rician noise

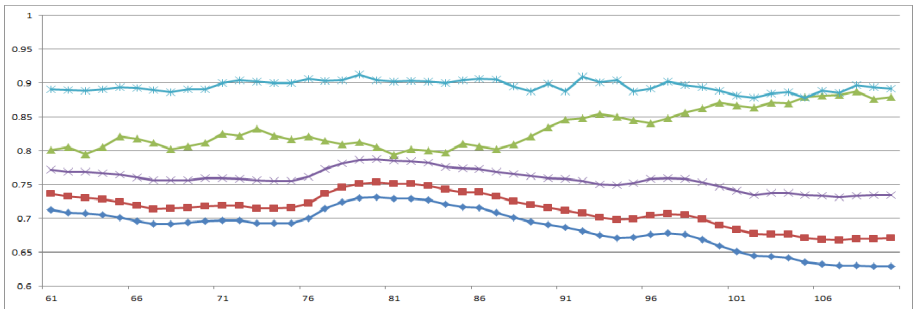

(e) SSIM comparison with Rician noise

Figure 3.2: Graphs for PSNR & SSIM comparison of T2 images with Gaussian noise and Rician noise for noise level 10.

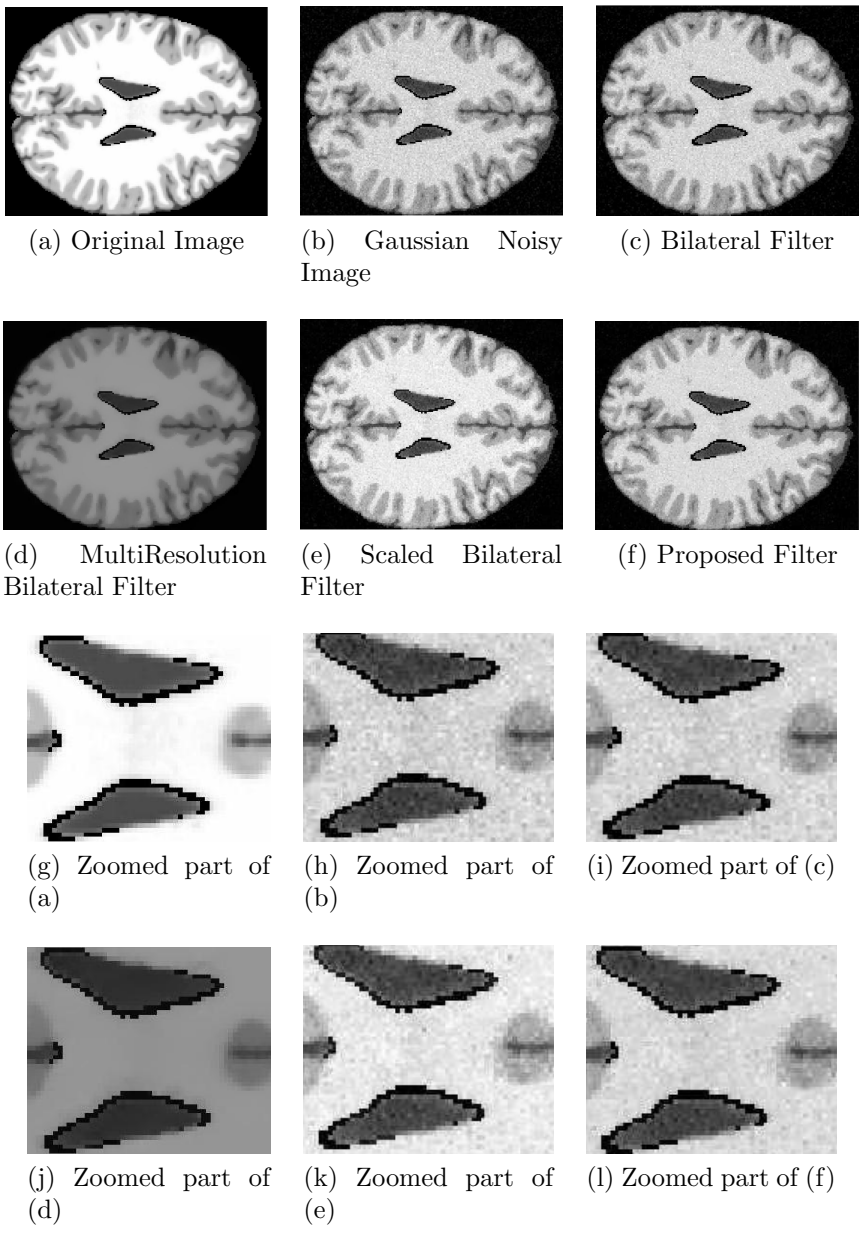

(a) Original Image (b) Gaussian Noisy Image (c) Bilateral Filter

(d) MultiResolution Bilateral Filter (e) Scaled Bilateral Filter (f) Proposed Filter

(g) Zoomed part of (a) (h) Zoomed part of (b) (i) Zoomed part of (c)

(j) Zoomed part of (d) (k) Zoomed part of (e) (l) Zoomed part of (f)

Figure 3.3: Results on Brain Web data (slice 100) having Gaussian noise with zero mean and standard deviation 5.

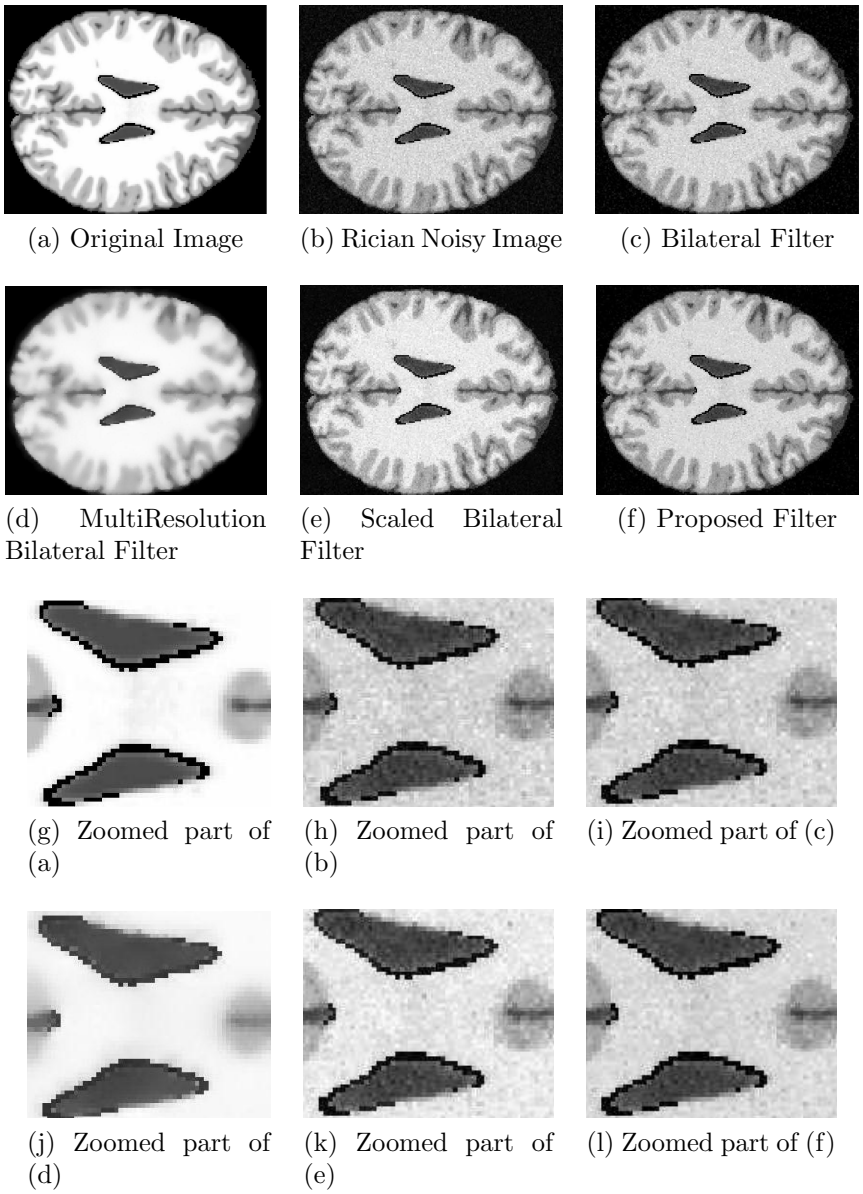

(a) Original Image (b) Rician Noisy Image (c) Bilateral Filter

(d) MultiResolution Bilateral Filter (e) Scaled Bilateral Filter (f) Proposed Filter

(g) Zoomed part of (a) (h) Zoomed part of (b) (i) Zoomed part of (c)

(j) Zoomed part of (d) (k) Zoomed part of (e) (l) Zoomed part of (f)

Figure 3.4: Results on Brain Web data (slice 100) having Rician noise with zero mean and standard deviation 10.

Table 3.6: Performance comparison of proposed denoising filter with other approaches on various quantitative measures under **Rician Noise** assumption on **T2** images of Brain Web database

Noise		Slice 70				Slice 100			
SD	Methods	PSNR	RMSE	MSSIM	FSIM	PSNR	RMSE	MSSIM	FSIM
3	Noisy Image	37.83	10.71	0.9123	0.9773	37.55	11.42	0.8787	0.9741
	Bilateral	40.17	6.25	0.972	0.9881	40.81	5.4	0.9738	0.9885
	Multi Resolution Bilateral	30.74	54.88	0.8868	0.9099	32.80	34.10	0.9468	0.9458
	Scaled Bilateral	39.17	7.88	0.9801	0.9913	38.79	8.6	0.9868	0.9923
	Proposed Method	40.6	5.66	0.98	0.9909	41.48	4.62	0.9861	0.9924
7	Noisy Image	30.5	58	0.7834	0.9128	30.21	61.93	0.7412	0.9005
	Bilateral	31.88	42.22	0.8238	0.9241	32.06	40.47	0.8006	0.9159
	Multi Resolution Bilateral	27.99	103.18	0.8430	0.8754	29.23	77.61	0.9044	0.9110
	Scaled Bilateral	32.54	36.21	0.866	0.9442	32.76	34.43	0.8653	0.9422
	Proposed Method	33.21	31.07	0.8953	0.956	34.07	25.46	0.9161	0.959
10	Noisy Image	27.42	117.88	0.6959	0.8644	27.13	126.03	0.6592	0.8642
	Bilateral	28.54	90.98	0.718	0.8725	28.65	88.74	0.6901	0.8578
	Multi Resolution Bilateral	26.28	153.24	0.8120	0.8522	27.14	125.76	0.8710	0.8838
	Scaled Bilateral	29.29	76.53	0.757	0.896	29.5	73.08	0.7429	0.8865
	Proposed Method	31.2	49.36	0.8921	0.9312	31.26	48.66	0.893	0.9434
15	Noisy Image	23.92	263.54	0.5782	0.7965	23.63	282.14	0.554	0.7722
	Bilateral	24.79	215.91	0.5849	0.8002	24.85	212.87	0.564	0.779
	Multi Resolution Bilateral	23.98	260.19	0.7603	0.8139	24.65	222.93	0.8209	0.8404
	Scaled Bilateral	25.57	180.15	0.6144	0.8222	25.71	174.51	0.5969	0.8043
	Proposed Method	28.3	96.19	0.7884	0.8987	28.52	91.39	0.7914	0.8946
20	Noisy Image	21.46	465	0.4908	0.7428	21.16	498.27	0.4763	0.7151
	Bilateral	22.03	407.82	0.4875	0.7406	22.05	405.47	0.4742	0.716
	Multi Resolution Bilateral	22.20	392.16	0.7092	0.7733	22.68	350.48	0.7705	0.7944
	Scaled Bilateral	22.92	331.81	0.5141	0.7625	23.0	326.71	0.5	0.7391
	Proposed Method	24.76	217.34	0.6114	0.8253	24.67	222.03	0.5865	0.8056
25	Noisy Image	19.56	720.13	0.4248	0.6987	19.26	771.56	0.4168	0.6697
	Bilateral	19.77	684.97	0.4133	0.6896	19.79	682.89	0.4061	0.6634
	Multi Resolution Bilateral	20.99	517.51	0.6712	0.7411	21.14	500.2480	0.7230	0.7513
	Scaled Bilateral	20.77	544.15	0.4378	0.7117	20.8	540.85	0.4281	0.6855
	Proposed Method	21.49	461.31	0.4746	0.7493	21.36	474.92	0.4585	0.7211

Results on Real database

The other two real datasets are having some pathological issues. The subject details of selected data from OASIS dataset are as follows: Subject ID:0018, Age: 39 (male), scan number: mpr-1, type: MPRAGE, voxel resolution: 1.0 mm x 1.0 mm x 1.25mm, Orientation: Sagital, TR (ms)= 9.7, TE (ms)= 4.0, TI(ms)= 20.0, Flip angle= 10, slice number used = 100. The results are shown in figure 3.5 along with their zoomed in portion for more clearity.

Another dataset is selected from BRATS data where the given challenge was to identify tumor region and other pathological disorder. The details of the subjects are as follows: Subject ID: 0015, having high grade gliomas, slice= 100. In the real datasets, the noise model was assumed to Rician in nature [11]. The Rician noise estimation was done using recently proposed method in [2]. The results are shown in figure 3.6. The figure 3.7 shows the estimated Tumor class in comparison with the ground truth provided by the organizers. The Dice coefficient is found to be 0.71 where labels are re-estimated using approach given in section 3.1 after denoising.

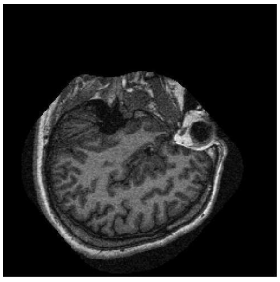

(a) OASIS database Image

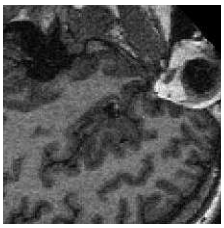

(b) Zoomed part of (a)

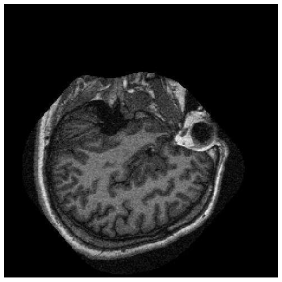

(c) Bilateral filtered Image

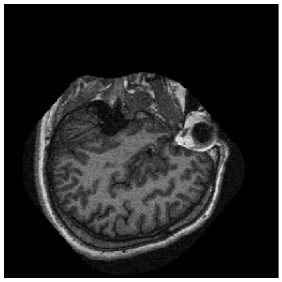

(d) MultiResolution Bilateral Filter

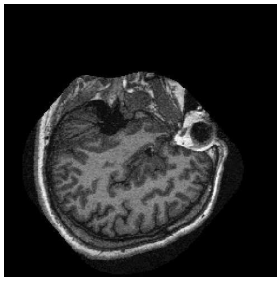

(e) Scaled Bilateral filtered Image

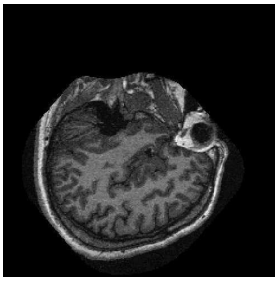

(f) Proposed filtered Image

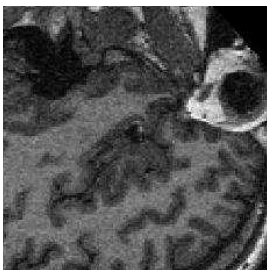

(g) Zoomed part of (b)

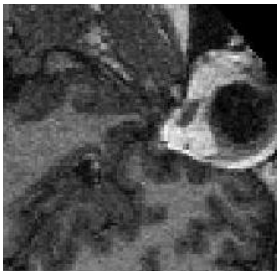

(h) Zoomed part of (c)

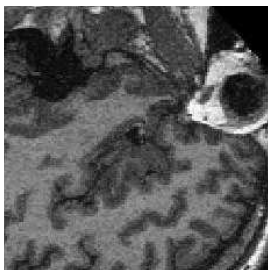

(i) Zoomed part of (e)

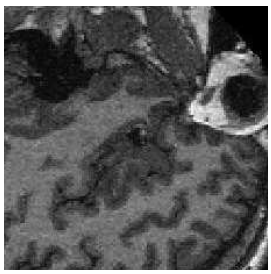

(j) Zoomed part of (f)

Figure 3.5: Result on MR slice from OASIS database

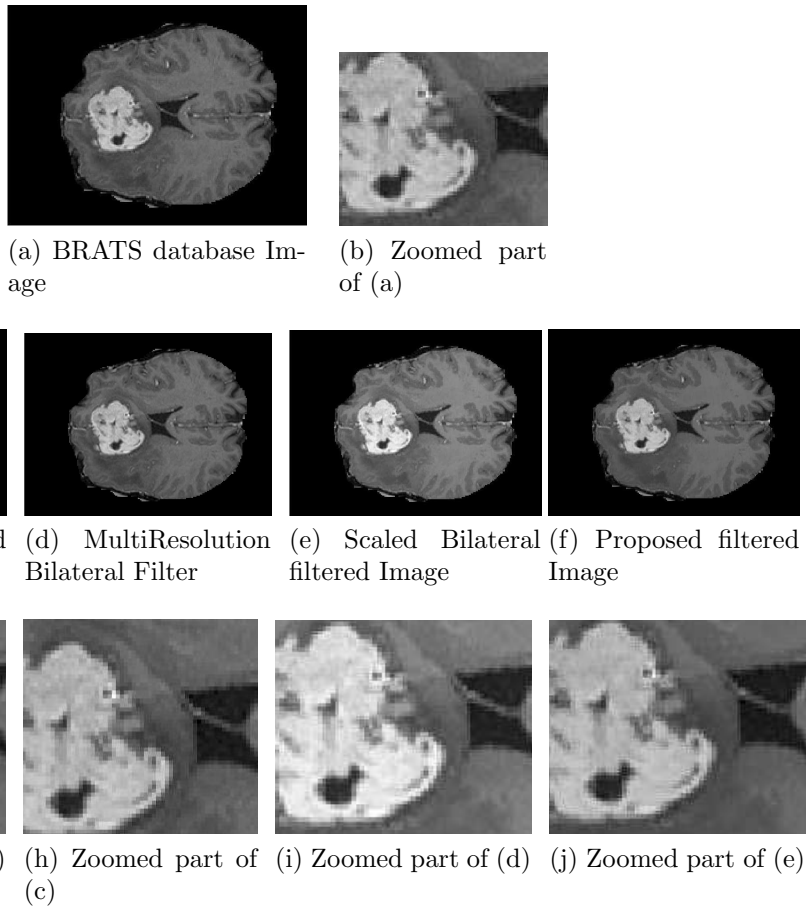

(a) BRATS database Image (b) Zoomed part of (a)

(c) Bilateral filtered Image (d) MultiResolution Bilateral Filter (e) Scaled Bilateral filtered Image (f) Proposed filtered Image

(g) Zoomed part of (b) (h) Zoomed part of (c) (i) Zoomed part of (d) (j) Zoomed part of (e)

Figure 3.6: Result on MR slice from MICCAI BRATS 2012 database

(a) Actual Tumor and Edema class in the image (b) Estimated Tumor class in the image

Figure 3.7: The comparison of actual tumor region and estimated region using Rough Class labels is shown where Dice coefficient is found to be 0.71.

3.5 Conclusion

Rough set has capacity to handle the uncertainty present in the data. This characteristic of RST enables it to be a suitable candidate to obtain Edge and Class information form the noisy image. The edge information and class information in-turn boost up the performance of the proposed filter. The obtained edge map is found to be continuous and closed and is capable of defining object boundaries even in noisy situations. It appears to be defining object boundaries in a better way compared to a couple of existing methodologies such as Canny Edge Detector, Active Contour methods. The performance of the proposed filter is found to be satisfactory when compared with the existing bilateral filters. Note that the performance of present filter for denoising is not compared with some of the recent techniques included within paradigm of non-local means. These methodologies are based on very different principle and hence has not been compared. The propose method can be extended under cross bilateral framework where a pair of images of similar characteristic are considered to denoise a single image having the same characteristic. For example, different modality images can be used to denoise Brain MR Image.

Chapter 4

Non Local Self Similar Image Denoising

More recent work on image denoising includes patch based mechanism. For the last one and half decades, it has matured a lot and is a front runner. In this work, an attempt is made to utilize rough set based image information (discussed in earlier chapters) in the framework of patch based image denoising.

The patch based processing coined the notion of *self-similar patches*. The similarity between two patches can be defined in terms of geometrical and structural perspective. The repetition of these kind of similar patches in the image are employed in *Non local self-similarity* (NLSS) fashion, as proposed in [93]. The term *non-local* leverage distance constraint between location of two patches in the image space rather than restricting in small window as done in Bilateral Filter. Philosophically, NLSS framework is based on photometric filter which eliminates least significant patch based on distance measure. Practically, searching of all similar patches for each underlying patch, in the image space, is computationally intensive process. Many methods restrict this search to sufficiently large predefined window, $W \times W$, which is not non local in *true* sense. The search window parameter, W, may set a trade-off between computation time and performance of the method.

4.1 State-of-the-art Methods

This section explains two primary methods of NLSS framework i.e. Non Local Means method [93] and Local Pixel Grouping based Principal Component Analysis (LPG-PCA) [97]. Brief overviews of variants of these methods are also mentioned thereafter.

Non Local Means Method

The Non Local Means (NLM) Method [93] is a successor of Bilateral filter method where a pixel is denoised by weighted average of similar pixels in its vicinity. For denoising a pixel, the difference between Gaussian ϵ-neighborhood of two pixel must fall below a threshold criteria defined according to the measure used. The method is non-local in terms of the space available to search similar pixel for any pixel which is restricted in its predecessor methods. For an image X, the filtered value at location p is:

$$X(p) = \sum_{\forall q \in X} S(p,q)X(q) \tag{4.1}$$

where $S(p,q)$ is the similarity function between pixel at location p and q. The function S is defined as follows:

$$S(p,q) = \frac{1}{Z_p} e^{\frac{G_\rho \|X(N_p) - X(N_q)\|^2}{h^2}}$$
$$0 \leq S(p,q) \leq 1, \sum_{\forall q \in X} S(p,q) = 1$$

where Z_p is the normalizing constant, h is the exponential decay control parameter, G_ρ is normalized Gaussian weighting function with zero mean and ρ standard deviation.

The above formulation of NLM consider all the pixels in the image space for computing weighted average for pixel at location p. However, this makes a time consuming task and increases computational complexity. As suggest, one can have a sufficiently large local search window around each pixel to get its similar pixel. Hence, NLM method has three main parameters: patch size, local search window size, W

and decaying parameter, h. The decaying parameter is kept equal to noise variance itself as suggested in [93]. The patch size is an open issue in computer vision problems where one can think of deriving adaptive patch size based on object homogeneity and shape etc. The patch size is kept square and fixed in all the experiments. The local search window parameter is crucial and sets a trade-off between computation time and performance of the method. Note that, when W is kept as the image size, then it would be said that similar patches are from anywhere in the image support.

LPG-PCA Method

The Local Pixel Grouping Principal Component Analysis (LPG-PCA) method [97] also adapts the local search window mechanism to search for similar pixels for a query pixel or patch. The idea is to get similar patches having same Gaussian neighborhood surrounding the current patch and thus perform the PCA operation to build basis vectors.

Let X be the matrix of n similar patches at location x in the image space and $\overline{X}$ denotes the centralized matrix of X. The co-variance matrix is calculated as $\Omega = \frac{1}{n}\overline{X}\overline{X}^T$. Using orthonormal transformation matrix P, PCA will de-correlate $\overline{X}$, i.e. $\overline{Y} = P\overline{X}$ such that covariance matrix of $\overline{Y}$ becomes diagonal. In general, the energy of a signal will concentrate on a subset of PCA transformed basis while the energy of noise will spread over the whole basis values. Hence, the noise has been suppressed by using LMMSE technique in LPG-PCA. The first stage denoised result is considered as input to the second stage and noise is again estimated. The second stage is replica of first stage of LPG-PCA. However, local search mechanism may not explore similarity for rare patches in local surroundings.

Figure 4.1 represents analogy of spatially window based NLSS denoising methods. Given a reference patch, P & R in figure, a window is considered (orange color) to search similar patches. However, one may ignore dissimilar patches also based on evaluation criteria within orange window. Then, matrices Ω_P & Ω_R are formed by arranging similar patches as one dimension vector in the columns including reference

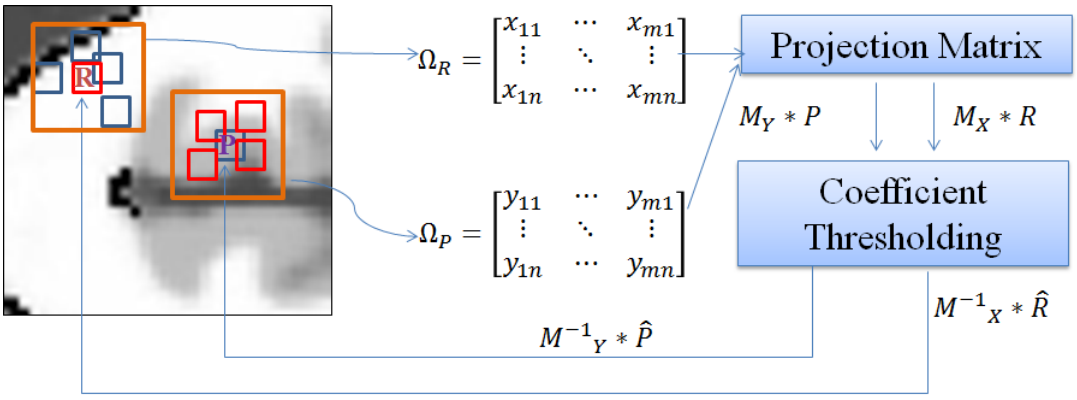

Figure 4.1: Conventional NLSS image denoising framework

patch P & R respectively. The Projection Matrix step is corresponding to transformation matrix like PCA etc. and reference patch is projected in the transformed domain. The lower coefficients below a certain threshold level in the transformed domain,, are replaced by zero, assuming to be correspond to noise [22]. These revised coefficients are reprojected to their spatial location in image space by multiplying them with inverse of projection matrix. In the image space, multiple estimation of pixel location is averaged out [22]. Figure 4.1 shows complete process for two patches and similarly repeated for all the possible patches in the image space.

Other Variants

Other than NLM and LPGPCA methods, K-SVD [98] is considered to another most influential method based on singular value decomposition (SVD). K-SVD become pioneer method to utilize dictionary based sparse denoising method in the natural image denoising and SVD further used in [99], [100]. In BM3D method [101], similarity between patches is defined based on Euclidean distance between patches. However, this method uses fixed basis matrices and restricts the similarity search in a window. This restriction led to a clustering based image denoising method. A brief representation is shown in Figure 4.2 The image patches are classified using clustering techniques such as K-Means, Mixture model and then a sparse dictionary is learned for these clusters. This laid the foundation of CSR [102], PLOW [103]. In [104], all image patches are

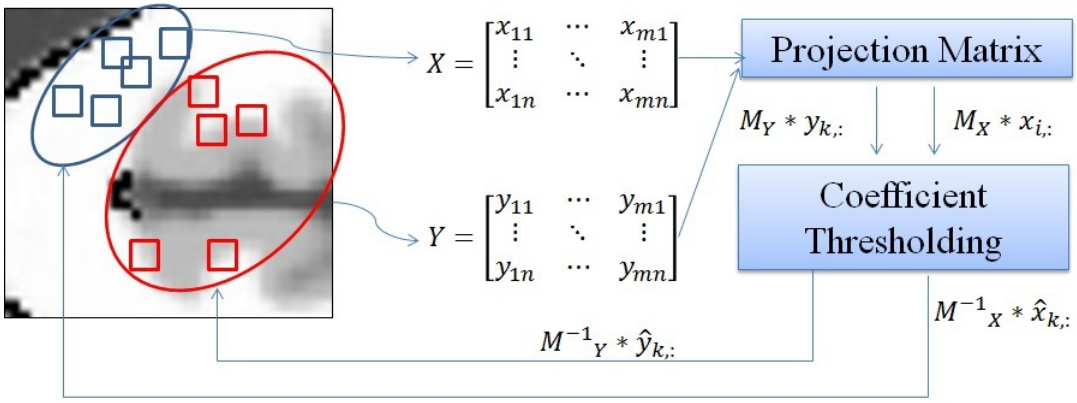

Figure 4.2: Clustering based NLSS image denoising framework

permuted by solving travelling salesman problem and then Wavelet based denoising is applied. The PCA method was first applied for denoising purpose in [105], extended in [97], [106] and for Poisson noise model in [107]. NLM methods further extended based on different similarity measures in [108], [109], [110], [111], [112]. However, there have been methods proposed in the literature based on Bayesian estimation like [113], Graph based [114] and wavelet based methods pioneered by [115] [1].

4.2 Proposed Approach

As discussed earlier, the main challenge in NLSS is to search similar patches for a patch of interest. The RST based information of REM and RCL (Chapter 2) is utilized for patch selection [2].

4.2.1 Patch selection using RST

Two patches are considered to be *similar* if their respective ϵ-neighborhoods possess the same property. Note that one can use a suitable metric to quantify this common property. Most of the research use Euclidean norm to define it. Unlike others, here

[1] Discussion on these methods are outside the scope of this thesis.

[2] This thesis assumes granules and patches to be different as per context assuming granules is small whereas patches could be bigger as of size 7×7 or more.

Rough Set Theory is used to identify similarity between patches non locally in a more principled way. Precisely, patches are clubbed together based on RCL information obtained as mentioned in Chapter 2. In Rough Set terminology, approximation spaces are defined for a set. Here, an object in the image space is referred a set. Hence, hereafter, approximation spaces are defined with respect to an object synonymous to a set. If a candidate patch is within a lower approximation of an object, then patches which constitute the lower approximation of this object are similar patches according to the definition of similarity given above. In precise, two patches within the lower approximation of an object will be similar. If a patch is in the upper approximation of an object but not in its lower approximation then the patch is in the boundary region of two distinct objects. This particular patch could also be in the upper approximation of the second object but not in its lower approximation. Any patch that is said to be similar of this patch has to have the same property.

A patch is classified in lower approximation of object C^k if all pixels have class label as k. A patch is classified to upper approximation of C^k, if any pixel has class label k. A clustering process is then define to club together similar pixels. If a patch has two class label (say p and q) then it is clubbed together with similar patch have labels p and q. All the possible combinations are been used in the clustering process. Hence, for K objects in an image, the total pools constructed would be $\sum_{i=1}^{K} \binom{K}{i}$. For example, if there are three objects in an image ($O_i, i = 1, 2, 3$) then pools/clusters constructed are: $\{\underline{O}_1, \underline{O}_2, \underline{O}_3, \{\overline{O}_1, \overline{O}_2\}, \{\overline{O}_1, \overline{O}_3\}, \{\overline{O}_2, \overline{O}_3\}, \{\overline{O}_1, \overline{O}_2, \overline{O}_3\}\}$ (where $\underline{O}_k$ and $\overline{O}_k$ represent lower and upper approximations of k^{th} object respectively and $\{\overline{O}_m, \overline{O}_n\}$ represents union of upper approximations of objects O_m and O_n).

If a candidate patch is within a lower approximation of an object, then patches which constitute the lower approximation of this object are similar according to the definition of similarity given above. If a patch is in the upper approximation of an object but not in its lower approximation then the patch is in the boundary region of two distinct objects. This particular patch could also be in the upper approximation of the second object but not in its lower approximation. Any patch that is said to be

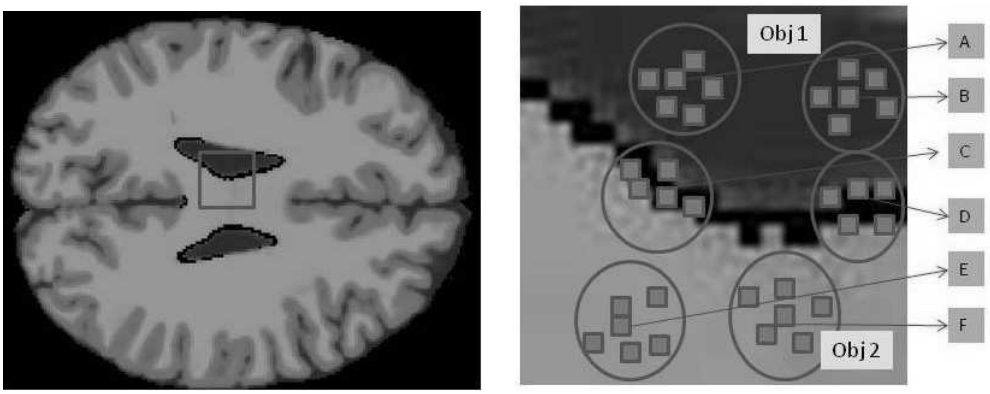

(a) (b)

Figure 4.3: A noise free T1 image is shown in (a) and zoomed part of box is shown in (b). In (b), groups of patches are shown in circle centered at patch A, B, C, D, E and F. The neighbor of patch A and B have same property and belong to same object and therefore for denoising patch A, one can use the patch B or vice versa. Similarly for patch E, one can use patch F for denoising and vice versa. The patches C and D are on boundary of two different objects as shown. For denoising them one can use patches which are falling on the boundary of two same objects. The conventional methods fail to take advantage of these kinds of similarity and Rough Set approach helps to look more in deeper to boundary patches.

similar of this patch has to have the same property. This implies that patches which are in the upper approximations but not in the lower approximations of two adjacent objects should be similar. The same concept is true for more than two adjacent objects. The concept of identifying similar patches is illustrated in Figure 4.3.

4.2.2 Algorithms

In Algorithm 1,a set of similar patches for each candidate patch in the noisy image are found and then denoising operation is performed. The proposed-1 algorithm corresponds to denoising under Non-Local Means (NLM) [93] framework whereas the Proposed-2 algorithm corresponds to PCA framework as suggested in [97].

The Algorithm 2 (Proposed 3) uses the same approach for deriving lower and upper approximation of all the objects. Unlike, finding similar patches for a candidate patch, a few pool of similar patches are constructed based on the patches either

within a object or on the boundary of two or more objects. Hence for K number of objects present in the image, the number of pool constructed would be $\sum_{i=1}^{K} \binom{K}{i}$. Here one point is important that how to know the number of objects (or class as described by RCL in Section 2). But in case of MRI, usually the number of classes (objects) is known as stated in literature. After generation of these pools, one can take PCA decomposition of each pool separately followed by Hard thresholding method as suggested in [106]. This will give a basis vector representation of each pool. Then, each patch in the noisy image, based on its class representation can be projected on to particular pool basis vector. Instead of finding similar patches for each candidate patch from noisy image, this method speeds up the process by computing basis vectors only for once. The same is depicted in Figure 4.2.

4.3 Experimental Results

This Section encompasses the qualitative and quantitative evaluation of the proposed methods along with some of the state-of-the-art methods.

4.3.1 Methods & parameters

The patch size, p, is kept square and fixed to 5×5 in all the experiments. The local search window parameter is crucial to balance between computation time and performance of the method. In fact, patch size, p, and search window size W are dependent on each other. Note that, when W is kept as the image size, then it would be said that similar patches are from anywhere in the image support. However this is an exhaustive search and would take a lot of computational time. In this study, we have consider two search windows for evaluation purpose. The NLM 1 method represents NLM method with local search window of size 25×25 around each pixel to denoise whereas NLM 2 method represents NLM method with local search window of size 101×101. The NLM1 shows impact of selecting small local search window whereas NLM 2 is more computational intensive process.

Input: Noisy Image (I_n), patch size (p)
Output: Denoised Image ($\hat{I}$), Rough Class Label (RCL)

a. Get the intensity thresholds from histogram of image I_n using parzen window method. Let there are $K-1$ thresholds.

b. Partition the image into non-overlapping 2×2 granules. Define the lower approximation and upper approximation of those K objects and obtain Rough Class Label (RCL) image.

c. Consider a patch of size $p \times p$ from noisy image, I_n, and get the corresponding class patch, C, from RCL image.

d. Find the number of classes present in C. The presence of single class indicate the homogeneous patch else it can be considered as heterogeneous patch.

e. For homogeneous patch, get the similar patches from the lower approximation of that class.

f. For heterogeneous patch, fetch the similar patches from the union of upper approximations of all the present classes in C.

g. Proposed 1: For NLM framework:

- Use all the similar patches (fetched from above mentioned method) to denoise the candidate patch as in [93] for both homogeneous and heterogeneous patches.

h. Proposed 2: For PCA framework:

- From all available similar patches, select *best* L patches among them. Apply PCA decomposition followed by wiener filtering as suggested in [97].

Algorithm 1: Proposal 1 and Proposal 2

Input: Noisy Image (I_n), patch size (p)
Output: Denoised Image ($\hat{I}$), Rough Class Label (RCL)

a. Get the intensity thresholds from histogram of image I_n using parzen window method. Let there are $K-1$ thresholds.

b. Partition the image into non-overlapping 2×2 granules. Define the lower approximation and upper approximation of those K objects and obtain Rough Class Label (RCL) image.

c. Construct the patch of size $p \times p$ around each location present in the all the approximation sets. This will create a pool of patches for an approximation set. Hence, there will be $\sum_{i=1}^{K} \binom{K}{i}$ pool of patches by considering all the possible overlapping of K objects.

d. Apply PCA decomposition of each pool individually followed by Hard thresholding method. Now, we will have the basis vectors for the pools.

e. Now, consider a patch of size $p \times p$ from noisy image, I_n and get the corresponding class patch, C from RCL image.

f. Find the classes present in the class patch, C. Accordingly, fetch the basis vector for combination present in C and project the candidate patch.

Algorithm 2: Proposal 3

In LPG-PCA method [97], the patch size p and local search window W need to be fixed. This method requires to select few best similar patches to compute PCA basis within the window size $W \times W$. Here, we have used $p = 5$ and $W = 41$ in all the experiments. The large number of patches may not be suitable for the basis computation in PCA. During experiments, by default it is fixed to 200. The LPG-PCA may not reveal similar patches for rare patches present at different places in the image and is restricted to get those many patches from local window area.

The proposed strategy for selecting similar patches from the image space removes the constraint of local search window W parameter from both state-of-the-art methods. The strategy has an intelligent way to get patches from the whole image. Hence, it is also adaptive in terms of number of patches used for each pixel for denoising current pixel or patch.

In another proposal under PCA framework, the formation of pool is remained same. Here, number of such pool will be $\sum_{i=1}^{K} \binom{K}{i}$ and $K = 4$ is used in all experiments (Hence, there will be 15 pools and these many PCA basis needs to be computed). Instead of selecting few best patches for a given candidate patch as in previous proposal, here whole pool is assumed to be similar and hence an equivalence relation. So, PCA is computed on each pool respectively. Then hard thresholding step is performed for coefficient shrinkage instead of wiener filtering. A comparison of hard thresholding and soft thresholding is presented in [106]. This proposal is also a non-iterative method in comparison to LPG-PCA method and found to have comparable performance. Note that PCA method inherently assume Gaussian distribution for noise in the data [116]. Hence, straight forward extension of all PCA methods under Rician noise assumption is not possible.

4.3.2 Phantom Database

The experiments have been carried out on 2D monochrome phantom human brain MRI images obtained from Brain Web Database [1]. The parameters are as follows:

RF = 20, protocol = ICBM, slice thickness = 1mm, volume size = $181 \times 217 \times 181$. The experimental set up considers two different noise model (Gaussian and Rician) at different noise levels along with two modalities, namely T1 and T2. Two slices are considered from both the modalities, namely slice 70 and 100 and adjusted to size 140×176 by truncating excessive background portions.

The quantitative evaluations of all the methods under Gaussian noise assumption is shown in Tables 4.1 and 4.2 for T1 and T2 image slices respectively. The proposed-1 and proposed-2 found to be comparable to their corresponding contemporary methods. At lower noise levels, proposed-3 could not perform up to desired level due to having large number of patches in the basis computation whereas at higher noise level it performance is quite encouraging. The proposed-3 is better in terms of all the measures in T2 images. The Figure 4.4 and 4.6 show noisy image and denoised results of slice 100 in T1 and T2 modality respectively. The zoomed part of these are shown in Figure 4.5 and 4.7 respectively for visual comparison. Similarly, Table 4.3 and 4.4 covers quantitative evaluation under Rician noise assumption for T1 and T2 images respectively.

4.3.3 Real database

All three proposed methods are also tested for real MRI data. In the real datasets, the noise model was assumed to be Rician in nature [11]. The problem in the real databases is the estimation of noise level present in terms of standard deviation or percentage level of maximum intensity. Numerous approaches have been proposed in the literature [15], [2], [13], [14]. A recently proposed approach [2] for estimation of Rician noise level in real MR image has been adopted in this work. The iterative method transforms heteroskedastic Rician noisy image into homoskedastic data via variance stabilization technique where additive white Gaussian noise (AWGN) estimation can be applied. The most common estimation of AWGN is Median Absolute Deviation or Mean Absolute Deviation (MAD) has been applied. Here, only

Table 4.1: Performance comparison of proposed denoising strategy with **NLM** and **LPG-PCA** approaches on various quantitative measures under *Gaussian Noise assumption* in BrainWeb database (**slice=70 & 100**, Modality = T1 and patch size $= 5 \times 5$). The bold figures represent best figure for each noise level for all measures.

Noise		Slice 70				Slice 100			
SD	Methods	PSNR	RMSE	MSSIM	FSIM	PSNR	RMSE	MSSIM	FSIM
3	Noisy	39.0033	8.1800	0.9472	0.9752	39.1824	7.8495	0.9345	0.9730
	NLM 1	38.4878	9.2110	0.9731	0.9902	40.0507	6.4270	0.9705	0.9918
	NLM 2	39.6999	6.9678	0.9753	0.9913	41.1318	5.0107	0.9724	0.9929
	Proposed 1	40.2146	6.1890	0.9761	0.9918	41.2662	4.8580	0.9730	0.9933
	LPGPCA	42.6899	3.5002	0.9792	0.9924	43.1492	3.1489	0.9757	0.9926
		42.8983	3.3362	**0.9807**	0.9930	43.4324	2.9501	**0.9781**	0.9934
	Proposed 2	**43.2144**	**3.1020**	0.9804	**0.9931**	**43.6717**	**2.7920**	0.9758	**0.9935**
	Proposed 3	41.4458	4.6613	0.9742	0.9820	40.9759	5.1939	0.9654	0.9789
5	Noisy	34.5663	22.7227	0.8776	0.9409	34.7454	21.8041	0.8541	0.9358
	NLM 1	37.2108	12.3595	0.9505	0.9842	38.4707	9.2472	0.9415	0.9867
	NLM 2	37.2210	10.9868	0.9516	0.9842	39.1392	7.9279	0.9434	0.9883
	Proposed 1	38.0013	10.3028	0.9520	0.9845	39.1804	7.8530	0.9438	0.9885
	LPGPCA	39.0903	8.0177	0.9554	0.9837	39.4677	7.3504	0.9459	0.9840
		39.2712	7.6906	**0.9585**	**0.9850**	39.7782	6.8432	**0.9516**	**0.9861**
	Proposed 2	**39.5599**	**7.1959**	0.9565	0.9845	**39.9363**	**6.5985**	0.9450	0.9848
	Proposed 3	38.0680	10.1456	0.9490	0.9632	37.3722	11.9085	0.9309	0.9552
7	Noisy	31.6438	44.5353	0.8028	0.9025	31.8229	42.7360	0.7735	0.8947
	NLM 1	35.9154	16.6547	0.9272	0.9770	37.0060	12.9561	0.9136	0.9811
	NLM 2	36.0394	16.1862	0.9276	0.9764	37.4026	11.8255	0.9157	0.9831
	Proposed 1	36.1936	15.6213	0.9276	0.9767	37.3974	11.8396	0.9157	0.9832
	LPGPCA	36.7490	13.7462	0.9307	0.9738	37.0637	12.7853	0.9150	0.9740
		36.8869	13.3166	**0.9358**	**0.9760**	37.3657	11.9264	**0.9246**	**0.9778**
	Proposed 2	**37.0354**	**12.8689**	0.9292	0.9734	**37.3969**	**11.8410**	0.9111	0.9735
	Proposed 3	35.6652	17.6426	0.9163	0.9394	35.0947	20.1190	0.8955	0.9311
10	Noisy	28.5457	90.8884	0.6971	0.8458	28.7248	87.2163	0.6679	0.8352
	NLM 1	34.0846	25.3877	0.8949	0.9647	34.9940	20.5910	0.8782	0.9705
	NLM 2	34.0291	25.7140	0.8956	0.9645	35.1379	19.9200	0.8806	0.9728
	Proposed 1	34.0798	25.4153	0.8957	0.9647	35.0181	20.4771	0.8803	0.9723
	LPGPCA	34.3078	24.1158	0.8954	0.9572	34.5764	22.6695	0.8724	0.9573
		34.4206	**23.4976**	**0.9046**	**0.9616**	**34.8828**	**21.1251**	**0.8898**	**0.9647**
	Proposed 2	34.3245	24.0232	0.8866	0.9535	34.6667	22.2029	0.8614	0.9525
	Proposed 3	33.7537	27.3977	0.8900	0.9205	33.2131	31.0295	0.8629	0.9081
15	Noisy	25.0248	204.4551	0.5524	0.7635	25.2036	196.2080	0.5323	0.7504
	NLM 1	31.4873	46.1692	0.8441	0.9383	32.0768	40.3088	0.8270	0.9455
	NLM 2	31.2278	49.0116	0.8461	0.9377	31.8915	42.0656	0.8298	0.9450
	Proposed 1	31.1918	49.4195	0.8459	0.9355	31.6760	44.2056	0.8282	0.9408
	LPGPCA	31.5384	45.6290	0.8391	0.9270	31.7780	43.1797	0.8106	0.9263
		31.6666	44.3021	0.8600	**0.9369**	**32.1150**	**39.9556**	**0.8450**	**0.9421**
	Proposed 2	31.1903	49.4368	0.8116	0.9143	31.5172	45.8527	0.7837	0.9116
	Proposed 3	**31.7306**	**43.6535**	**0.8678**	0.9142	31.1681	49.6906	0.8183	0.8820

Table 4.2: Performance comparison of proposed denoising filter with **NLM** and **LPG-PCA** approaches on various quantitative measures under *Gaussian Noise assumption* in Brain Web database (**slice=70 & 100**, Modality = T2 and patch size = 5×5). The bold figures represent best figure for each noise level for all measures.

Noise		Slice 70				Slice 100			
SD	Methods	PSNR	RMSE	MSSIM	FSIM	PSNR	RMSE	MSSIM	FSIM
3	Noisy	39.0062	8.1745	0.9490	0.9793	39.1840	7.8466	0.9372	0.9769
	NLM 1	34.0656	25.4989	0.9724	0.9873	34.9016	21.0340	0.9698	0.9889
	NLM 2	35.3489	18.9754	0.9745	0.9886	36.0625	16.1002	0.9270	0.9911
	Proposed 1	36.2715	15.3436	0.9757	0.9892	36.4523	14.7179	0.9730	0.9918
	LPGPCA	42.3015	3.8276	0.9816	0.9932	42.8303	3.3888	0.9784	0.9937
		42.4723	3.6801	**0.9830**	**0.9937**	**43.0882**	**3.1935**	**0.9809**	**0.9944**
	Proposed 2	**42.6202**	**3.5568**	0.9823	0.9936	43.0856	3.1953	0.9779	0.9940
	Proposed 3	40.7245	5.5033	0.9734	0.9840	40.6771	5.5638	0.9691	0.9834
7	Noisy	31.6750	44.2159	0.8124	0.9199	31.8474	42.4950	0.7852	0.9102
	NLM 1	32.6468	35.3506	0.9296	0.9744	33.3213	30.2658	0.9175	0.9786
	NLM 2	33.4319	29.5045	0.9312	0.9754	34.2722	24.3143	0.9206	0.9814
	Proposed 1	34.1362.	25.0877	0.9325	0.9762	34.6377	22.3518	0.9218	0.9819
	LPGPCA	36.0440	16.1691	0.9378	0.9763	36.4815	14.6194	0.9238	0.9773
		36.1306	15.8496	**0.9428**	**0.9784**	36.7300	13.8064	**0.9340**	**0.9807**
	Proposed 2	**36.3703**	**14.9987**	0.9337	0.9759	**36.7415**	**13.7697**	0.9172	0.9760
	Proposed 3	35.8224	17.0153	0.9527	0.9639	34.5427	22.8460	0.8995	0.9398
10	Noisy	28.5974	89.8134	0.7166	0.8746	28.7699	86.4757	0.6893	0.8600
	NLM 1	31.4787	46.2607	0.8992	0.9628	31.1529	39.6084	0.8845	0.9676
	NLM 2	32.0328	40.7189	0.9011	0.9646	32.8020	34.1101	0.8878	0.9700
	Proposed 1	32.5938	35.7845	0.9031	0.9657	33.0595	32.1464	0.8883	0.9706
	LPGPCA	33.3753	29.8916	0.9042	0.9615	33.8047	27.0778	0.8852	0.9627
		33.4093	29.6586	0.9141	**0.9654**	**34.0192**	**25.7730**	0.9036	**0.9696**
	Proposed 2	**33.5845**	**28.4861**	0.8909	0.9586	33.9640	26.1026	0.8693	0.9580
	Proposed 3	33.4118	29.6414	**0.9265**	0.9463	33.7583	27.3682	**0.9369**	0.9509
15	Noisy	25.0997	200.9597	0.5917	0.8094	25.2559	193.8616	0.5722	0.7896
	NLM 1	29.6076	71.1740	0.8494	0.9398	30.1840	62.3271	0.8371	0.9453
	NLM 2	29.7120	69.4833	0.8499	0.9405	30.4111	59.1526	0.8395	0.9466
	Proposed 1	29.9421	65.8976	0.8518	0.9418	30.5809	56.8844	0.8398	0.9478
	LPGPCA	30.3258	60.3261	0.8488	0.9355	30.7441	54.7858	0.8276	0.9356
		30.3370	60.1702	0.8731	**0.9444**	30.9306	52.4832	0.8650	**0.9508**
	Proposed 2	30.3740	59.6811	0.8174	0.9273	30.7362	54.8854	0.7949	0.9240
	Proposed 3	**30.6543**	**55.9308**	**0.8848**	0.9228	**31.0021**	**51.6257**	**0.9042**	0.9276
20	Noisy	22.6240	355.3679	0.5015	0.7565	22.7724	343.4283	0.4899	0.7338
	NLM 1	27.8462	104.9507	0.8006	0.9162	28.5052	91.7404	0.7938	0.9225
	NLM 2	27.6370	112.2367	0.7982	0.9139	28.4627	92.6419	0.7949	0.9232
	Proposed 1	27.6093	112.6486	0.7987	0.9140	28.5006	91.8375	0.7943	0.9235
	LPGPCA	28.1483	99.3691	0.7925	0.9101	28.5555	90.6843	0.7736	0.9071
		28.2037	98.3366	0.8383	**0.9249**	28.7354	87.0052	0.8345	**0.9318**
	Proposed 2	28.0775	101.2349	0.7466	0.8965	28.4334	93.2697	0.7278	0.8895
	Proposed 3	**28.5616**	**90.5563**	**0.8436**	0.8994	**28.8346**	**85.0403**	**0.8596**	0.9008
25	Noisy	20.7071	552.5522	0.4342	0.7120	20.8551	534.0331	0.4285	0.6880
	NLM 1	26.5430	144.1393	0.7553	0.8949	27.0817	137.3239	0.7524	0.9002
	NLM 2	25.8927	167.4194	0.7495	0.8874	26.6663	140.1048	0.7506	0.8972
	Proposed 1	25.5882	179.5794	0.7476	0.8834	26.3774	149.7409	0.7467	0.8915
	LPGPCA	26.4655	146.7378	0.7364	0.8857	26.8252	135.0712	0.7212	0.8787
		26.5483	143.9617	**0.8068**	**0.9059**	27.0183	129.1955	0.8069	**0.9128**
	Proposed 2	26.2834	153.0173	0.6799	0.8665	26.6040	142.1273	0.6648	0.8554
	Proposed 3	**27.0504**	**128.2455**	0.8005	0.8800	**27.1099**	**126.4993**	**0.8119**	0.8747

Table 4.3: Performance comparison of proposed denoising filter with **NLM** approach on various quantitative measures under *Rician Noise assumption* in Brain Web database (**slice=70 & 100**, Modality = T1 and patch size = 5×5). The bold figures represent best figure for each noise level for all measures.

Noise		Slice 70				Slice 100			
SD	Methods	PSNR	RMSE	MSSIM	FSIM	PSNR	RMSE	MSSIM	FSIM
3	Noisy	37.8322	10.7118	0.9068	0.9730	37.5516	11.4267	0.8713	0.9701
	NLM 1	38.4189	9.3581	0.9853	0.9899	40.1874	6.2279	0.9906	0.9918
	NLM 2	39.6518	7.0453	0.9872	0.9912	41.4113	4.6984	0.9923	0.9929
	Proposed 1	**40.2500**	**6.1387**	**0.9880**	**0.9917**	**41.7100**	**4.3862**	**0.9930**	**0.9934**
5	Noisy	33.3959	29.7505	0.8384	0.9358	33.1147	31.7401	0.7937	0.9290
	NLM 1	37.3165	12.0623	0.9772	0.9840	38.7274	8.7165	0.9851	0.9871
	NLM 2	37.7701	10.8660	0.9778	0.9843	39.5639	7.1893	0.9868	0.9887
	Proposed 1	**38.1135**	**10.0400**	**0.9783**	**0.9846**	**39.6512**	**7.0463**	**0.9871**	**0.9889**
7	Noisy	30.4746	58.2935	0.7705	0.8943	30.1928	62.2019	0.7248	0.8839
	NLM 1	36.1236	15.8754	0.9672	0.9772	37.3746	11.9020	0.9780	0.9817
	NLM 2	36.1493	15.7817	0.9668	0.9766	37.9375	10.4552	0.9798	0.9837
	Proposed 1	**36.2880**	**15.2855**	**0.9668**	**0.9769**	**37.8837**	**10.5855**	**0.9797**	**0.9838**
10	Noisy	27.3799	118.8753	0.6734	0.8336	27.0967	126.8861	0.6332	0.8193
	NLM 1	34.3661	23.7943	0.9489	0.9651	35.5171	18.2546	0.9644	0.9717
	NLM 2	**34.2259**	**24.5747**	**0.9489**	**0.9648**	**35.6979**	**17.5103**	**0.9664**	**0.9732**
	Proposed 1	34.2188	24.6152	0.9487	0.9647	35.4986	18.3323	0.9657	0.9724
15	Noisy	23.8689	266.8053	0.5358	0.7467	23.5821	285.0160	0.5089	0.7285
	NLM 1	**31.7086**	**43.8749**	**0.9088**	**0.9380**	**32.6333**	**35.4610**	**0.9316**	**0.9477**
	NLM 2	31.3893	47.2223	0.9103	0.9367	32.1920	39.2538	0.9317	0.9435
	Proposed 1	31.1989	49.3388	0.9082	0.9297	31.5710	45.2879	0.9272	0.9344

Table 4.4: Performance comparison of proposed denoising filter with **NLM** approach on various quantitative measures under *Rician Noise assumption* in Brain Web database (**slice=70 & 100**, Modality = T2 and patch size = 5×5). The bold figures represent best figure for each noise level for all measures.

Noise		Slice 70				Slice 100			
SD	Methods	PSNR	RMSE	MSSIM	FSIM	PSNR	RMSE	MSSIM	FSIM
3	Noisy	37.8331	10.7096	0.9123	0.9773	37.5530	11.4230	0.8787	0.9741
	NLM 1	34.0044	25.8607	0.9834	0.9871	34.8524	21.2736	0.9983	0.9886
	NLM 2	35.3224	19.0916	0.9854	0.9884	36.0799	16.0358	0.9905	0.9909
	Proposed 1	**36.2392**	**15.4581**	**0.9867**	**0.9891**	**36.5527**	**14.3817**	**0.9914**	**0.9917**
7	Noisy	30.4961	58.0055	0.7834	0.9129	30.2117	61.9311	0.7412	0.9005
	NLM 1	32.6043	35.6982	0.9652	0.9738	33.4493	29.3867	0.9770	0.9785
	NLM 2	33.4922	29.0980	0.9669	0.9750	34.5264	22.9317	0.9801	0.9816
	Proposed 1	**34.2211**	**24.6019**	**0.9683**	**0.9757**	**34.9021**	**21.0313**	**0.9808**	**0.9820**
10	Noisy	27.4166	117.8750	0.6959	0.8644	27.1262	126.6260	0.6592	0.8462
	NLM 1	31.4948	46.0890	0.9476	0.9622	32.3291	38.0341	0.9643	0.9681
	NLM 2	32.0600	40.4654	0.9494	0.9641	33.0714	32.0585	0.9679	0.9711
	Proposed 1	**32.6502**	**35.3234**	**0.9517**	**0.9656**	**33.3904**	**29.7880**	**0.9685**	**0.9717**
15	Noisy	23.9223	263.5408	0.5782	0.7965	23.6261	282.1416	0.5540	0.7742
	NLM 1	29.6345	70.7341	0.9095	0.9401	30.4214	59.0123	0.9355	0.9485
	NLM 2	29.6681	70.1899	0.9099	0.9413	30.5742	56.9715	0.9380	0.9500
	Proposed 1	**29.8437**	**67.4079**	**0.9115**	**0.9422**	**30.7240**	**55.0406**	**0.9382**	**0.9508**
20	Noisy	21.4563	464.9964	0.4908	0.7428	21.1562	498.2680	0.4763	0.7151
	NLM 1	**27.8369**	**107.0012**	**0.8655**	**0.9178**	**28.6805**	**88.1106**	**0.9005**	**0.9285**
	NLM 2	27.4349	117.3792	0.8618	0.9131	28.3237	95.6555	0.9002	0.9260
	Proposed 1	27.2309	123.0242	0.8607	0.9100	28.2561	97.1561	0.8980	0.9226
25	Noisy	19.5567	720.1252	0.4248	0.6987	19.2571	771.5618	0.4168	0.6696
	NLM 1	**26.2158**	**155.4194**	**0.8216**	**0.8963**	**27.0615**	**127.9178**	**0.8627**	**0.9073**
	NLM 2	25.2324	194.9111	0.7986	0.8672	25.9354	165.7835	0.8456	0.8806
	Proposed 1	24.6450	223.1435	0.7849	0.8522	25.2038	196.2009	0.8157	0.8558

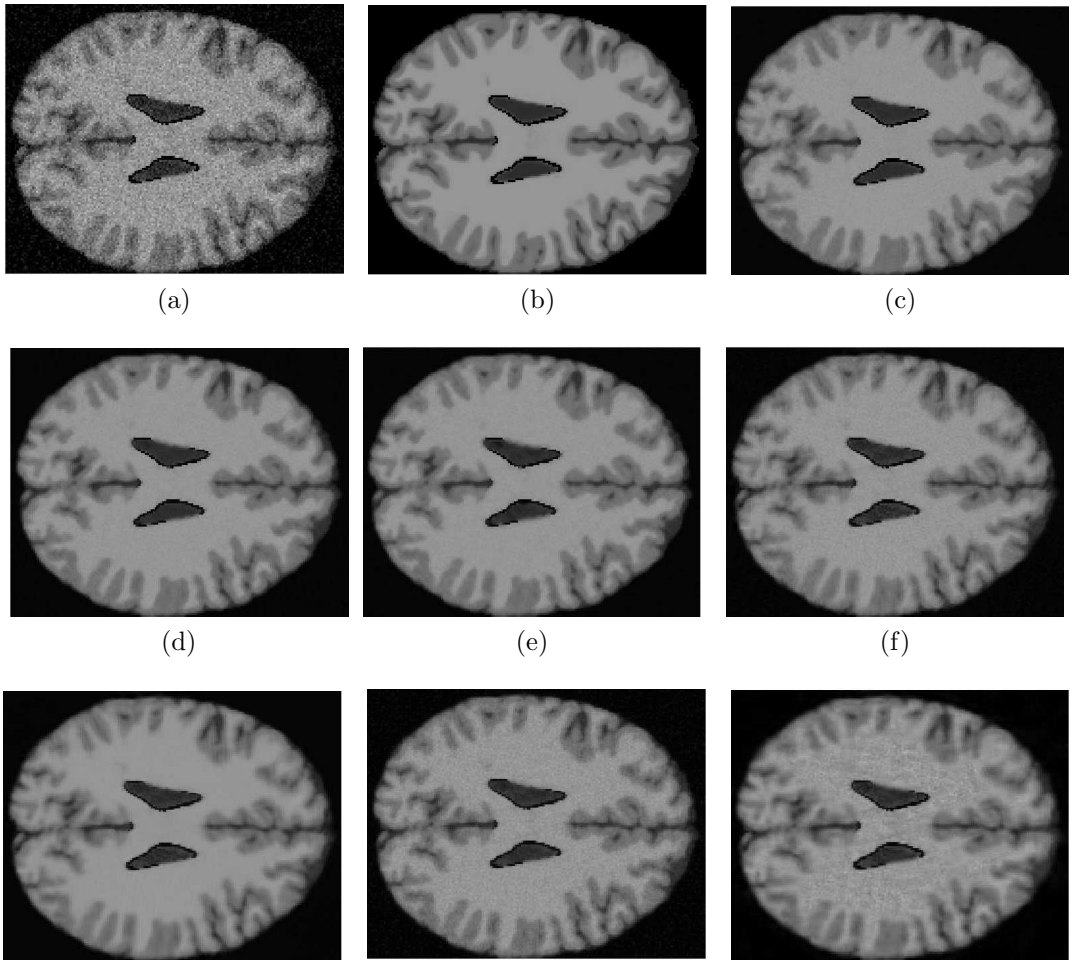

Figure 4.4: T1 Image (a) Noisy image with Gaussian noise sd=15 (b) Original Image (c) NLM1 method (d) NLM2 method (e) Proposed1 method (f) LPGPCA phase 1 method (g) LPGPCA phase 2 method (h) Proposed2 method (i) Porposed3 method

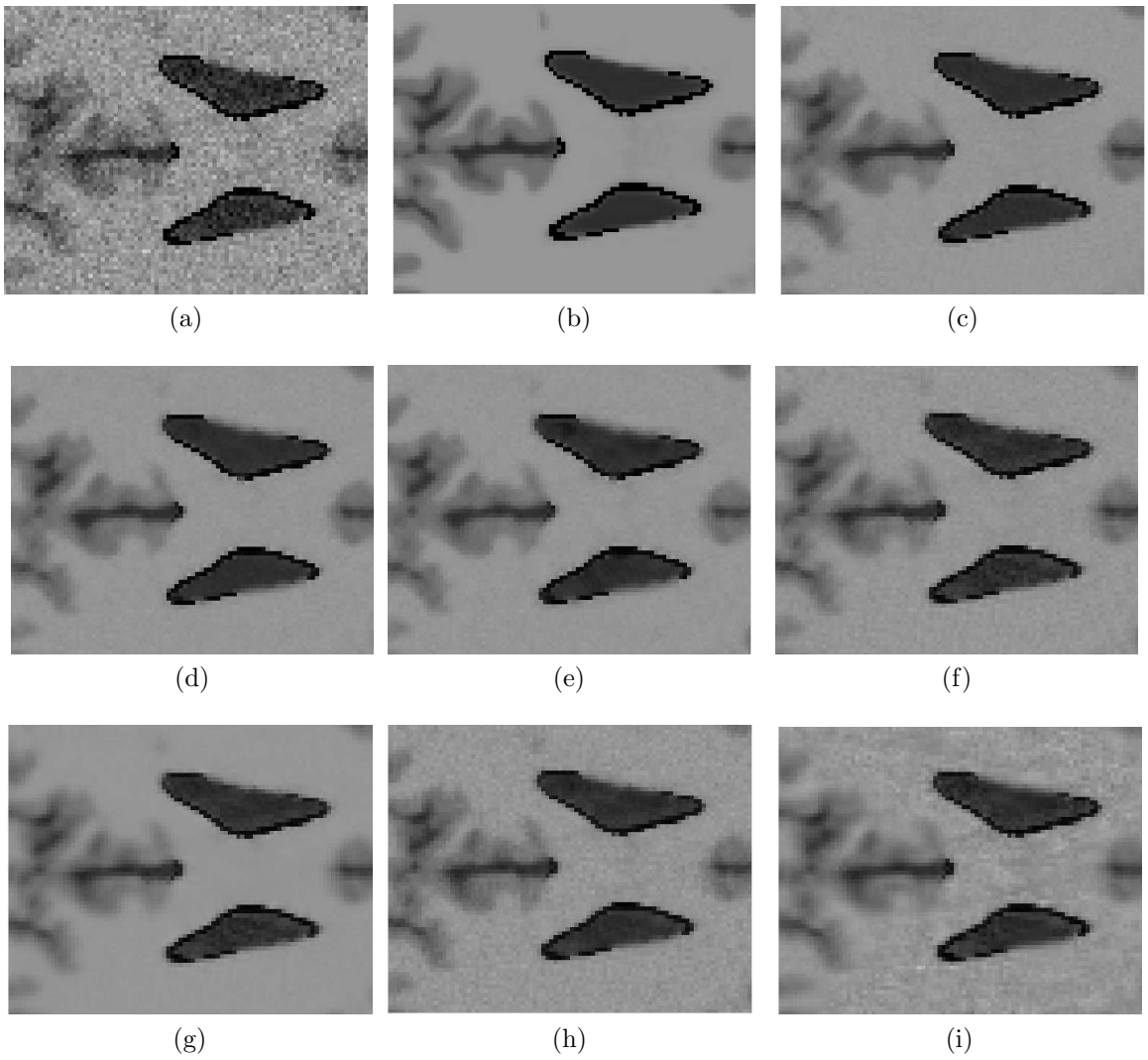

(a) (b) (c)

(d) (e) (f)

(g) (h) (i)

Figure 4.5: Zoomed part of images from Figure 4.4 respectively.

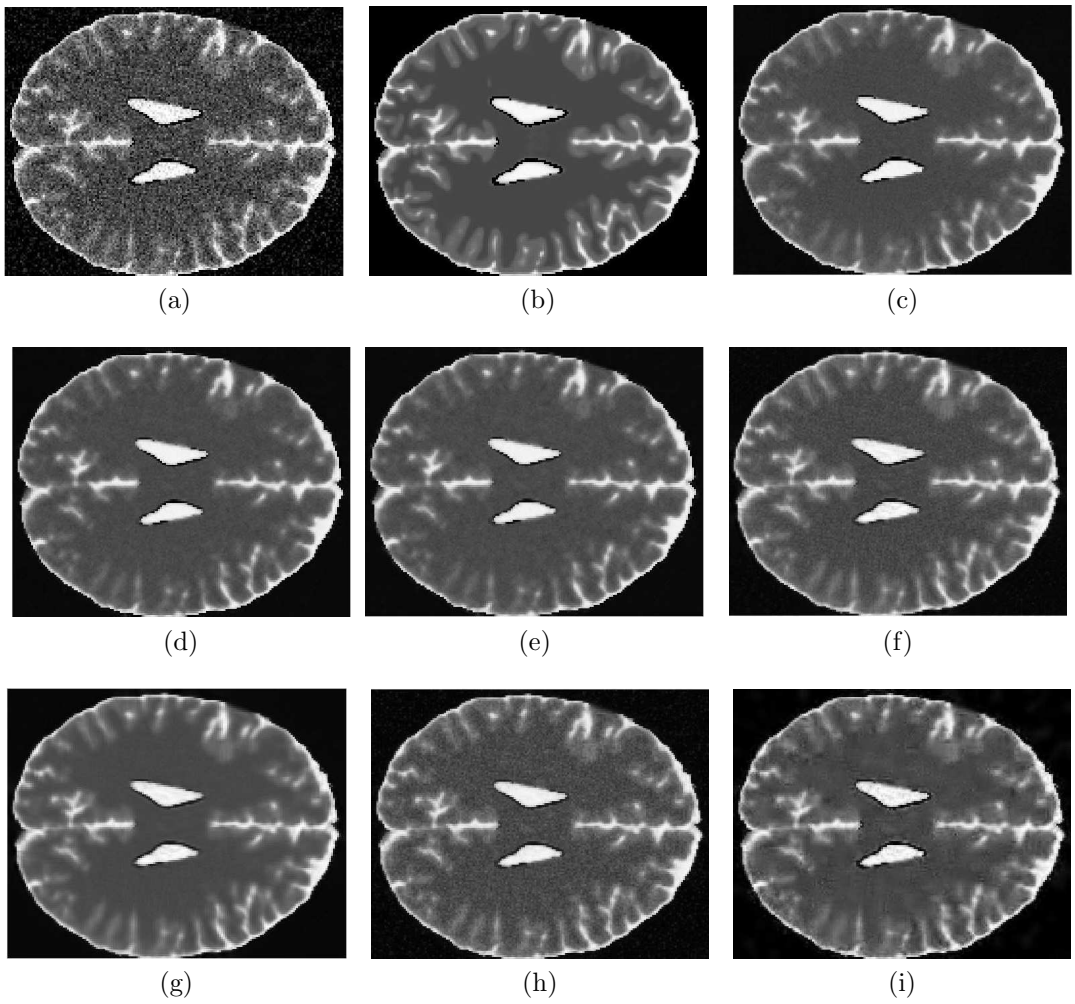

Figure 4.6: T2 Image (a) Noisy image with Gaussian noise sd=25 (b) Original Image (c) NLM1 method (d) NLM2 method (e) Proposed1 method (f) LPGPCA phase 1 method (g) LPGPCA phase 2 method (h) Proposed2 method (i) Porposed3 method

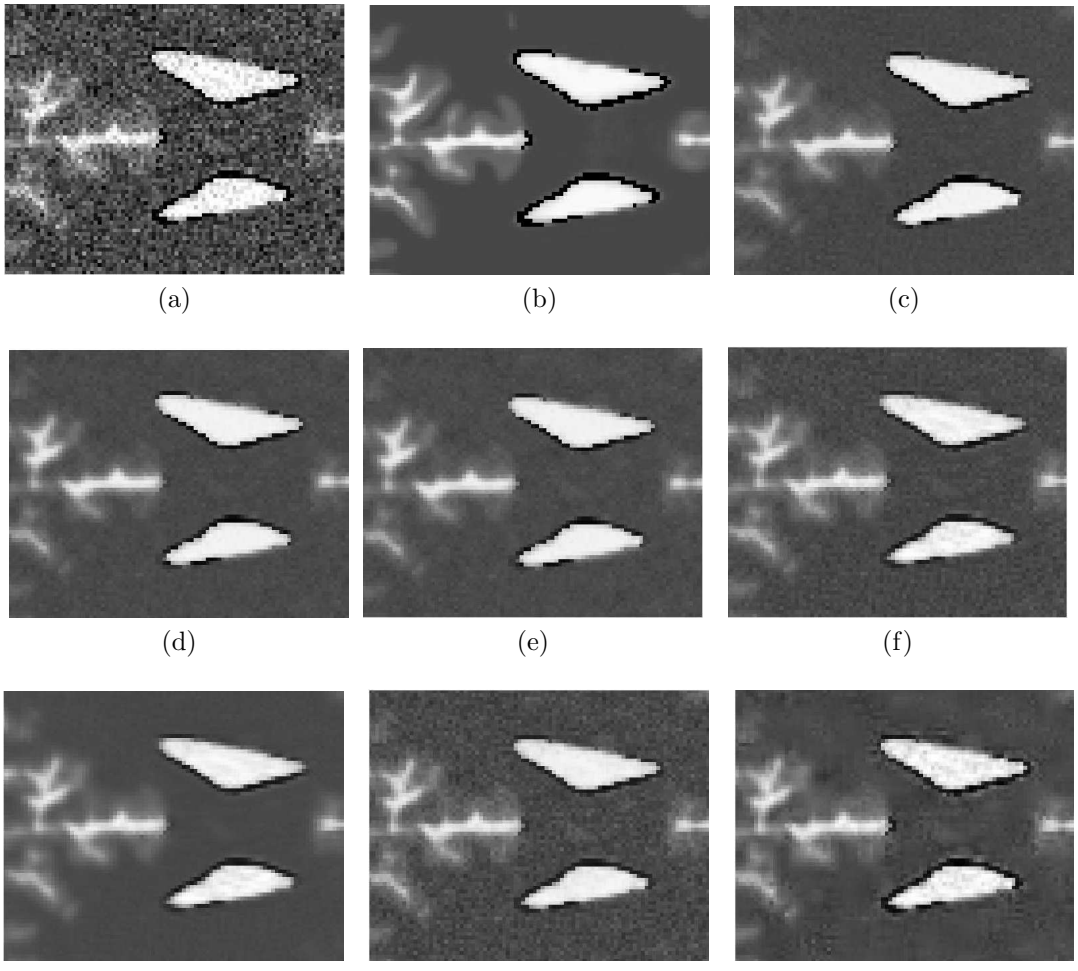

(a) (b) (c)

(d) (e) (f)

(g) (h) (i)

Figure 4.7: Zoomed part of images from Figure 4.6 respectively.

Non-local Means denoising methods have been applied since direct implementation of PCA method under Rician noise data is not possible.

In this work, experiments have been performed on real MR images from two publically available real MR image databases. The first one is extracted from OASIS database [7] which does not have any pathological disorder. The subject details of selected data from OASIS dataset are as follows: Subject ID:0018, Age: 39 (male), scan number: mpr-1, type: MPRAGE, voxel resolution:$1.0mm \times 1.0mm \times 1.25mm$, Orientation: Sagital, TR (ms)= 9.7, TE (ms)= 4.0, TI(ms)= 20.0, Flip angle= 10, slice number used = 100. The noise standard deviation estimated for the image is 4.66. The results are shown in Figure 4.8 along with their zoomed in portion for more clarity. Note that experiments have been conducted for a large number of slices, however the result of only two slices are presented here.

Another dataset is selected from Multimodal Brain Tumor Segmentation Challenge (BRATS) [8] data where actual challenge was to identify tumor region and other pathological disorder. The details of the subjects are as follows: Subject ID: 0015, having high grade gliomas, slice= 100. The standard deviation of the image estimated is 2.55. The results are shown in Figure 4.9.

4.4 Conclusion

A rigorous framework for patch based medical image denoising problem using Rough Set Theory has been presented. There is a twofold implication of this work. Under the noisy environment, imprecise information has been used to denoise the image and another is the joint framework for image segmentation and denoising problem. The contribution of this work is providing a fundamental way to explore similar patches adapting to object boundary information. The proposed strategy of patch selection is more informative in comparison to other methods which also use clustering approach for patch selection (Refer to Figure 4.3). Instead of hard clustering approach, the proposal also considers the adjacent boundary information between objects for getting the similar patches. All proposed algorithms are tested for various phantom and real

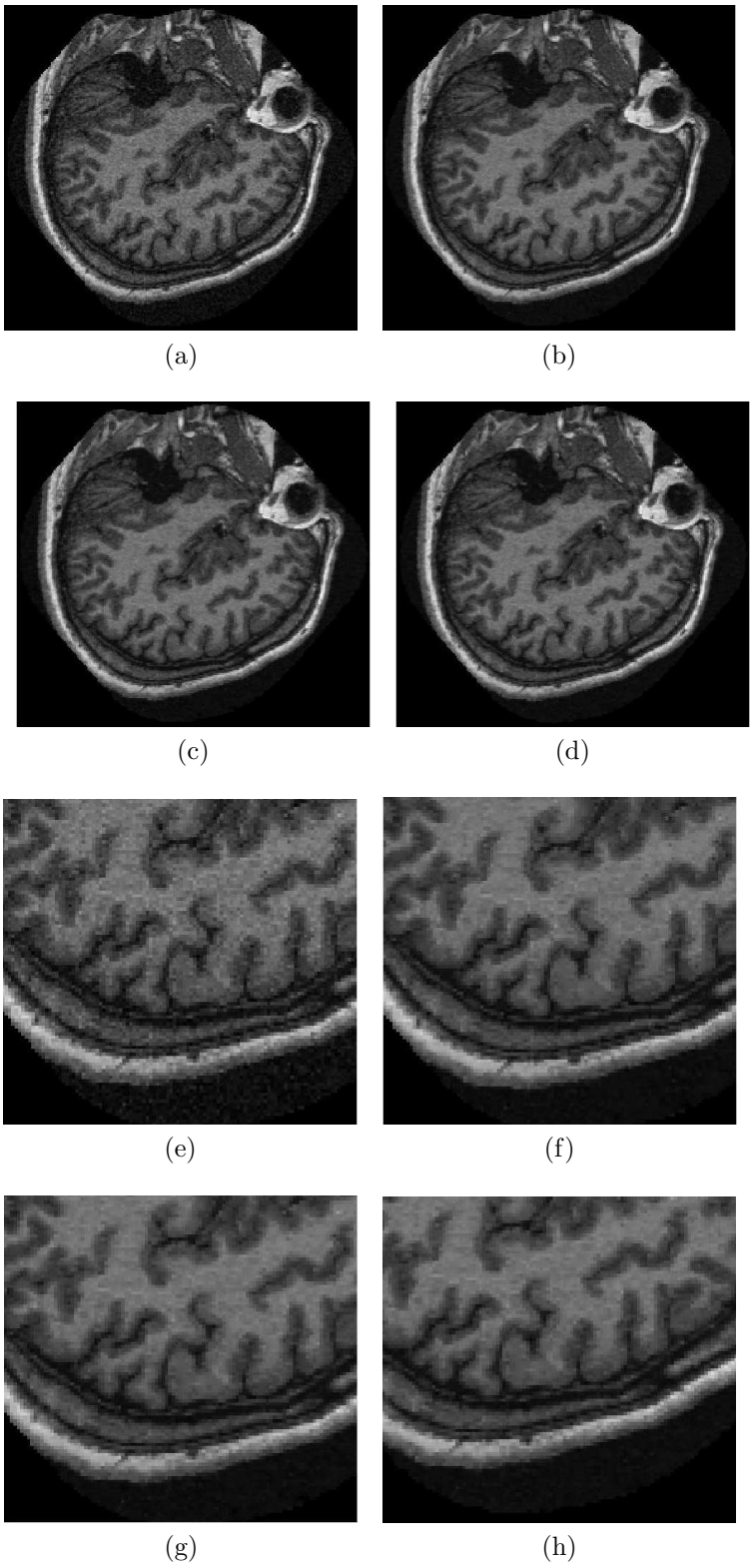

Figure 4.8: (a) Noisy image with noise sd=4.66 estimated by [2], (b) NLM 1 method, (c) NLM 2 method (d) Proposed 1 method (e)-(h) zoomed parts of images (a)-(d) respectively.

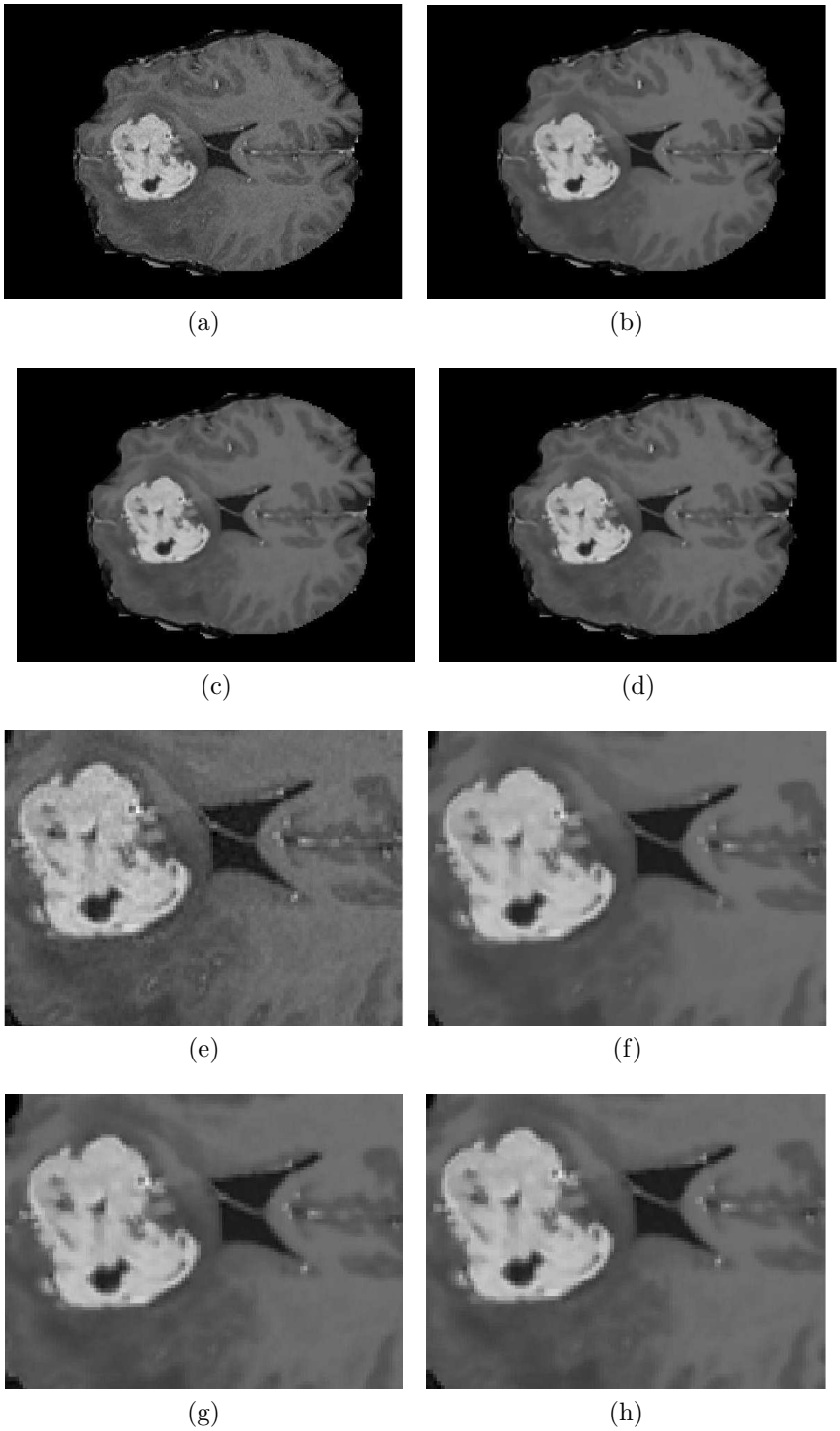

Figure 4.9: (a) Noisy image with noise sd=2.55 estimated by [2], (b) NLM 1 method, (c) NLM 2 method (d) Proposed 1 method (e)-(h) zoomed parts of images (a)-(d) respectively.

MR images. The results are very encouraging and comparable to some of the state-of-the-art methods.

The problem in the predecessor frameworks of denoising is time complexity if one explores whole image space for each patch in the image. It surely cannot be applied as an online process; however the joint framework of denoising and segmentation could be an added advantage. To speed up the process, the Proposal 3 is proposed to scarifies the accuracy a little. Here the numbers of PCA operations to be performed are very less as compared to LPG-PCA method. The proposal 3 tries to model object details in PCA basis whereas LPG-PCA models local structure of image in basis vectors. However, Gaussian assumption in data restricts application PCA methods to Rician noisy data. The next chapter studies impact of PCA method and its kernel variant on Rician noisy data.

Chapter 5

Rician Noise Removal using KPCA

As mentioned earlier that, noise most naturally acquired in MR images is Rician in nature. So, it requires a different treatment. In this chapter, we first discuss, briefly, the nature of Rician noise and then propose a mechanism based on Kernel Principal Component Analysis (KPCA) that can remove Rician noise in a better way.

It has been shown that the intensities of MR images represent magnitude of underlying complex data which follows Rice distribution [2]. The real and imaginary parts are modeled as independently distributed Gaussian with means a_r and a_i respectively, and with same variance σ^2. The pdf of Rician random variable y can be defined as follows:

$$f_Y(y|a,\sigma) = \frac{y}{\sigma^2} e^{\left(-\frac{y^2+a^2}{2\sigma^2}\right)} I_0\left(\frac{ya}{\sigma^2}\right), y > 0 \tag{5.1}$$

where $a = \sqrt{a_r^2 + a_i^2}$ is underlying noise free signal amplitude and $I_n(z)$ is n^{th} order modified bessel function of first kind. Asymptotic approximation of modified bessel function of first kind, $I_0(x)$, is given by

$$I_0(x) = \frac{e^x}{\sqrt{2\pi x}}\left[1 + \frac{1}{8x}\left(1 + \frac{9}{2(8x)}\left(1 + \ldots\right)\right)\right] \tag{5.2}$$

Let SNR be the signal to noise ratio (here, it is a/σ). When SNR is high, the

Rician distribution approaches Gaussian with mean $\sqrt{a^2+\sigma^2}$ and variance σ^2; when SNR approaches zero (that is only noise is present, $a \to 0$) [11]. In this case, Rician distribution becomes Rayleigh distribution and the pdf becomes

$$f_Y(y|a \to 0, \sigma) = \frac{y}{\sigma^2} e^{\left(-\frac{y^2}{2\sigma^2}\right)} \tag{5.3}$$

Hence, the conventional methods for Rician noise removal first try to find the background portion in the Medical images where no signal is assumed. Hence, one can use Rayleigh distribution on background portion and Gaussian distribution in the rest (where SNR is assumed to be high enough) [19], [117]. However under the noisy condition, it is difficult to find proper background in the image.

The recent methods use the principle of non-local similarity (as proposed in [93]) for image restoration task, where the first step involves finding out the similar patches (in terms of some predefined criteria such as Euclidean distance) that are similar to a given reference patch from the image. Thereafter, orthonormal basis is inferred for each patch and shrinkage is performed on the coefficients obtained when the patch is projected based on that basis. Hence coefficients are sparse in nature as described in [118], [101], [100].

Out of recently proposed techniques, BM3D [101] seems to be most popular. The BM3D technique creates a 3D stack of similar patches, projects it onto a 3D basis (tensor product of 2D-DCT and 1D-Haar), and performs hard thresholding of these coefficients followed by basis inversion, thereby allowing for a coupled update of the coefficients [101]. Another class of methods such as [102], first try to cluster similar patches and then learns basis for each cluster instead of searching the similar patches for each underlying reference patch. However, due to nature of noise, straight forward implication of natural image denoising methods has not been advocated for medical images. The NLM method has been extended for Medical Image denoising problem in [20] where bias correction needs to be considered. The BM3D has been extended using a suitable invertible transformation of the medical data into another

domain where data behaves like Gaussian distributed in resultant domain. The most commonly known such kind of transformation for this purpose is Anacombe's Transformation, also known as Variance Stabilization Technique (VST). Recently, VST has been proposed in [2] for Rician distributed data and BM3D method is referred as BM3D+VST method. The BM3D+VST method can be summarized mathematically as follows:

$$\hat{y} = VST^{-1}(BM3D(VST(z, \sigma), \sigma_{VST}), \sigma) \tag{5.4}$$

where VST^{-1} denotes the inverse Variance Stabilization transform, σ_{VST} is the stabilized standard deviation induced by VST and z denotes the additive white Gaussian noise whose true intensity is represented by y.

The aim of this chapter is to explore a direct technique that can handle Rician noise suitably giving rise to noise removal as good as BM3D+VST, if not better. We have extended PCA based method using Rough Set based clustering proposed in previous chapter to Rician noise model and bias term correction is also made, referred as ER-PCA in the paper. We have proposed a new Kernel based PCA (KPCA) method for Rician noise. However, we have adopted the clustering strategy used in Algorithm 2 (Proposal 3, Chapter 4), which is non-local approach in *true-sense*. As per our knowledge, KPCA has not been applied for Rician noise removal in medical image yet. The kernel based methods can find non-linearity of data in Feature space. Recently, kernel based methods have been used in Medical imaging in [119], [120], [121]. However, choice of appropriate or optimal kernel for given data is undecidable [121]. In the current proposal, the Gaussian kernel is used and the performance of noise removal technique is at par with the state-of-the-art methods.

The chapter has been arranged in following manner: Section 5.1 presents proposed method using KPCA. Section 5.2 compares proposed method with other state-of-the-art methods.

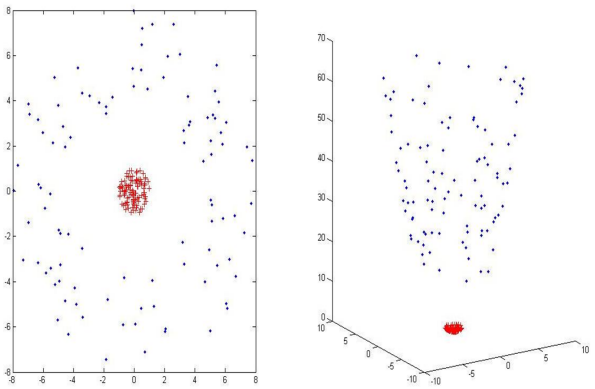

Figure 5.1: Transformation of two circular data sets into higher dimension space using kernel method where separation between them is more prominent and can be classified using linear hyper-surface.

5.1 Proposed Method using KPCA

5.1.1 Kernel Principal Component Analysis

A nonparametric variant of PCA, known as Kernel Principal Component Analysis (KPCA) has been explored for Rician noise removal. The KPCA tries to explore the structure in the data in Feature space instead of data space and tries to capture higher-order dependencies in the data. In Figure 5.1, two class data is shown in circular form and transformed to higher dimension for classification purpose, where transformation is $\phi(x) : (x_1, x_2) \rightarrow (x_1, x_2, x_1^2+x_2^2)$. Hence, one can find a plane (linear surface) in higher dimensions which is not possible in two dimensions for given data points.

In KPCA, this nonlinearity is introduced by first mapping the data into another space F using a nonlinear map $\Phi : R^N \rightarrow F$, before a standard linear PCA is carried out in F using the mapped samples $\phi(x_k)$. The map Φ and the space F are determined implicitly by the choice of a kernel function k, which acts as a similarity measure. This mapping computes the dot product between two input samples x and y mapped into F via

$$k(x; y) = \Phi(x).\Phi(y) \tag{5.5}$$

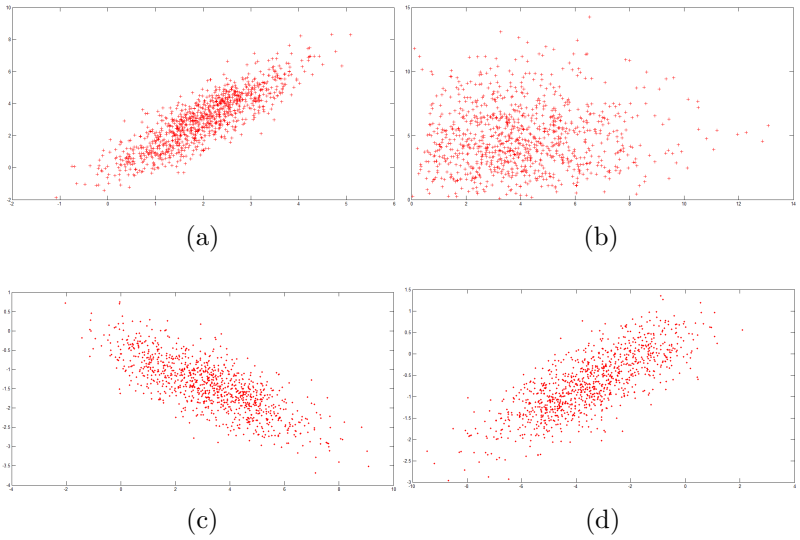

(a) (b)

(c) (d)

Figure 5.2: Reconstruction using PCA and KPCA over synthetic data with Rician noise. (a) Synthetic Data, (b) Rician Noisy Data, (c) Reconstruction using PCA and (d) Reconstruction using KPCA.

One can show that if k is a positive definite kernel, then there exists a map Φ into a dot product space F such that Eq.5.5 holds. The space F then has the structure of a Reproducing Kernel Hilbert Space (RKHS) [119].

The identity Eq.5.5 is important for KPCA since PCA in F can be formulated entirely in terms of inner products of the mapped samples. Thus, we can replace all inner products by evaluations of the kernel function. This has two important consequences: first, inner products in F can be evaluated without computing $\Phi(x)$ explicitly. This allows to work with a very high-dimensional, possibly infinite-dimensional RKHS F. Second, if a positive definite kernel function is specified, we need to know neither Φ nor F explicitly to perform KPCA since only inner products are used in the computations. Commonly used positive definite kernel functions are *polynomial kernel* of degree $d \in N, k(\mathbf{x}, \mathbf{y}) = (\mathbf{x}.\mathbf{y})^d$ or $k(\mathbf{x}, \mathbf{y}) = (\mathbf{x}.\mathbf{y} + 1)^d$ or Gaussian kernel of width $\sigma > 0$, $k(\mathbf{x}, \mathbf{y}) = exp\left(-\left\|\mathbf{x} - \mathbf{y}\right\|^2 / 2\sigma^2\right)$. In all the experiment, Gaussian Kernel has been used which is isotropic stationary in nature and also satisfy Mercer's Theorem [121].

In PCA, the covariance matrix is defined as $C = \frac{1}{N-1} X^t X$ where is X is called

Data matrix containing samples in columns. The covariance matrix in case of KPCA of size $M \times M$, calculated by

$$C_F = \frac{1}{N} \sum_{i=1}^{N} \phi(\mathbf{x}_i)\phi(\mathbf{x}_i)^T \tag{5.6}$$

Its eigenvalues and eigenvectors are given by $C_F\mathbf{v}_k = \lambda_k\mathbf{v}_k$, where $k = 1, 2, \ldots, M$. Mathematical simplification lead to $\mathbf{v}_k = \sum_{i=1}^{N} a_{ki}\phi(x_i)$ and hence $\mathbf{a}_k$ (N-dimensional column vector of a_{ki}) can be solved by $C_F\mathbf{a}_k = \lambda_k N\mathbf{a}_k$. If projected dataset $\phi(\mathbf{x}_i)$ does not have zero mean, one can use Gram matrix $\tilde{C_F}$ to substitute the kernel matrix C_F which is given by

$$\tilde{C_F} = C_F - \mathbf{1}_N C_F - C_F\mathbf{1}_N + \mathbf{1}_N C_F \mathbf{1}_N \tag{5.7}$$

where $\mathbf{1}_N$ is the $N \times N$ matrix with all elements equal to $1/N$.

An experiment has been performed as shown in Figure 5.2 where rician noise added in the synthetic data. Here, KPCA (with Gaussian kernel) is able to preserve orientation of the data in a better way as compared to PCA based reconstruction.

5.1.2 Proposed Approach

The outline of approach can be described as follows:

a. Get the clusters of the given noisy image using Rough set based method (as described in Chapter 4).

b. For each cluster, get the Basis vectors using KPCA method along pixel positions. For patches of size $p \times p$, Kernel matrix would of size $p^2 \times p^2$. Hence, the method is data adaptive in nature.

c. Project the noisy image patches using the obtained basis vectors in the KPCA domain.

d. Apply coefficient shrinkage method on these projected patches to get the denoised patches. Transform patches back to image space.

e. Remove the bias term from denoised image for each pixel.

$$I_{unbiased} = \sqrt{max(\hat{I}(i,j)^2 - 2h^2, 0)} \tag{5.8}$$

where h is the standard deviation of the noise and $\hat{I}$ is the image obtained by step (4). Figure 5.3 shows the method in a block diagram.

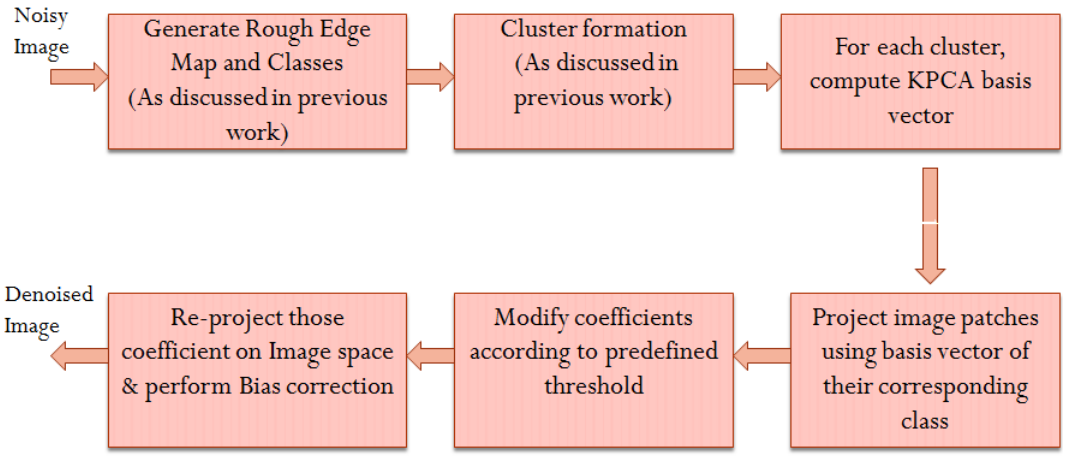

Figure 5.3: Flow chart of proposed method using KPCA

5.2 Experimental Results

This Section encompasses qualitative and quantitative evaluation of the proposed method along with some of the state-of-the-art methods. Experiments have been carried out on 2D monochrome phantom human brain MRI images obtained from Brain Web Database [1]. The parameters are as follows: RF = 20, protocol = ICBM, slice thickness = 1mm, volume size = 181x217x181. The experimental set up considers Rician noise model at different noise levels along with two modalities, namely T1 and T2. The simulated database provides the ground truth image for evaluating denoising

performance which most of the time is unavailable with real database. The Rician noise addition and bias correction are done as suggested in [122] and [20] respectively. The evaluation measures used are Peak-Signal-to-Noise Ratio (PSNR), Root Mean Square Error (RMSE), Structural Similarity Index (SSIM) [95] and Feature Similarity Index (FSIM) [96].

For comparison, four state-of-the-art methods are considered: Unbiased Non Local Means (UNLM method) presented in [20], BM3D+VST method proposed in [101], RS-NLM method proposed in Chapter 4 (Algorithm 1). The PCA based method proposed in the Chapter 4 (Algorithm 2) has been extended in this work for Rician noise, referred as ER-PCA. The parameters of all methods are kept default as suggested by respective authors. In all the experiments, patch size is kept as 5×5. The proposed KPCA method does not use VST method. Table 5.1 and Table 5.2 represent quantitative results for two slices 70 and 100 of T1 MR and T2 MR images respectively. The performance of ER-PCA is comparable to UNLM and BM3D+VST methods. The proposed KPCA method outperforms ER-PCA and preserves structure better than other state-of-the-art methods. BM3D+VST is observed to be very robust and hence performance of the proposed method is tested taking BM3D+VST as benchmark. Figure 5.4 shows difference of PSNR and SSIM measure for KPCA method with reference to BM3D+VST (zero level on vertical axis) of 50 slices (from 61^{st} to 110^{th} slice of database mentioned above) with noise standard deviation equal to 15 for both T1 and T2 modalities. The negative value indicates BM3D+VST perform better and, in reverse, positive value is indicator of better performance of KPCA method. From the Figure 5.4, PSNR of KPCA is falls below BM3D+VST method whereas it preserves structure of the image better in terms of SSIM measure. This is also visually evident in Figure 5.5 for the slice 100 of T1 modality at noise level 15.

5.3 Conclusion

In this chapter, an approach for removing Rician noise from brain MR images using Kernel PCA has been proposed. Being a manifold learning method, KPCA explores a

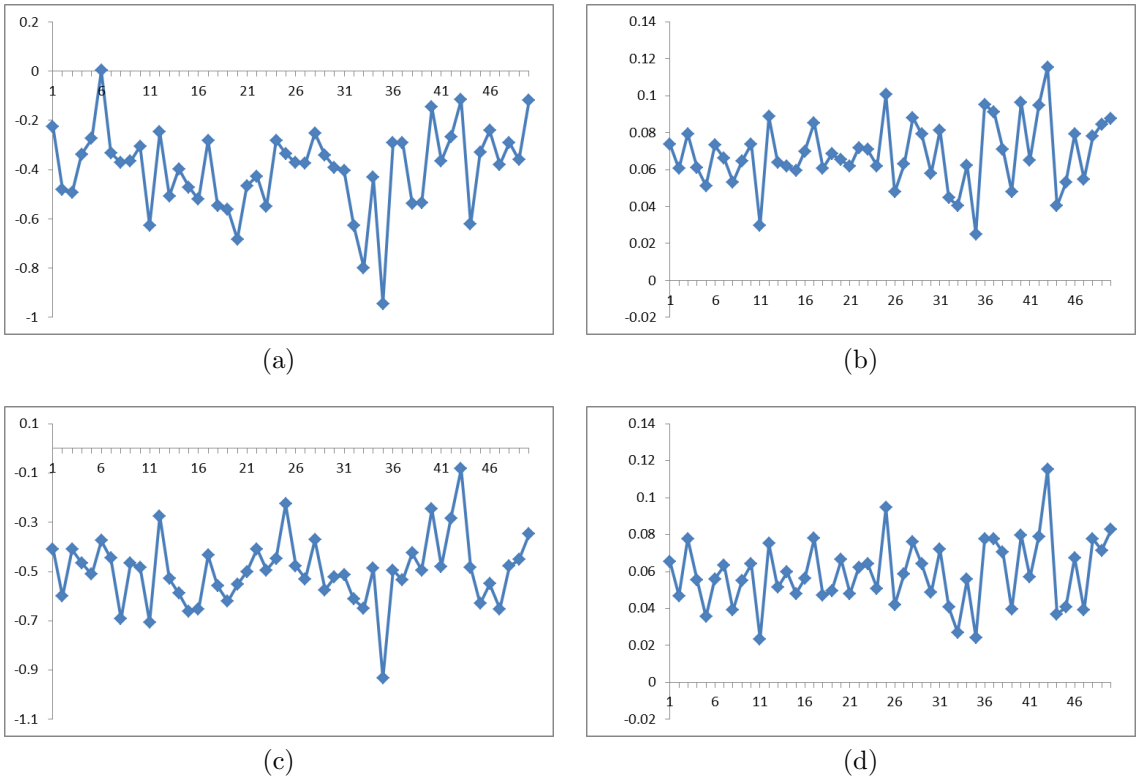

Figure 5.4: Difference comparison of KPCA with reference to BM3D+VST method (at zero level vertically) for 50 slices for noise standard deviation equal to 15 (a) T1 images with PSNR difference values, (b) T1 images with SSIM difference values, (c) T2 images with PSNR difference values and (d) T2 images with SSIM difference values.

Table 5.1: Performance comparison of proposed denoising strategy with different approaches on various quantitative measures under *Rician Noise assumption* in Brain Web database (**slice=70 & 100**, Modality = T1, image size = 181 × 217 and patch size = 5 × 5). Best figures are shown in Bold.

Noise		Slice 70				Slice 100			
SD	Methods	PSNR	RMSE	MSSIM	FSIM	PSNR	RMSE	MSSIM	FSIM
5	Noisy	32.4293	37.1660	0.6134	0.9296	32.2588	38.6549	0.5564	0.8922
	UNLM [20]	39.0519	8.0889	0.9832	0.9845	40.1551	6.2744	0.9882	0.9887
	BM3D+VST [2]	**40.9727**	**5.1937**	0.9602	0.9843	41.4921	4.6118	0.9602	0.9857
	RS-NLM	39.8595	6.7163	**0.9851**	**0.9853**	**41.5829**	**4.5164**	**0.9914**	**0.9913**
	ER-PCA	40.4514	5.8606	0.9791	0.9764	39.9719	6.5447	0.9689	0.9563
	KPCA	40.2107	6.1946	0.9197	0.9797	41.2223	4.9073	0.9866	0.9850
10	Noisy	26.4115	148.5702	0.4717	0.8149	26.2398	154.5629	0.4183	0.7567
	UNLM [20]	35.9894	16.3733	0.9608	0.9643	36.9916	12.9993	0.9707	0.9724
	BM3D+VST [2]	**36.3738**	**14.9866**	0.9040	0.9607	36.8590	13.4025	0.9132	0.9653
	RS-NLM	35.8260	17.0011	**0.9631**	**0.9645**	**37.2231**	**12.3246**	**0.9762**	**0.9770**
	ER-PCA	35.7387	17.3464	0.9389	0.9439	36.3168	15.1846	0.9597	0.9484
	KPCA	36.1061	15.9395	0.9586	0.9522	36.6642	14.0172	0.9682	0.9628
15	Noisy	22.8950	333.8752	0.3744	0.7177	22.7220	347.4434	0.3331	0.6495
	UNLM [20]	33.5147	28.9475	0.9299	**0.9391**	**34.4622**	**23.2732**	0.9453	**0.9498**
	BM3D+VST [2]	**33.7666**	**27.3162**	0.8583	0.9368	34.2393	24.4992	0.8684	0.9447
	RS-NLM	32.1179	39.9292	0.9273	0.9244	32.5856	35.8523	**0.9472**	0.9448
	ER-PCA	33.2440	30.8093	0.9133	0.9178	33.8155	27.0103	0.9377	0.9287
	KPCA	33.4097	29.6557	**0.9323**	0.9262	34.0241	25.7438	0.9469	0.9404

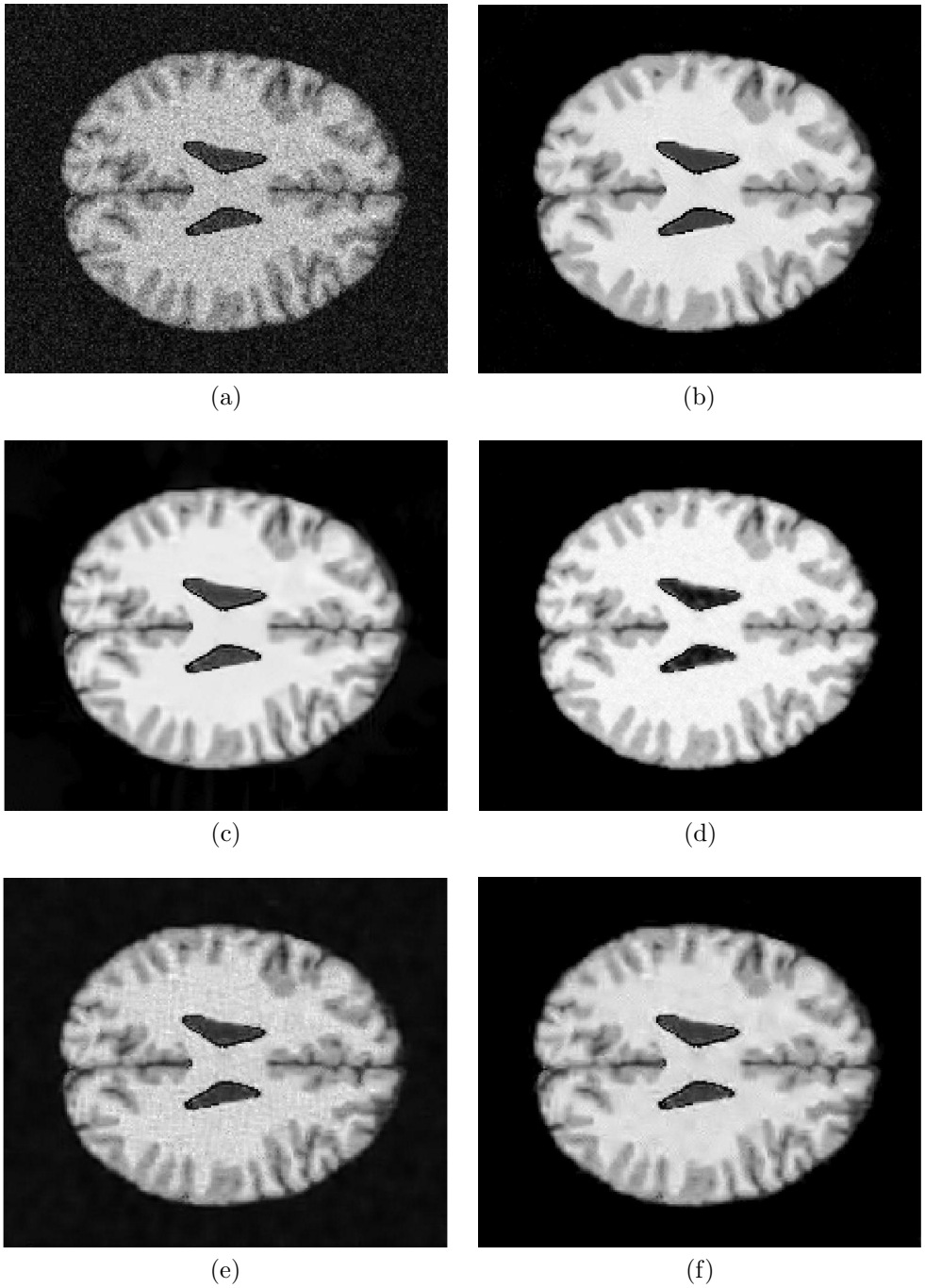

Figure 5.5: (a) Synthetic Noisy T1 Image with Rician noise standard deviation=15 and PSNR =22.7220 dB, Denoised image using (b) UNLM method, PSNR = 34.4622 dB, (c) BM3D+VST method, PSNR = 34.2393 dB, (d) RS-NLM method, PSNR = 32.5856 dB, (e) ER-PCA method, PSNR = 33.8155 dB, (f) KPCA method, PSNR = 34.0241 dB.

Table 5.2: Performance comparison of proposed denoising strategy with different approaches on various quantitative measures under *Rician Noise assumption* in Brain Web database (**slice=70 & 100**, Modality = T2, image size = 181 × 217 and patch size = 5 × 5). Best figures are shown in Bold.

Noise		Slice 70				Slice 100			
SD	Methods	PSNR	RMSE	MSSIM	FSIM	PSNR	RMSE	MSSIM	FSIM
5	Noisy	32.4349	37.1185	0.6257	0.9365	32.2639	38.6095	0.5691	0.9052
	UNLM [20]	34.4831	23.1617	0.9822	0.9813	35.2666	19.3385	0.9869	0.9858
	BM3D+VST [2]	**40.4738**	**5.8305**	0.9648	**0.9861**	**41.0752**	**5.0764**	0.9663	0.9885
	RS-NLM	36.9814	13.0300	**0.9856**	0.9835	37.6322	11.2166	**0.9915**	**0.9900**
	ER-PCA	39.8618	6.7127	0.9783	0.9727	39.1934	7.8297	0.9610	0.9473
	KPCA	37.8578	10.6487	0.8002	0.9782	38.1996	9.8429	0.7610	0.9797
10	Noisy	26.4322	147.8642	0.4956	0.8356	26.2550	154.0201	0.4408	0.7757
	UNLM [20]	32.9818	32.7262	0.9618	0.9623	33.8132	27.0246	0.9710	0.9687
	BM3D+VST [2]	**35.7377**	**17.3504**	0.9181	**0.9681**	35.8044	17.0860	0.9683	0.9637
	RS-NLM	34.5041	23.0502	**0.9691**	0.9676	35.2411	19.4522	**0.9799**	**0.9766**
	ER-PCA	34.8288	21.3894	0.9432	0.9323	34.5457	22.8303	0.9262	0.9008
	KPCA	35.0519	20.3182	0.8527	0.9567	**36.1329**	**15.8413**	0.9184	0.9727
15	Noisy	22.9275	331.3825	0.4131	0.7519	22.7460	345.5293	0.3676	0.6776
	UNLM [20]	31.4832	46.2121	0.9346	0.9408	32.1181	39.9271	0.9472	0.9456
	BM3D+VST [2]	**32.8504**	**33.7321**	0.8769	**0.9496**	**33.1694**	**31.3427**	0.8855	**0.9567**
	RS-NLM	31.9206	41.7849	**0.9446**	0.9452	32.6973	34.9423	**0.9601**	0.9543
	ER-PCA	31.7529	43.4297	0.9034	0.8973	31.7770	43.1894	0.8989	0.8718
	KPCA	32.3606	37.7592	0.9363	0.9346	32.8539	33.7049	0.9516	0.9439
20	Noisy	20.4499	518.2594	0.3540	0.6871	20.2642	611.8738	0.3162	0.6059
	UNLM [20]	30.0502	64.2771	0.9063	0.9205	30.5757	56.9519	0.9199	0.9216
	BM3D+VST [2]	**30.7168**	**55.1319**	0.8426	**0.9303**	**30.9691**	**52.0201**	0.8508	**0.9398**
	RS-NLM	29.4113	74.4654	0.9109	0.9104	30.1086	63.4192	0.9293	0.9137
	ER-PCA	29.6008	71.2860	0.8723	0.8785	29.6002	71.2947	0.8647	0.8527
	KPCA	30.1448	62.8934	**0.9129**	0.9144	30.6031	56.5941	**0.9316**	0.9245
25	Noisy	18.5384	910.4194	0.3095	0.6362	18.3487	951.0736	0.2774	0.5520
	UNLM [20]	28.6394	88.9483	0.8777	0.9012	29.1108	79.7989	0.8914	0.8987
	BM3D+VST [2]	**29.0589**	**80.7598**	0.8109	**0.9114**	**29.2912**	**76.5527**	0.8269	**0.9227**
	RS-NLM	26.4734	146.4670	0.8599	0.8492	26.6486	140.6762	0.8696	0.8372
	ER-PCA	28.0567	101.7219	0.8576	0.8824	28.1251	100.1314	0.8529	0.8685
	KPCA	28.1995	98.4298	**0.8792**	0.8814	28.3402	95.2919	**0.8932**	0.8785

suitable transformation for image representation through sparse bases. This method learns basis vectors from data itself unlike BM3D+VST method where basis vectors are kept fixed. The limitation of KPCA method is the selection of suitable kernel which is yet unanswered. If the nature of data is not known a-prior then one can try various kernels to find a suitable one. However, commonly used Gaussian kernel in KPCA, found to perform comparable with other state-of-the-art methods. The PCA based method proposed in previous chapter has also been implemented to remove Rician noise, but it fails to attend superior performance over KPCA. The proposed method is implemented on synthetic data for quantitative evaluation since ground truth data is available for it.

Chapter 6

3D MRI Denoising

3D MRI provides more insight into data and their inter slice relationship. With this in mind, researchers, in recent days, prefer to work directly on 3D data. However, large dimensions increase computation hugely and correlation between the dimensions play major role. The search of relationship of data among different dimensions is a highly sought. One class of method deploys non-local means strategy while deriving feature set from the raw data/pre-processed data. Mainly, methods [123], [124], [125], [120], [16] follow NLM process. Another class of methods transform data to Gaussian space using VST, then perform denoising and invert back to data space [122], [126].

6.1 State-of-the-art Methods for 3D denoising

Many state-of-the-art methods for 3D image denoising are extensions of their 2D counterpart versions. However, computational complexity becomes a crucial factor during the extension. The 3D MR image denoising was introduced in modern literature in [123] and then followed by [124], [125], [120], [122], [126], [16] etc. Instead of playing with patches in 2D images, here a voxel is defined as 3D cube centered at location (i, j, k) in $\mathcal{R}^3$. Hence, a voxel is simply counterpart of a patch of size $w \times w \times w$. Consequently, exploring relationship among intensity values in $\mathcal{R}^3$ is highly sought and thus leads to computational intensive process.

The Optimized Blockwise NLM (OBNLM, [123]) is extension of Non Local Means method [93]. OBNLM tweak the computation of similarity weight between voxels and constrained to have predefined criteria for mean and variance of both the voxels. At the same time, it adopted the block-wise strategy to drop restoration of adjacent n voxels which effectively reduce the computational load by n^3 times instead of processing each voxel in the image space. A similar approach has been adopted in [124], [122]. In case of ABONLM method [124], denoising is performed under Wavelet framework using adaptive soft wavelet coefficient mixing (ASCM) approach.

A non-parametric kernel regression framework has also been adopted for 3D MR image denoising in Unbiased Kernel Regression method [120]. UKR is rooted on a zeroth order 3D kernel regression and similarity weight between voxels is derived on small sized feature vectors based image intensity and gradient information. The sparseness and self-similarity has been unified in PRI-NLM method [125]. PRI-NLM incorporate rotational invariant version of NLM [109] and discrete cosine transform hard thresholding for sparsity purpose.

One of the most well know BM3D method has been extended to 3D MR image denoising as BM4D method [122]. Similar to BM3D, BM4D is also equipped with collaborative filtering notion where similar voxels are arranged in fourth dimension. It is also a two stage method where the output of first stage guides the second stage and uses hard thresholding in first pass and wiener filtering in second pass. Ideally, BM4D is designed for Gaussian noise whereas Variance Stabilization Technique (VST) has been adopted to deal with Rician noise in 3D MRI data [122]. The VST based scheme is also adopted in two phased HOSVD-R method [126] which is also a natural extension of HOSVD method proposed in [100].

Recently, another two stage method PRI-NL-PCA [16] was proposed based on sparsity and self-similarity of voxels. It is encompassed within PCA thresholding strategy in first stage where rotational invariant NLM method is deployed in second stage. The next section describes the current proposal.

6.2 Proposed Method

6.2.1 Kernel Principal Component Analysis

Kernel Principal Component Analysis (KPCA) is described in Chapter 5, however we are reminding the reader about the salient features of it. KPCA induces non-linearity by projecting data to kernel space via similarity measuring kernel function. A standard linear PCA operation is then carried out in the kernel space. In PCA, the covariance matrix is defined as $C = \frac{1}{N-1}X^tX$ where is X is called Data matrix containing samples in columns. The covariance matrix in case of KPCA of size $M \times M$, calculated by

$$C_F = \frac{1}{N}\sum_{i=1}^{N}\phi(\mathbf{x}_i)\phi(\mathbf{x}_i)^T \tag{6.1}$$

Its eigenvalues and eigenvectors are given by $C_F\mathbf{v}_k = \lambda_k\mathbf{v}_k$, where $k = 1, 2, \ldots, M$. Mathematical simplification lead to $\mathbf{v}_k = \sum_{i=1}^{N} a_{ki}\phi(x_i)$ and hence $\mathbf{a}_k$ (N-dimensional column vector of a_{ki}) can be solved by $C_F\mathbf{a}_k = \lambda_k N\mathbf{a}_k$. If projected dataset $\phi(\mathbf{x}_i)$ does not have zero mean, one can use Gram matrix $\tilde{C_F}$ to substitute the kernel matrix C_F which is given by

$$\tilde{C_F} = C_F - \mathbf{1}_N C_F - C_F\mathbf{1}_N + \mathbf{1}_N C_F \mathbf{1}_N \tag{6.2}$$

where $\mathbf{1}_N$ is the $N \times N$ matrix with all elements equal to $1/N$ (Refer to Chapter 5 for more details).

6.2.2 Proposed Method

The 3D MR image denoising is extension of method used in Chapter 5 for slice image denoising. In this work, Rough Class Label (RCL) and Rough Edge Map (REM) notion is extended to 3D data in similar fashion via rough entropy optimization criteria. Here, we refer a patch as voxel.

The method proposed in Chapter 5 for 2D images has been extended for 3D data in this chapter. We have extended Rough Set based RCL and REM information (Chapter 2) for 3D data and the pool formation uses voxels (cube). A voxel ($N \times N \times N$) is first converted into vector format ($N^3 \times 1$). Afterwords, RST based pooling process creates pool of similar voxels globally. The basis vectors from KPCA method (Chapter 5), are then truncated using hard thresholding approach. The denoised vector is projected back to image space. The proposed method is a single phase process whereas methods proposed in [122], [126], [16] are two phase methods 5where output of first phase used as informed input to the next phase.

The outline of present work can be described as follows:

a. Get the clusters of voxels ($p \times p \times p$) from the given noisy image using Rough set based method (as described in Chapter 4).

b. For each cluster, get the basis vectors using KPCA method along pixel positions. For cluster matrix of size $p^3 \times N$, kernel matrix would be of size $p^3 \times p^3$, where N is number of voxels in the cluster.

c. Project the noisy image patches on the obtained basis vectors in the KPCA domain.

d. Apply coefficient shrinkage method on these projected patches to get the denoised patches. Transform them back to image space.

e. Remove the bias term from each pixel of the denoised image i.e. $\hat{I}_{unbiased}(i,j,k) = \sqrt{max(\hat{I}(i,j,k)^2 - 2h^2, 0)}$, where h is the standard deviation of noise and $\hat{I}$ is the image obtained by step (4).

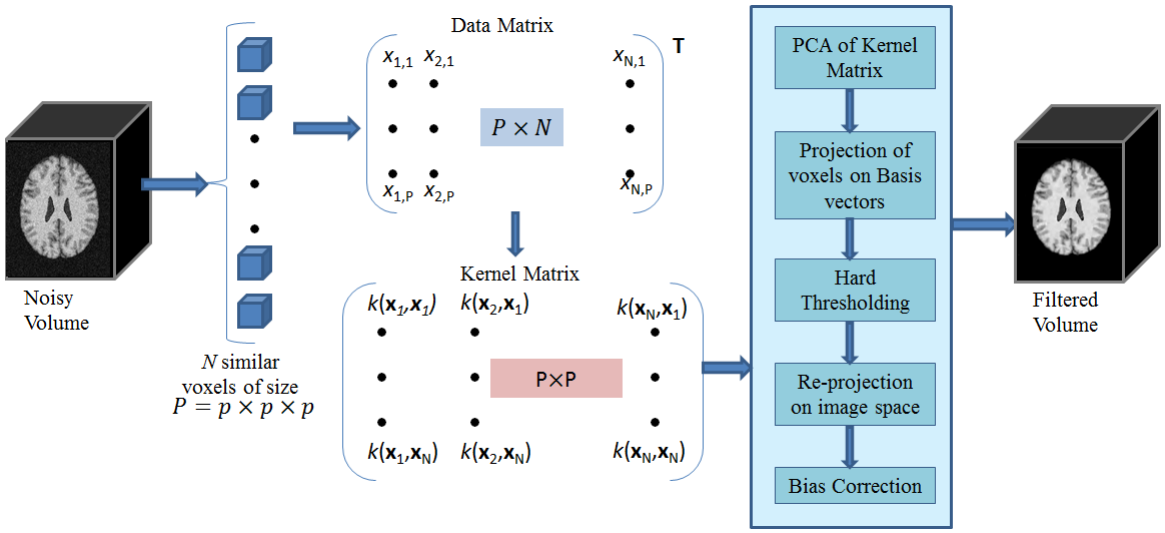

Figure 6.1: Flowchart of Proposed Method

6.3 Experimental Results

6.3.1 Validation on Phantom Database

The experiments have been carried out on Brain Web database [1] with T1, T2 and PD modalities. The Simple Kernel is parameter free whereas other kernels, referred in this work, have one parameter. Kernels with more than one parameters will increase the computation drastically. For this reason, such kernels are not considered. The kernels used in this work are mentioned in Table 6.1 with their respective parameters. In this work, exhaustive experimental results are presented in Figure 6.2 and 6.3 for finding optimized kernel parameter values. The parameter values are evaluated in the range 10^{-3} to 10^{6} with incremental step 10. The proposed method with single threaded MATLAB implementation takes around 45 minutes on core i7 processor, 2.10 GHz and 8 GB RAM machine. The UKR is observed to have same computational time whereas BM4D with MATLAB/C implementation takes 11 minutes and others run in less than five minutes.

The proposed method has been compared with UKR [120], PRI-NLM [125], BM4D [122], PRI-NL-PCA [16]. Table 6.2 shows reconstruction error of all methods when

Table 6.1: Various Kernel used in this work

Kernel Name	Expression	Parameter
Simple/Linear	$\mathbf{x}^T\mathbf{y}$	-
Gaussian	$exp\left(-\frac{\|\mathbf{x}-\mathbf{y}\|^2}{2h^2}\right)$	h
Laplacian	$exp\left(-\frac{\|\mathbf{x}-\mathbf{y}\|}{h}\right)$	h
Multiquadratic	$\sqrt{\|\mathbf{x}-\mathbf{y}\|^2+h^2}$	h
Sigmoid	$tanh\left(\|\mathbf{x}-\mathbf{y}\|^2+h^2\right)$	h

Table 6.2: Results of state-of-the-art Methods for *Noise Free* Data for T1, T2 and PD modalities (represented row-wise against each method)

	Modality	PSNR	RMSE	SSIM	BC
UKR	T1	12.45	60.83	0.7063	0.8519
	T2	11.55	67.45	0.7045	0.8819
	PD	7.24	110.73	0.7044	0.8519
PRI-NLM	T1	12.45	60.83	0.7064	0.8548
	T2	11.57	67.31	0.7053	0.8594
	PD	7.25	11.61	0.7060	0.8618
BM4D	T1	47.64	1.06	0.9976	0.9955
	T2	40.57	2.39	0.9966	0.9923
	PD	54.76	0.47	0.9989	0.9529
PRI-NL-PCA	T1	56.24	0.39	0.9997	0.9734
	T2	46.32	1.23	0.9995	0.9763
	PD	48.07	1.01	0.9994	0.9783
KPCA	T1	**296.48**	**0.0**	**1.0**	**0.9988**
	T2	**200.14**	**0.0**	**1.0**	**0.9963**
	PD	**263.69**	**0.0**	**1.0**	**0.9901**

no noise is present in image. In oracle situation, image (3D volume data here) must be exactly reconstructed with result in PSNR = Infinity, RMSE = 0, SSIM = 1.0 and Bhattacharya Coefficient (BC) = 1.0. The proposed method reconstructs image better than other state-of-the-art methods in terms of all the measures. Although, PSNR of proposed method is not around Infinity but very high than that of other methods.

Table 6.3, 6.4 and 6.5 present denoising results for T1, T2 and PD modality respectively. All the tables present results with various noise levels ($\sigma = 5, 10, 15, 20, 25$). In the table, 2×2 block represents PSNR (top-left), RMSE (top-right), SSIM (bottom-left) and BC (bottom-right). The best result along each noise is represented in bold figure for all the measures. At lower noise level, KPCA method performed compara-

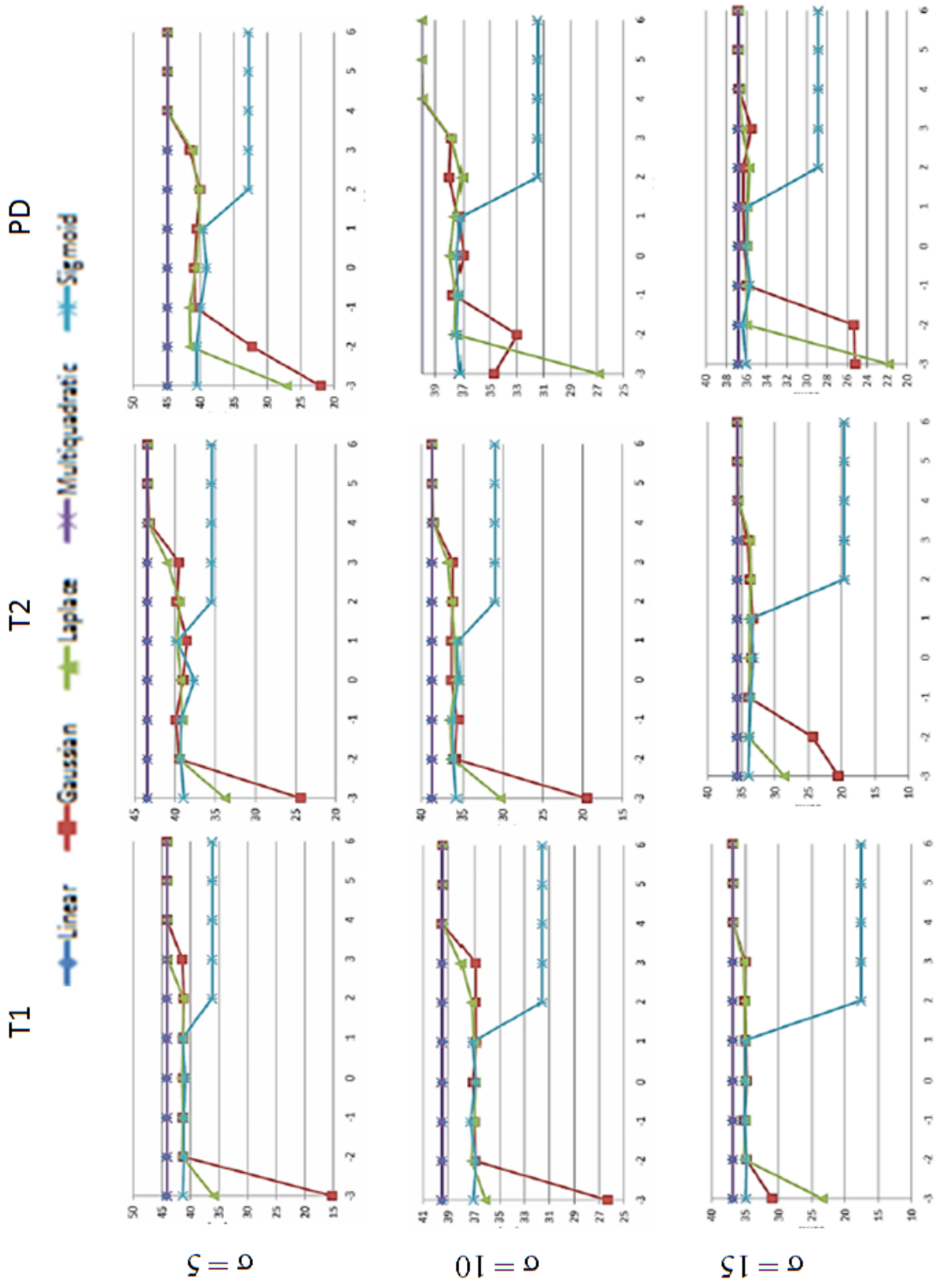

Figure 6.2: Performance of various kernels over PSNR values with different noise levels and modalities

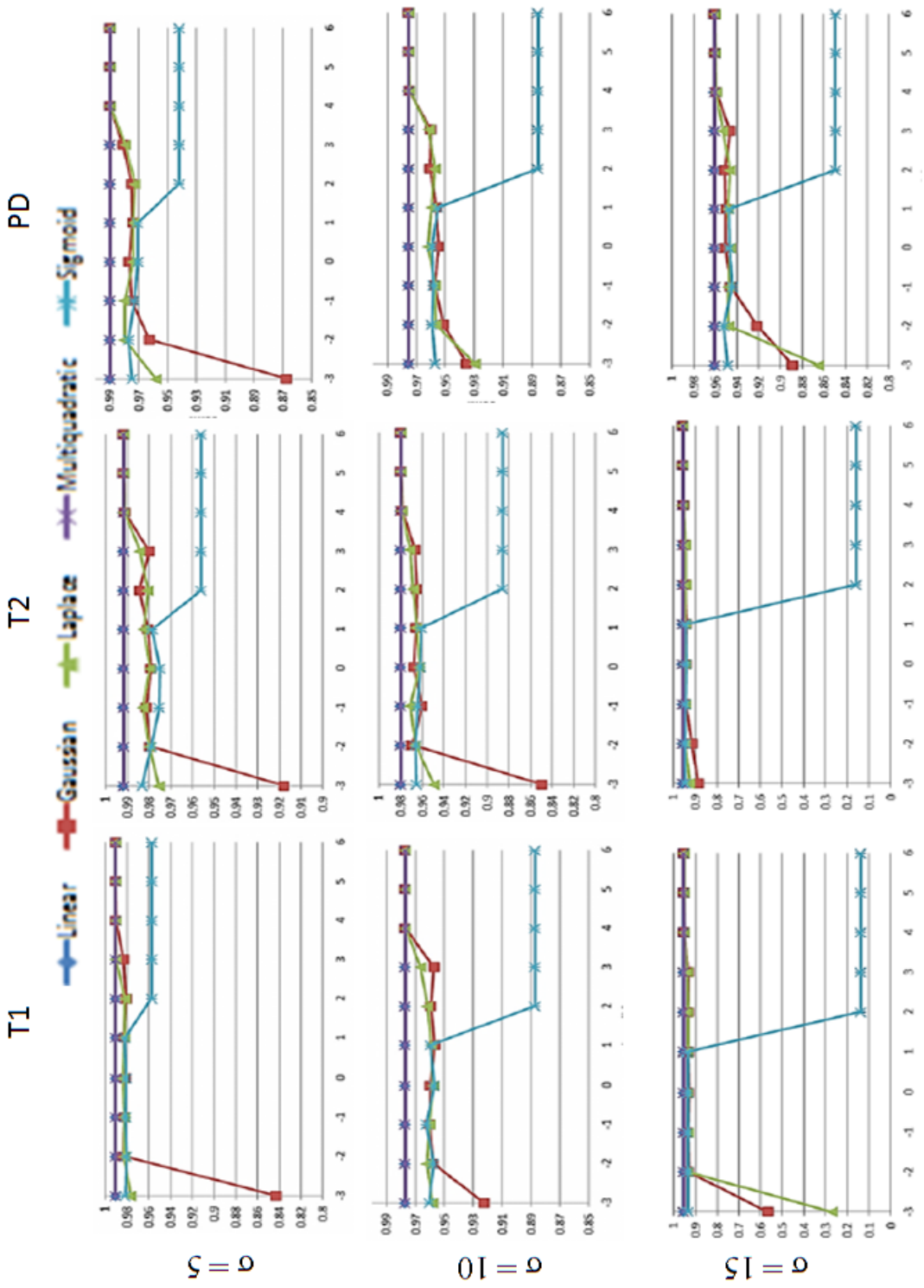

Figure 6.3: Performance of various kernels over SSIM values with different noise levels and modalities

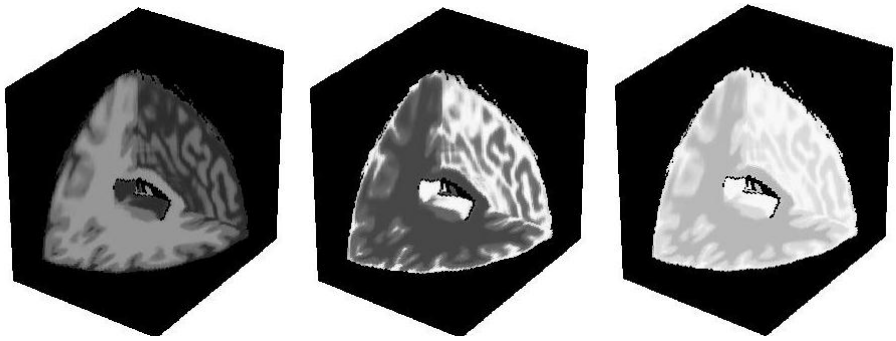

(a) T1 volume (b) T2 volume (c) PD volume

Figure 6.4: Original volumes of T1, T2, PD data from BrainWeb Database

ble to other methods in all the modalities. At higher level, PSNR of proposed method falls very down whereas it is able to preserve the structure of medical data far better than other state-of-the-methods. At the same time, proposed method also stood best in probabilistic measure BC. The kernel method may not be able to project data on manifold under high noisy condition that might cause the fall in PSNR values. However, a simple pre-processing such as mean or median filtering can be applied at higher noise level as done in [120].

6.3.2 Results on Real Databases

The other two real datasets are having some pathological issues. The subject details of selected data from OASIS dataset [7] are as follows: Subject ID: 012, 018, Age: 30 and 39 (both male) respectively, scan number: mpr-1, type: MPRAGE, voxel resolution: 1.0 mm x 1.0 mm x 1.25mm, Orientation: Sagittal, TR (ms)= 9.7, TE (ms)= 4.0, TI(ms)= 20.0, Flip angle= 10. The 3D cross sectional view of subject results are shown in Figure 6.8 and 6.9 for subject 012 and 018 respectively and Figure 6.10 shows 2D view of a portion of Subject 018.

6.4 Conclusion

Kernel method is explored in this work to deal with Rician noise present in the MRI data. Being signal dependent noise, applicability of linear denoising operation such as PCA is not advisable. It is expected in the present work that kernel method may project the nonlinear data in the linear feature space. We have an extended Rough Set based clustering method to collect similar voxels conditioned on class and edge information. These similar voxels are then used to define kernel matrix via kernel function. We have experimented with a small set of kernels having one parameter. However, it can be exercised with other known kernel with suitable parameter estimation method or data adaptive kernel for rician model can be thought of.

The proposed method is non-iterative and single stage method as opposed to some of predecessor methods like BM4D, PRI-NL-PCA etc. In this work, intensity value is used as a feature in clustering step and in kernel space however more features can be considered like gradient information as in UKR. The predecessor methods restrict the search space for searching similar voxels. However, current method exploits the whole volume and thereby forms clusters for similar voxels.

Table 6.3: Results of state-of-the-art Methods for T1 modality (represented row-wise against each method). In each 2×2 block, top-left figure is PSNR, top-right is RMSE, bottom-left is SSIM and bottom-right is BC measure. The figure against each noise level is represented in Bold face.

$\sigma \rightarrow$	5		10		15		20		25	
Noise	31.78	06.57	25.76	13.13	22.25	19.69	19.75	26.24	17.82	32.77
	0.3473	0.3497	0.2170	0.2910	0.1583	0.2859	0.1209	0.3033	0.0949	0.3207
UKR	36.04	04.02	30.59	07.53	33.72	05.25	32.11	06.32	32.85	05.81
	0.5084	0.5373	0.3359	0.2760	0.6507	0.7809	0.6364	0.8210	0.7762	0.8902
PRI-NLM	**45.16**	**01.41**	**39.95**	**02.56**	**36.91**	**03.64**	**34.84**	**04.62**	**33.27**	**05.53**
	0.9527	0.9009	0.8769	0.8291	0.8129	0.8173	0.7734	0.8276	0.7297	0.8225
BM4D	43.81	06.57	39.17	02.81	36.50	03.81	34.61	04.74	33.14	05.62
	0.9452	0.9008	0.8729	0.8690	0.8167	0.8597	0.7735	0.8549	0.7390	0.8518
PRI-NL-PCA	40.36	02.45	35.01	04.53	32.0	06.41	29.90	08.16	28.32	09.78
	0.6640	0.4699	0.4918	0.5332	0.4243	0.5705	0.3864	0.5930	0.3662	0.6173
KPCA	44.09	01.59	39.45	02.72	36.83	03.67	32.93	05.76	32.11	06.33
	0.9904	**0.9818**	**0.9770**	**0.9760**	**0.9535**	**0.9641**	**0.9446**	**0.9505**	**0.9391**	**0.9446**

Table 6.4: Results of state-of-the-art Methods for T2 modality (represented row-wise against each method). In each 2×2 block, top-left figure is PSNR, top-right is RMSE, bottom-left is SSIM and bottom-right is BC measure. The figure against each noise level is represented in Bold face.

$\sigma \rightarrow$	5		10		15		20		25	
Noise	31.78	06.57	25.76	13.11	22.26	19.65	19.77	26.17	17.84	32.67
	0.3540	0.3496	0.2341	0.2894	0.1850	0.2671	0.1552	0.2259	0.1344	0.2559
UKR	35.79	04.14	30.12	07.95	31.03	07.16	29.87	08.19	28.74	09.32
	0.5141	0.5411	0.3434	0.3204	0.4739	0.6155	0.5732	0.7732	0.4727	0.6726
PRINLM3D	**43.87**	**01.63**	**39.41**	**02.73**	**36.62**	**03.76**	**34.25**	**04.94**	**32.09**	**06.34**
	0.9537	0.8942	0.8819	0.8247	0.8216	0.8148	0.7845	0.8244	0.7414	0.8184
BM4D	42.95	01.82	38.11	03.17	35.21	04.43	33.09	05.65	31.41	06.86
	0.9460	0.8971	0.8746	0.8660	0.8201	0.8566	0.7790	0.8525	0.7458	0.8500
PRI-NL-PCA	40.1	02.52	34.45	04.83	31.21	07.02	28.90	09.15	27.03	11.34
	0.6818	0.4872	0.4745	0.5154	0.3980	0.5359	0.3624	0.5536	0.3361	0.5518
KPCA	43.46	01.71	38.65	02.98	35.58	04.24	26.97	11.42	26.39	12.22
	0.9916	**0.9797**	**0.9798**	**0.9732**	**0.9564**	**0.9597**	**0.9434**	**0.9638**	**0.9364**	**0.9585**

Table 6.5: Results of state-of-the-art Methods for PD modality (represented row-wise against each method). In each 2×2 block, top-left figure is PSNR, top-right is RMSE, bottom-left is SSIM and bottom-right is BC measure. The figure against each noise level is represented in Bold face.

$\sigma \rightarrow$	5		10		15		20		25	
Noise	31.78	06.57	25.78	13.10	22.28	19.61	19.81	26.07	17.89	32.48
	0.3430	0.3455	0.2074	0.2842	0.1493	0.2609	0.1163	0.2466	0.0955	0.2347
UKR	36.22	03.94	36.28	03.91	34.26	04.94	30.71	07.43	28.98	09.07
	0.5112	0.5422	0.6616	0.7192	0.7614	0.8462	0.6648	0.8133	0.4693	0.6645
PRINLM3D	**45.67**	**01.33**	**41.04**	**02.26**	**38.02**	**03.20**	**35.61**	**04.23**	**33.45**	**05.42**
	0.9528	0.8922	0.8800	0.8205	0.8181	0.8079	0.7793	0.8162	0.7340	0.8094
BM4D	44.46	01.53	39.38	02.74	36.22	03.94	33.88	05.16	32.01	06.40
	0.9455	0.8946	0.8731	0.8629	0.8175	0.8520	0.7754	0.8458	0.7419	0.8414
PRI-NL-PCA	40.64	02.37	34.99	04.53	31.58	06.72	29.04	09.01	27.02	11.37
	0.6879	0.4927	0.4935	0.5350	0.4049	0.5457	0.3513	0.5364	0.3203	0.5325
KPCA	44.88	01.45	40.02	02.54	36.83	03.67	27.34	10.95	26.94	11.47
	0.9898	**0.9770**	**0.9756**	**0.9717**	**0.9608**	**0.9671**	**0.9468**	**0.9705**	**0.9399**	**0.9564**

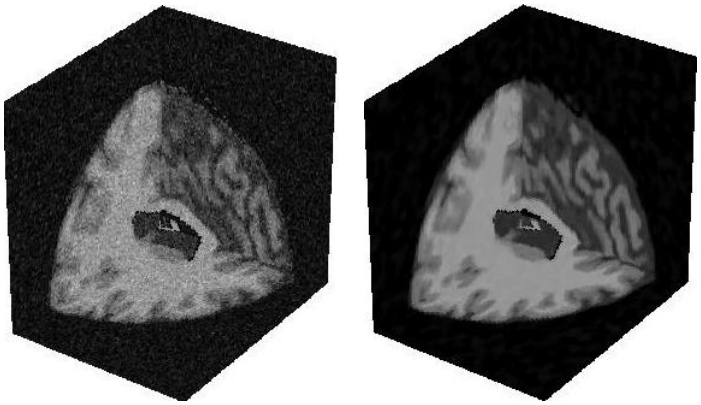

(a) Noisy volume

(b) UKR

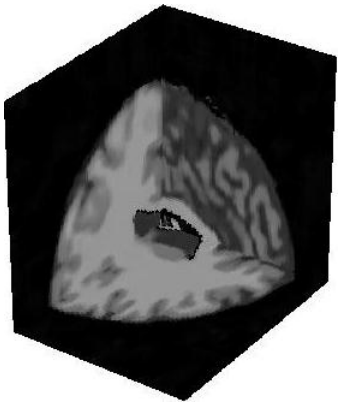

(c) PRINLM3D

(d) BM4D

(e) PRINLPCA

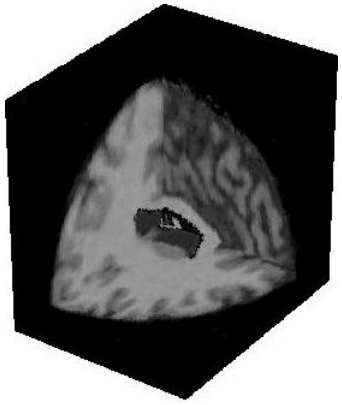

(f) Proposed

Figure 6.5: Comparison of various methods on T1 from BrainWeb Database

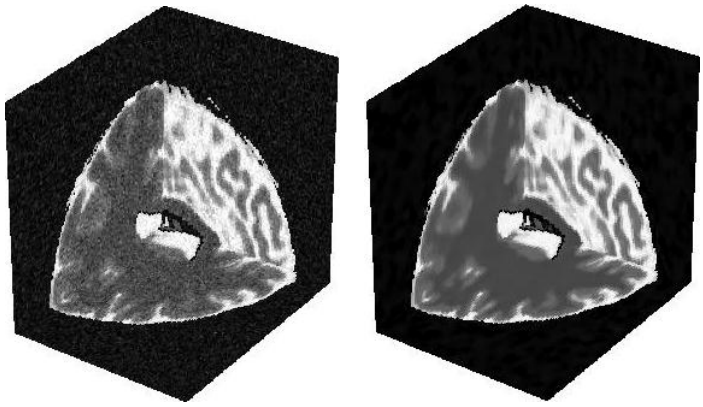

(a) Noisy volume (b) UKR

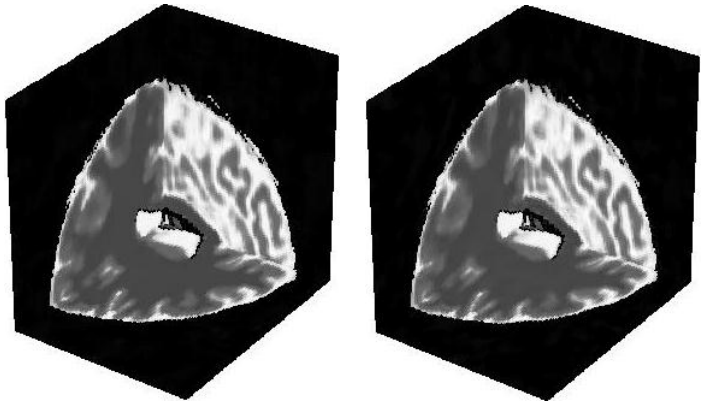

(c) PRINLM3D (d) BM4D

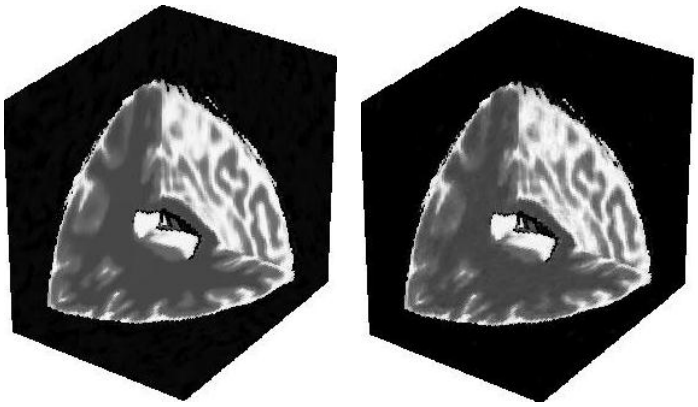

(e) PRINLPCA (f) Proposed

Figure 6.6: Comparison of various methods on T2 from BrainWeb Database

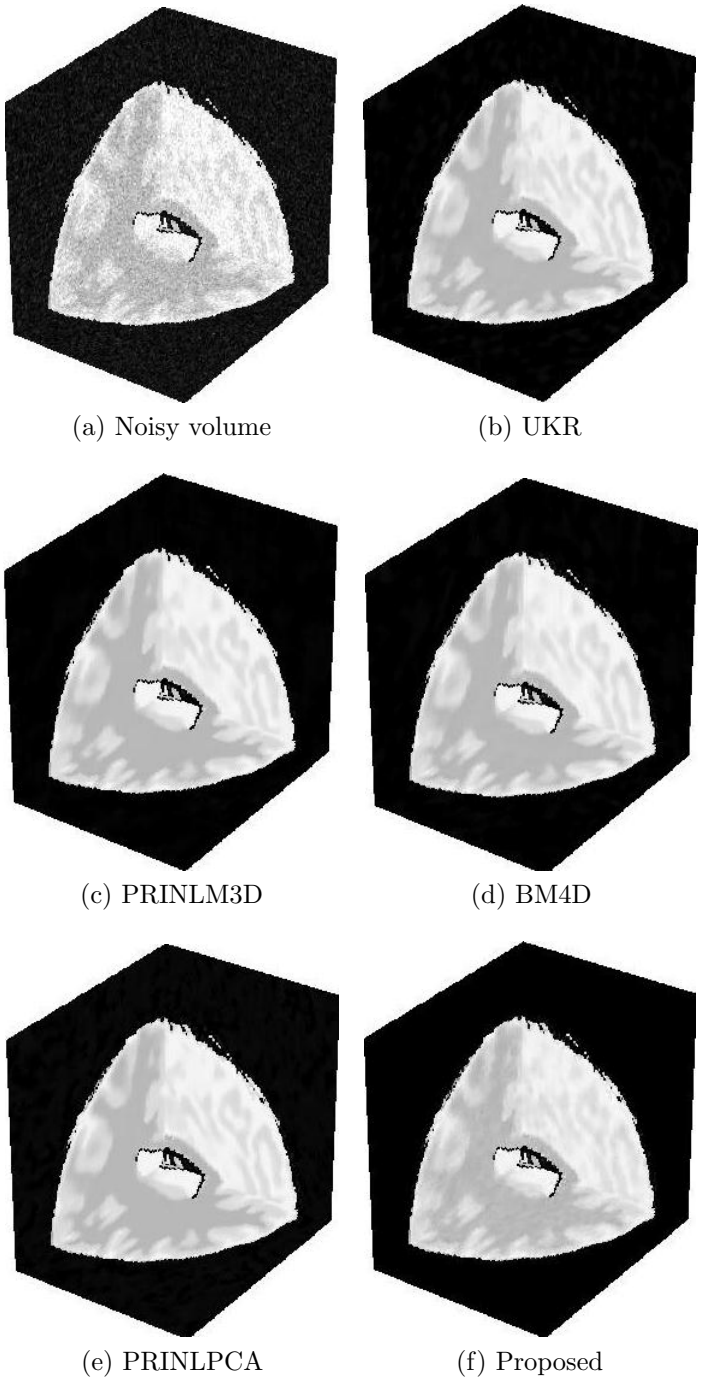

(a) Noisy volume (b) UKR

(c) PRINLM3D (d) BM4D

(e) PRINLPCA (f) Proposed

Figure 6.7: Comparison of various methods on PD from BrainWeb Database

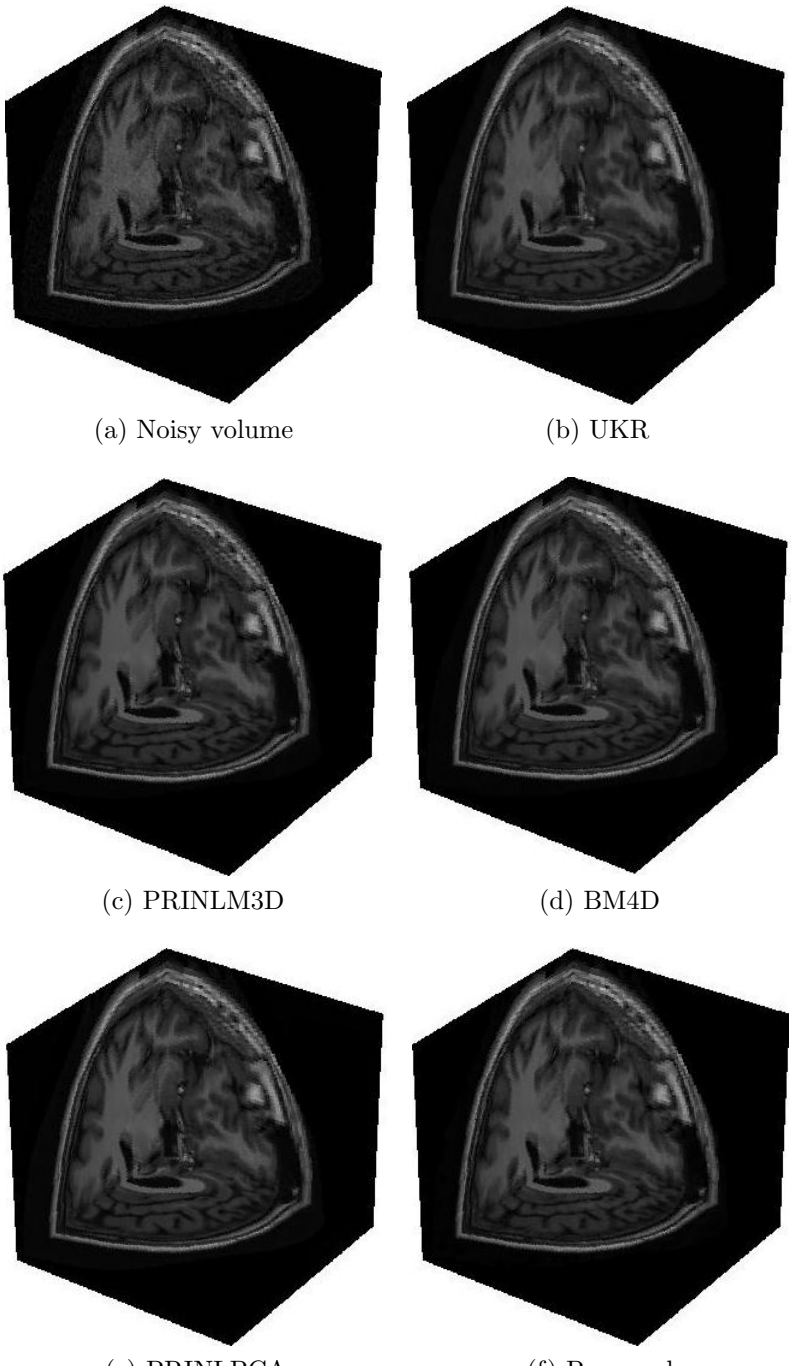

(a) Noisy volume (b) UKR

(c) PRINLM3D (d) BM4D

(e) PRINLPCA (f) Proposed

Figure 6.8: Comparison of various methods on subject 012 from OASIS Database

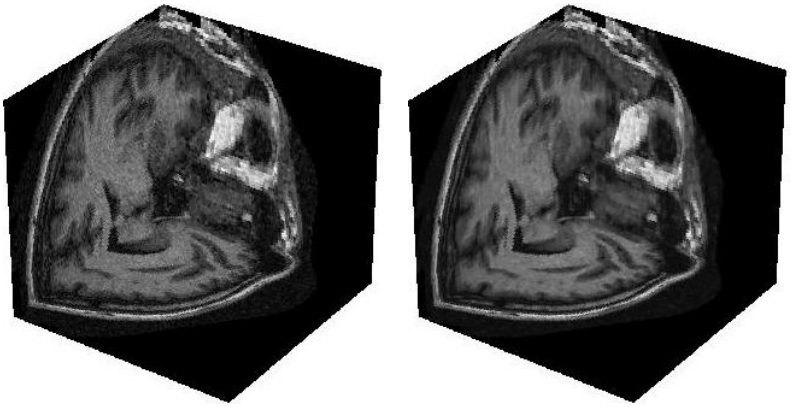

(a) Noisy volume (b) UKR

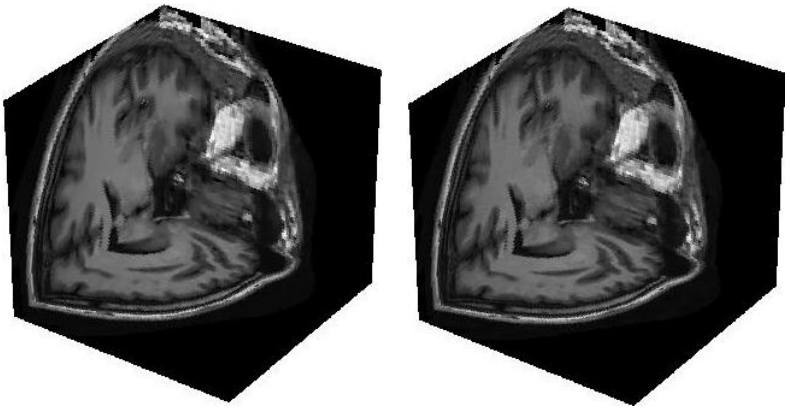

(c) PRINLM3D (d) BM4D

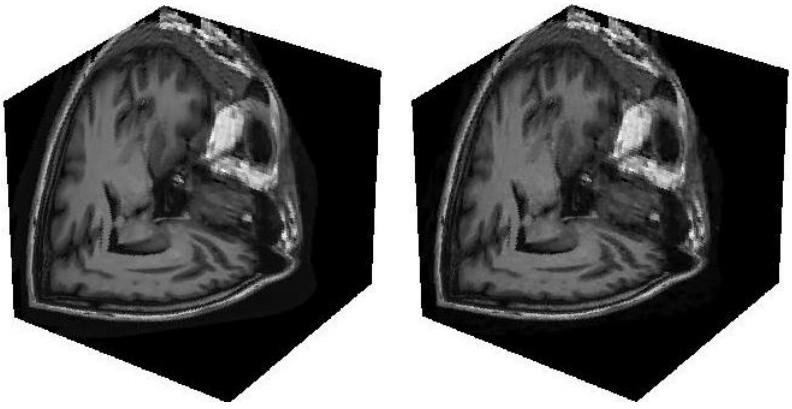

(e) PRINLPCA (f) Proposed

Figure 6.9: Comparison of various methods on subject 018 from OASIS Database

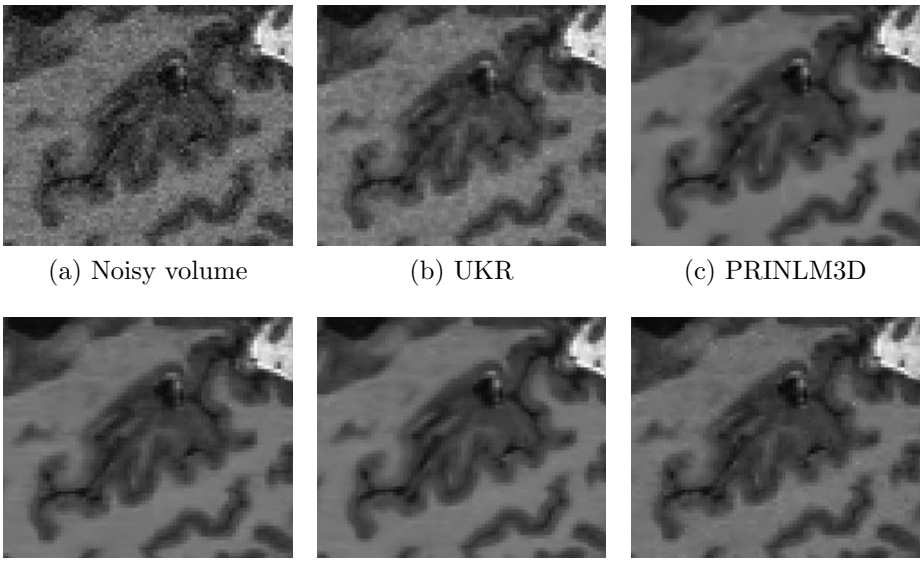

(a) Noisy volume (b) UKR (c) PRINLM3D

(d) BM4D (e) PRINLPCA (f) Proposed

Figure 6.10: Comparison of various methods on subject 018 with zoom from OASIS Database

Chapter 7

Conclusion & Future Work

Medical Image Denoising plays a crucial role in Computer Aided Diagnostic (CAD) system where a good quality image can better be utilized in disease identification, segmentation of normal and abnormal tissues etc. This work started with some notion of segmentation and edge detection problems in medical images preceded by noise removal. The methods of noise removal in this thesis are revolving around utilizing the notion of uncertainty management using Rough Set Theory (RST). Although, RST has been used in past for segmentation purpose extensively, this is an early attempt to use it in image denoising framework as prior information.

This thesis interlinked uncertainty model defined by Rough Set in the image denoising framework where data is assumed to be corrupted by signal dependent noise. The prior information derived in RST framework is applied on three denoising frameworks. The spectrum of frameworks varies from pixel level aggregation to patch level aggregation and spread from bias correction to sparsity conditions.

This chapter summarizes the work accomplished in this thesis and discusses limitations and possibilities to extend it in various directions.

7.1 Winding Up

Being non-invasive technique, MRI offers a great help to diagnostic system by acquiring structural information of human anatomy. However, there is always a chance to get attenuated by various error sources, mentioned in Chapter 1. This thesis is an endeavor to use Rough Set Theory (RST [30]) explored to remove Rician noise model present in MRI. Main contributions of the thesis are listed below.

a. RST, being known for uncertainty handling capability, has been explored on noisy MR images. A novel multi-class thresholding method is proposed to generate Rough Class Label (RCL) and Rough Edge Map (REM) information. This scheme is adaptive in terms of number of objects present in the image and edges obtained here are closed and continuous. It also provides accessibility to visualize an object of interest and its boundary information.

b. A more informative denoising filter is proposed under Bilateral filter framework [35]. RCL and REM information are used to define a weighing term along with spatial and photometric weights for pixel based denoising mechanism.

c. The notion of non-local self similarity (NLSS) widen the use of similar neighborhoods in denoising instead of a pixel level processing in conventional methods. This is also generalized to patch based processing where two locationally far apart similar patches contribute to denoise each other. However, this process involves heavy computational burden. Under this situation, a clustering based framework is proposed which adhere to NLSS notion more appropriately. This provides a unique and more intuitive gathering of similar patches and then proceeds for denoising task. Hence, the number of computations get lowered down to an extent.

d. A non additive signal dependent Rician noise present in MRI makes the applicability of the natural image denoising methods unfair for MRI. However, this has been made possible by variance stabilization technique proposed in [2] to

an extent. To deal with above mentioned problem, a Kernel Principal Component Analysis (KPCA) based method with RCL and REM information has been proposed. The results laid a new direction to explore KPCA for signal dependent noisy environment.

e. Structure preserving property of previous proposal lays to explore it for 3D data denoising. The REM and RCL information are extended to explore relationship in 3D. Here, instead of dealing with patches, similarity criteria is redefined for voxels (cubes) and clustering based denoising framework is adopted as mentioned earlier. Kernel Principal Component Analysis (KPCA) indeed preserves structure, after denoising, better than its contemporary methods.

7.2 Contributions

This section gives a final glimpse of this thesis with an outline of the problem addressed in each chapter and solution addressed in that regard.

- The notion of Rough Set based class label and edge map information (i.e. RCL and REM) is defined in Chapter 2 using multilevel histogram thresholding and rough entropy optimization.

- REM and RCL are used as regularization factor in the Bilateral Filter to prevent distortion at edges in the noisy images in Chapter 3. The proposed filter can be regarded as Trilateral Filter.

- Patch based medical image denoising problem is addressed in Chapter 4. Rough Set based clustering approach is proposed for transformed domain based non-local MR image denoising problem.

- Kernel Principal Component Analysis (KPCA) method is adopted to deal with Rician nature of noise present in MR images in Chapter 5. In this, data is first projected to kernel space via function mapping then non local clustering

based denoising framework is adopted in kernel space and inverted back to get denoised MR image.

- Chapter 6 is an extension of methods proposed in Chapter 2 and Chapter 5 from 2D images to 3D volume MR data.

7.3 Overall Conclusion

The current work is an early attempt to explore Rough Set Theory for medical image denoising under various frameworks. Starting from filter approaches, more sophisticated and recent mechanism of patch based denoising are attempted. All methods proposed are found to be as efficient as their contemporary methods, if not better. All experiments are performed on phantom datasets; however the same is explored for some real datasets as and when possible.

This work is complete by extending the proposals to denoise the 3D MRI which is gaining lots of attention in recent times. Finally, it is concluded that soft computing approach, specifically Rough Set Theory is successfully applied to MR image denoising and the results are encouraging to researchers for further studies towards possible extensions.

7.4 Future Work

The performance comparison of image denoising methods, on Real images like natural or medical, is quite subjective if no gold standard is available. This thesis compares methods on phantom database that is similar to Real human brain MRI scans, some results are also shown on Real MRI data. Brain related diseases such as brain tumor, multiple sclerosis etc. are analyzed based on change in Cerebrospinal Fluid (CSF), Gray Matter (GM) and White Matter (WM) over a period of time. Hence, one needs to keep track of the details of these tissues in MRI scans and hence must be preserved intact during denoising process. This work considers four objects, namely

CSF, GM, WM and rest as Background [1]. Using these four objects/classes, RCL and REM information (Chapter 2) is derived and further used for various denoising frameworks. Methods presented here can be applied to MRI scan of human body such as cardiac, knee by adopting number of objects present in them. Note that one can acquire number of classes according to domain knowledge.

At the end of Chapter 3, a result is presented on brain tumor class estimation. The dice coefficient was found to be 0.71 which is far behind from 1.0 in ideal situation. Hence, one can further take this coefficient values towards unity aiming more feature preservation during denoising. This can also be extendable for identification of other diseases and there by supporting clinical practice and diagnostic.

In Non Local Self Similar (NLSS) framework (Chapter 4), thesis proposes a novel clustering technique based on RCL and REM information between patches. The conventional clustering methods such as K-Means, Finite Mixture Models, segment an image in K number of clusters if there are K objects with crisp boundary. The proposed approach assumes rough boundary where overlapping between multiple objects is possible. Hence, method constructs all possible combinations of K objects as clusters. Clusters, thus formed are not analyzed statistically on the ground of compactness such as mean, standard deviation in the thesis. Such inclusions may enhance the robustness of proposed denoising framework during basis vector formation.

In Chapters 5 and 6, manifold based KPCA denoising framework for Rician noise removal in the 2D and 3D MRI images is presented. During this work, limited subset of kernels having single parameter is experimented. However, this work can further be investigated using various other kernels with a mechanism to adjust kernel parameters. One interesting line of work could be to design a Rician kernel or data adaptive kernel specifically to deal Ricianity conditions. A more analytical study of manifold based methods can be looked upon to investigate behavior of Rician noise under high noisy environment. While performing patch and voxel based denoising, patch and voxel

[1] One can remove skull part in MRI data from some available tools but such methods are outside the scope of the thesis

are converted to their one dimensional representation which may lose the relation up to some extent. A 2D or 3D PCA/KPCA method can be investigated in the light of preserving structural information in the raw data.

REFERENCES

[1] D. L. Collins, A.P. Zijdenbos, V. Kollokian, J.G. Sled, N.J. Kabani, C.J. Holmes, and A.C. Evans. Design and construction of a realistic digital brain phantom. *IEEE Trans. on Medical Imaging*, 17(3):463–468, June 1998.

[2] Alessandro Foi. Noise estimation and removal in mr imaging: The variance-stabilization approach. In *ISBI*, pages 1809–1814, 2011.

[3] TM Hudson, DJ Hamlin, WF Enneking, and H Pettersson. Magnetic resonance imaging of bone and soft tissue tumors: early experience in 31 patients compared with computed tomography. *Skeletal radiology*, 13(2):134–146, 1985.

[4] WD Zimmer, TH Berquist, RA McLeod, FH Sim, DJ Pritchard, TC Shives, LE Wold, and GR May. Bone tumors: Magnetic resonance imaging versus computed tomography. *Radiology*, 155(3):709–718, 1985.

[5] Timothy G Feeman. *The mathematics of medical imaging: a beginners guide*. Springer Science & Business Media, 2010.

[6] K Kirk Shung, Michael Smith, and Benjamin MW Tsui. *Principles of medical imaging*. Academic Press, 2012.

[7] Daniel S Marcus, Tracy H Wang, Jamie Parker, John G Csernansky, John C Morris, and Randy L Buckner. Open access series of imaging studies (oasis): cross-sectional mri data in young, middle aged, nondemented, and demented older adults. *Journal of Cognitive Neuroscience*, 19(9):1498–1507, 2007.

[8] B. Menze, A. Jakab, S. Bauer, M. Reyes, M. Prastawa, and K. V. Leemput. Multimodal brain tumor segmentation chanllenge. In *MICCAI Conference*, October 2012.

[9] P. Milanfar. A tour of modern image filtering. *IEEE Signal Processing Magazine*, pages 106–128, Jan 2013.

[10] Santiago Aja-Fernández and Antonio Tristán-Vega. A review on statistical noise models for magnetic resonance imaging. *LPI, ETSI Telecomunicacion, Universidad de Valladolid, Spain, Tech. Rep*, 2013.

[11] Hákon Gudbjartsson and Samuel Patz. The rician distribution of noisy mri data. *Magnetic Resonance in Medicine*, 34(6):910–914, 1995.

[12] ER McVeigh, RM Henkelman, and MJ Bronskill. Noise and filtration in magnetic resonance imaging. *Medical physics*, 12:586, 1985.

[13] Pierre Gravel, Gilles Beaudoin, and Jacques A De Guise. A method for modeling noise in medical images. *IEEE Transactions on Medical Imaging*, 23(10):1221–1232, 2004.

[14] Ranjan Maitra and David Faden. Noise estimation in magnitude mr datasets. *Medical Imaging, IEEE Transactions on*, 28(10):1615–1622, 2009.

[15] Pierrick Coupé, José V Manjón, Elias Gedamu, Douglas L Arnold, Montserrat Robles, D Louis Collins, et al. Robust rician noise estimation for mr images. *Medical image analysis*, 14(4):483–493, 2010.

[16] José V Manjón, Pierrick Coupé, and Antonio Buades. Mri noise estimation and denoising using non-local pca. *Medical image analysis*, 22(1):35–47, 2015.

[17] Guido Gerig, Olaf Kubler, Ron Kikinis, and Ferenc A Jolesz. Nonlinear anisotropic filtering of mri data. *Medical Imaging, IEEE Transactions on*, 11(2):221–232, 1992.

[18] Tim McInerney and Demetri Terzopoulos. Deformable models in medical image analysis: a survey. *Medical image analysis*, 1(2):91–108, 1996.

[19] Jan Sijbers, Arnold J. den Dekker, Paul Scheunders, and Dirk Van Dyck. Maximum likelihood estimation of rician distribution parameters. *IEEE Transaction on Medical Imaging*, 17(3):357–361, 1998.

[20] J. V. Manjon, J. C. Caballero, G. G. Marti, L. Marti-Baonmati, and M. Robles. Mri denoising using non local means. *Medical Image Analysis*, 12:514–523, 2008.

[21] Yasuyuki Taki, Benjamin Thyreau, Shigeo Kinomura, Kazunori Sato, Ryoi Goto, Ryuta Kawashima, and Hiroshi Fukuda. Correlations among brain gray matter volumes, age, gender, and hemisphere in healthy individuals. *PloS one*, 6(7):e22734, 2011.

[22] J Mohan, V Krishnaveni, and Yanhui Guo. A survey on the magnetic resonance image denoising methods. *Biomedical Signal Processing and Control*, 9:56–69, 2014.

[23] Krit Somkantha, Nipon Theera-Umpon, and Sansanee Auephanwiriyakul. Boundary detection in medical images using edge following algorithm based on intensity gradient and texture gradient features. *Biomedical Engineering, IEEE Transactions on*, 58(3):567–573, 2011.

[24] John Canny. A computational approach to edge detection. *Pattern Analysis and Machine Intelligence, IEEE Transactions on*, 8(6):679–698, 1986.

[25] Luminita A Vese and Tony F Chan. A multiphase level set framework for image segmentation using the mumford and shah model. *International journal of computer vision*, 50(3):271–293, 2002.

[26] Koen Van Leemput, Frederik Maes, Dirk Vandermeulen, and Paul Suetens. Automated model-based bias field correction of mr images of the brain. *IEEE Transactions on Medical Imaging*, 18(10):885–896, 1999.

[27] Abhirup Banerjee and Pradipta Maji. Rough sets for bias field correction in mr images using contraharmonic mean and quantitative index. *IEEE Transactions on Medical Imaging*, 32(11):2140–2151, 2013.

[28] Partha Sarathi Mukherjee and Peihua Qiu. Efficient bias correction for magnetic resonance image denoising. *Statistics in medicine*, 32(12):2079–2096, 2013.

[29] Shanshan Wang, Yong Xia, Pei Dong, Jianhua Luo, Qiu Huang, Dagan Feng, and Yuanxiang Li. Bias correction for magnetic resonance images via joint entropy regularization. *Bio-medical materials and engineering*, 24(1):1239–1245, 2014.

[30] Zdzisław Pawlak. Rough sets. *International Journal of Computer & Information Sciences*, 11(5):341–356, 1982.

[31] A. E. Hassanien, A. Abraham, J. F. Peters, G. Schaefer, and C. Henry. Rough sets and near set in medical imaging: A review. *IEEE Trans on Information Technology in Biomedicine*, 13(6):955–968, Nov. 2009.

[32] Aboul Ella Hassanien, Ajith Abraham, James F Peters, and Janusz Kacprzyk. Rough sets in medical imaging: foundations and trends. *Computational Intelligence in Medical Imaging: Techniques and Applications*, pages 47–87, 2008.

[33] Sebastian Widz, Kenneth Revett, and Dominik Ślezak. A rough set-based magnetic resonance imaging partial volume detection system. In *Pattern Recognition and Machine Intelligence*, pages 756–761. Springer, 2005.

[34] Yi Xie. On medical image filtering based on rough set theory. In *Fifth International Conference on Fuzzy Systems and Knowledge Discovery (FSKD)*, volume 5, pages 276–280. IEEE, 2008.

[35] C. Tomasi and R. Manduchi. Bilateral filtering for gray and color images. In *IEEE International Conference on Computer Vision*, pages 839–846, 1998.

[36] Bernhard Schölkopf, Alexander Smola, and Klaus-Robert Müller. Kernel principal component analysis. In *Artificial Neural NetworksICANN'97*, pages 583–588. Springer, 1997.

[37] Jing Tao Yao. Information granulation and granular relationships. In *Granular Computing, IEEE International Conference on*, volume 1, pages 326–329, 2005.

[38] Lotfi A Zadeh. Some reflections on soft computing, granular computing and their roles in the conception, design and utilization of information/intelligent systems. *Soft Computing-A fusion of foundations, methodologies and applications*, 2(1):23–25, 1998.

[39] Zdzislaw Pawlak. Rough sets and data mining. In *Proceedings of the Australiasia-Pacific Forum on Intelligent Processing and Manufacturing of Materials*, 1997.

[40] Torgeir R Hvidsten and Jan Komorowski. Rough sets in bioinformatics. In *Transactions on rough sets VII*, pages 225–243. Springer, 2007.

[41] Francis EH Tay and Lixiang Shen. Economic and financial prediction using rough sets model. *European Journal of Operational Research*, 141(3):641–659, 2002.

[42] Aboul Ella Hassanien and Jafar MH Ali. Rough set approach for generation of classification rules of breast cancer data. *Informatica*, 15(1):23–38, 2004.

[43] YM Lazim, M Nordin A Rahman, and Farham Mohamed. Clustering model of multimedia data by using rough sets theory. In *Computer & Information Science (ICCIS), 2012 International Conference on*, volume 1, pages 336–340. IEEE, 2012.

[44] Pawan Lingras. Rough set clustering for web mining. In *Fuzzy Systems, 2002. FUZZ-IEEE'02. Proceedings of the 2002 IEEE International Conference on*, volume 2, pages 1039–1044. IEEE, 2002.

[45] Sankar K Pal and James F Peters. *Rough Fuzzy Image Analysis: Foundations and Methodologies*. CRC Press, 2010.

[46] Bing Zhou. Multi-class decision-theoretic rough sets. *International Journal of Approximate Reasoning*, 55(1):211–224, 2014.

[47] Phillip A Laplante and Colin J Neill. Modeling uncertainty in software engineering using rough sets. *Innovations in Systems and Software Engineering*, 1(1):71–78, 2005.

[48] Cheng-Dong Wu, Ying Zhang, Meng-Xin Li, and Yong Yue. A rough set ga-based hybrid method for robot path planning. *International Journal of Automation and Computing*, 3(1):29–34, 2006.

[49] Andrew Kusiak. Rough set theory: a data mining tool for semiconductor manufacturing. *Electronics Packaging Manufacturing, IEEE Transactions on*, 24(1):44–50, 2001.

[50] Lotfi A Zadeh. Fuzzy sets. *Information and control*, 8(3):338–353, 1965.

[51] Albrecht Pietsch. Approximation spaces. *Journal of Approximation Theory*, 32(2):115–134, 1981.

[52] James F Peters. Near sets. general theory about nearness of objects. *Applied Mathematical Sciences*, 1(53):2609–2029, 2007.

[53] Zdzisław Pawlak. Rough sets and fuzzy sets. *Fuzzy sets and Systems*, 17(1):99–102, 1985.

[54] Ranjit Biswas. Rough sets are fuzzy sets. *BUSEFAL*, 83:24–31, 2000.

[55] Didier Dubois and Henri Prade. Rough fuzzy sets and fuzzy rough sets*. *International Journal of General System*, 17(2-3):191–209, 1990.

[56] Chris Cornelis, Martine De Cock, and Anna Maria Radzikowska. Fuzzy rough sets: From theory into practice. *Handbook of Granular Computing*, pages 533–552, 2008.

[57] S. K. Pal, B. Uma Shankar, and P. Mitra. Granular computing, rough entropy and object recognition. *Pattern Recognition Letters*, 26:2509–2517, 2005.

[58] Xuguang Chen. *A Rough Set Approach to Face Recognition*. PhD thesis, Faculty of Graduate Studies and Research, University of Regina, 2014.

[59] Pradipta Maji and Shaswati Roy. Rough-fuzzy clustering and unsupervised feature selection for wavelet based mr image segmentation. *PloS one*, 10(4), 2015.

[60] Shaswati Roy and Pradipta Maji. A new post-processing method to detect brain tumor using rough-fuzzy clustering. In *Pattern Recognition and Machine Intelligence*, pages 407–417. Springer, 2015.

[61] Shoji Hirano and Shusaku Tsumoto. Rough representation of a region of interest in medical images. *International Journal of Approximate Reasoning*, 40(1):23–34, 2005.

[62] S Widz, D Slezak, and K Revett. Application of rough set based dynamic parameter optimization to mri segmentation. In *IEEE Annual Meeting of the Information Processing NAFIPS*, volume 1, pages 440–445, 2004.

[63] Roman W Swiniarski. Rough sets and bayesian methods applied to cancer detection. In *Rough Sets and Current Trends in Computing*, pages 609–616. Springer, 1998.

[64] Shoji Hirano and Shusaku Tsumoto. Segmentation of medical images based on approximations in rough set theory. In *Rough Sets and Current Trends in Computing*, pages 554–563. Springer, 2002.

[65] Aboul Ella Hassanien and Jafar M Ali. Rough set approach for classification of breast cancer mammogram images. In *Fuzzy logic and applications*, pages 224–231. Springer, 2006.

[66] P. Munshi and S. K. Mitra. A rough set based binarization technique for fingerprint images. In *IEEE International Conference on Signal Processing Computing and Control*, pages 1–6, March 2012.

[67] Pradipta Maji and Sankar K Pal. Rough set based generalized fuzzy-means algorithm and quantitative indices. *Systems, Man, and Cybernetics, Part B: Cybernetics, IEEE Transactions on*, 37(6):1529–1540, 2007.

[68] Pawan Lingras and Georg Peters. Rough clustering. *Wiley Interdisciplinary Reviews: Data Mining and Knowledge Discovery*, 1(1):64–72, 2011.

[69] Anca Loredana Ion. Rough sets and gaussian mixture model in medical image diagnosis. *Annals of the University of Craiova-Mathematics and Computer Science Series*, 38(4):50–62, 2011.

[70] Abhirup Banerjee and Pradipta Maji. Rough sets and stomped normal distribution for simultaneous segmentation and bias field correction in brain mr images. *Image Processing, IEEE Transactions on*, 24(12):5764–5776, 2015.

[71] Pradipta Maji and Shaswati Roy. Sobt-rfw: Rough-fuzzy computing and wavelet analysis based automatic brain tumor detection method from mr images. *Fundamenta Informaticae*, 142(1-4):237–267, 2015.

[72] Michael Kass, Andrew Witkin, and Demetri Terzopoulos. Snakes: Active contour models. *International journal of computer vision*, 1(4):321–331, 1988.

[73] Mitra Basu. Gaussian-based edge-detection methods-a survey. *Systems, Man, and Cybernetics, Part C: Applications and Reviews, IEEE Transactions on*, 32(3):252–260, 2002.

[74] Vicent Caselles, Ron Kimmel, and Guillermo Sapiro. Geodesic active contours. *International journal of computer vision*, 22(1):61–79, 1997.

[75] Tony F Chan and Luminita A Vese. Active contours without edges. *Image Processing, IEEE Transactions on*, 10(2):266–277, 2001.

[76] Milan Sonka, Vaclav Hlavac, and Roger Boyle. *Image processing, analysis, and machine vision*. Cengage Learning, 2014.

[77] P. Perona and J. Malik. Scale space and edge detection using anisotropic diffusion. *IEEE Trans on Pattern Ana. and Machine Intell.*, 12(7):629–639, July 1990.

[78] Joachim Weickert. *Anisotropic diffusion in image processing*, volume 1. Teubner Stuttgart, 1998.

[79] Michael J Black, Guillermo Sapiro, David H Marimont, and David Heeger. Robust anisotropic diffusion. *IEEE Transactions on Image Processing*, 7(3):421–432, 1998.

[80] VB Surya Prasath and Arindama Singh. Edge detectors based anisotropic diffusion for enhancement of digital images. In *Computer Vision, Graphics & Image Processing, 2008. ICVGIP'08. Sixth Indian Conference on*, pages 33–38. IEEE, 2008.

[81] Michael Elad. On the origin of the bilateral filter and ways to improve it. *Image Processing, IEEE Transactions on*, 11(10):1141–1151, 2002.

[82] Giovanni Sicuranza. *Nonlinear image processing*. Access Online via Elsevier, 2000.

[83] Shashaank M Aswatha, Jayanta Mukhopadhyay, and Partha Bhowmick. Image denoising by scaled bilateral filtering. In *Computer Vision, Pattern Recognition,*

Image Processing and Graphics (NCVPRIPG), 2011 Third National Conference on, pages 122–125. IEEE, 2011.

[84] Sylvain Paris and Frédo Durand. A fast approximation of the bilateral filter using a signal processing approach. In *Computer Vision–ECCV 2006*, pages 568–580. Springer, 2006.

[85] Yinxue Zhang, Xuemin Tian, and Peng Ren. An adaptive bilateral filter based framework for image denoising. *Neurocomputing*, 140:299–316, 2014.

[86] Ming Zhang and Bahadir K Gunturk. Multiresolution bilateral filtering for image denoising. *Image Processing, IEEE Transactions on*, 17(12):2324–2333, 2008.

[87] Fatih Porikli. Constant time o(1) bilateral filtering. In *Computer Vision and Pattern Recognition, IEEE Conference on*, pages 1–8, 2008.

[88] Qingxiong Yang, Narendra Ahuja, and Kar-Han Tan. Constant time median and bilateral filtering. *International Journal of Computer Vision*, pages 1–12, 2014.

[89] Wilbur CK Wong, Albert CS Chung, and Simon CH Yu. Trilateral filtering for biomedical images. In *Biomedical Imaging: Nano to Macro, 2004. IEEE International Symposium on*, pages 820–823. IEEE, 2004.

[90] Roman Garnett, Timothy Huegerich, Charles Chui, and Wenjie He. A universal noise removal algorithm with an impulse detector. *IEEE Transactions on Image Processing*, 14(11):1747–1754, 2005.

[91] Herng-Hua Chang, Tung-Ju Hsieh, Yun-Ni Ting, and Woei-Chyn Chu. Rician noise removal in mr images using an adaptive trilateral filter. In *Biomedical Engineering and Informatics (BMEI), 2011 4th International Conference on*, volume 1, pages 467–471. IEEE, 2011.

[92] Sylvain Paris, Pierre Kornprobst, Jack Tumblin, and Frédo Durand. Bilateral filtering: Theory and applications. *Foundations and Trends® in Computer Graphics and Vision*, 4(1):1–73, 2008.

[93] A. Buades, B. Coll, and J. M. Morel. A non local algorithm for image denoising. In *IEEE Computer Vision and Pattern Recognition*, pages 60–65, 2005.

[94] P. Coupe, P. Yger, S. Prima, P. Hellier, C. Kervrann, and C. Barillot. An optimized blockwise nonlocal means denoising filter for 3d magnetic resonance images. *IEEE Trans on Medical Imaging*, 27(4):425–441, April 2008.

[95] Z. Wang, A. C. Bovik, H. R. Sheikh, and E. P. Simoncelli. Image quality assessment: From error visibility to structural similarity. *IEEE Trans on Image Processing*, 13(4):600–612, April 2004.

[96] L. Zhang, L. Zhang, X. Mou, and D. Zhang. Fsim: A feature similarity index for image quality assessment. *IEEE Trans on Image Processing*, 20(9):2378–2386, Sept 2011.

[97] L. Zhang, W. Dong, D. Zhang, and G. Shi. Two-stage image denoising by principal component analysis with local pixel grouping. *Pattern Recognition*, 43(4):1531–1549, April 2010.

[98] Michal Aharon, Michael Elad, and Alfred Bruckstein. K-svd: An algorithm for designing overcomplete dictionaries for sparse representation. *IEEE Transactions on Signal Processing*, 54(11):4311–4322, 2006.

[99] Jeff Orchard, Mehran Ebrahimi, and Alexander Wong. Efficient nonlocal-means denoising using the svd. In *Image Processing, 2008. ICIP 2008. 15th IEEE International Conference on*, pages 1732–1735. IEEE, 2008.

[100] A. Rajwade, A. Rangarajan, and A. Banerjee. Image denoising using the higher singular value decomposition. *IEEE Trans on Pattern Ana. and Machine Intell.*, 35(4):849–862, April 2013.

[101] K. Dabov, A. Foi, V. Katkovnik, and K. Egiazarian. Image denoising by sparse 3d transform domain collaborative filtering. *IEEE Trans on Image Processing*, 16(8):2080–2095, Augest 2007.

[102] Weisheng Dong, Xin Li, D Zhang, and Guangming Shi. Sparsity-based image denoising via dictionary learning and structural clustering. In *Computer Vision and Pattern Recognition (CVPR), 2011 IEEE Conference on*, pages 457–464. IEEE, 2011.

[103] Priyam Chatterjee and Peyman Milanfar. Patch-based near-optimal image denoising. *Image Processing, IEEE Transactions on*, 21(4):1635–1649, 2012.

[104] Idan Ram, Michael Elad, and Israel Cohen. Image processing using smooth ordering of its patches. *Image Processing, IEEE Transactions on*, 22(7):2764–2774, 2013.

[105] D. D. Muresan and R. T. Parks. Adaptive principal components and image denoising. In *IEEE International Conference on Image Processing*, pages 1101 – 1104, 2003.

[106] C. A. Deledalle, J. Salmon, and A. Dalalyan. Image denoising with patch based pca: local versus global. In *BMVC*, 2011.

[107] Joseph Salmon, Zachary Harmany, Charles-Alban Deledalle, and Rebecca Willett. Poisson noise reduction with non-local pca. *Journal of Mathematical Imaging and Vision*, pages 1–16, 2013.

[108] Sebastian Zimmer, Stephan Didas, and Joachim Weickert. A rotationally invariant block matching strategy improving image denoising with non-local means. In *Proc. 2008 International Workshop on Local and Non-Local Approximation in Image Processing*, pages 135–142, 2008.

[109] Zexuan Ji, Qiang Chen, Quan-Sen Sun, and De-Shen Xia. A moment-based nonlocal-means algorithm for image denoising. *Information Processing Letters*, 109(23):1238–1244, 2009.

[110] Abdul Rehman and Zhou Wang. Ssim-based non-local means image denoising. In *Image Processing (ICIP), 2011 18th IEEE International Conference on*, pages 217–220. IEEE, 2011.

[111] Alvaro Pardo. Analysis of non-local image denoising methods. *Pattern Recognition Letters*, 32(16):2145–2149, 2011.

[112] Alessandro Foi and Giacomo Boracchi. Foveated self-similarity in nonlocal image filtering. In *IS&T/SPIE Electronic Imaging*, pages 829110–829110. International Society for Optics and Photonics, 2012.

[113] Chao-Tsung Huang. Bayesian inference for neighborhood filters with application in denoising. In *Proceedings of the IEEE Conference on Computer Vision and Pattern Recognition*, pages 1657–1665, 2015.

[114] Masaki Onuki and Yuichi Tanaka. Trilateral filter on graph spectral domain. In *Image Processing (ICIP), 2014 IEEE International Conference on*, pages 2046–2050. IEEE, 2014.

[115] Robert D Nowak. Wavelet-based rician noise removal for magnetic resonance imaging. *Image Processing, IEEE Transactions on*, 8(10):1408–1419, 1999.

[116] Michael Collins, Sanjoy Dasgupta, and Robert E Schapire. A generalization of principal component analysis to the exponential family. In *NIPS 2001*, 2001.

[117] Lili He and Ian R. Greenshields. A nonlocal maximum likelihood estimation method for rician noise reduction in mr images. *IEEE Transaction on Medical Imaging*, 28(2):165–172, 2009.

[118] Michael Elad and Michal Aharon. Image denoising via sparse and redundant representations over learned dictionaries. *Image Processing, IEEE Transactions on*, 15(12):3736–3745, 2006.

[119] Guillaume Charpiat, Matthias Hofmann, Bernhard Schölkopf, et al. Kernel methods in medical imaging. *Handbook of Biomedical Imaging*, 2010.

[120] E. L. Rubio and Maria N. F. Nunez. Kernel regression based feature extraction for 3d mr image denoising. *Medical Image Analysis*, 15:498–513, 2011.

[121] Veronika A Zimmer, Karim Lekadir, Corné Hoogendoorn, Alejandro F Frangi, and Gemma Piella. A framework for optimal kernel-based manifold embedding of medical image data. *Computerized Medical Imaging and Graphics*, 41:93–107, 2015.

[122] M. Maggioni, V. Katkovnik, K. Egiazarian, and A. Foi. Nonlocal transform domain filter for volumetric data denoising and reconstruction. *IEEE Trans on Image Processing*, 22(1):119–133, Jan 2013.

[123] P. Coupe, P. Yger, S. Prima, P. Hellier, C. Kervrann, and C. Barillot. An optimized blockwise non local means denoising filter for 3d magnetic resonance images. *IEEE Transactions on Medical Imaging*, 27(4):425–441, April 2008.

[124] Pierrick Coupé, José V Manjón, Montserrat Robles, Louis D Collins, et al. Adaptive multiresolution non-local means filter for 3d mr image denoising. *IET Image Processing*, 2011.

[125] José V Manjón, Pierrick Coupé, Antonio Buades, D Louis Collins, and Montserrat Robles. New methods for mri denoising based on sparseness and self-similarity. *Medical image analysis*, 16(1):18–27, 2012.

[126] Xinyuan Zhang, Zhongbiao Xu, Nan Jia, Wei Yang, Qianjin Feng, Wufan Chen, and Yanqiu Feng. Denoising of 3d magnetic resonance images by using higher-order singular value decomposition. *Medical image analysis*, 19(1):75–86, 2015.

Publication

The list of publications out of the work is as under:

- Journals

  (1) Ashish Phophalia and Suman K. Mitra, 3D MR Brain Image Denoising using Kernel Principal Component Analysis (Manuscript Prepared)

  (2) Ashish Phophalia and Suman K. Mitra, Rough Set based Bilateral Filter design for Denoising Brain MR Images, pp. 1-14, vol. 33, **Applied Soft Computing**, Elsevier, 2015 (Impact Factor = 2.68).

  (3) Ashish Phophalia, Ajit Rajwade and Suman K. Mitra, Rough set based Image Denoising for Brain MR Images, Special Issue on Image Restoration Methods, pp. 24-35, vol. 103, **Signal Processing**, Elsevier, 2014. (Impact Factor = 2.24)

- Conferences

  (1) Ashish Phophalia and Suman K. Mitra, 3D MRI denoising using Rough set theory and Kernel embedding method, 1st International Workshop on Patch-based Techniques in Medical Imaging, MICCAI 2015, LNCS 9467, 2015 (In Press).

  (2) Ashish Phophalia and Suman K. Mitra, Rician Noise Removal approach for Brain MR Images using Kernel Principal Component Analysis, Sixth Pattern Recognition and Machine Intelligence (PReMI), LNCS 9124, pp. 545-553, Springer, 2015.

  (3) Ashish Phophalia, Suman K. Mitra, Ajit Rajwade, Object Boundary Detection using Rough Set Theory, In Proc of fourth National Conference on Computer Vision Pattern Recognition Image Processing and Graphics (NCVPRIPG), 2013.

  (4) Ashish Phophalia, Suman K. Mitra, Ajit Rajwade, Medical Image Denoising from similar patches derived by Rough Set, In Proc IEEE Second International Conference on Image Information Processing (ICIIP), 2013.

  (5) Ashish Phophalia, Suman K. Mitra, Ajit Rajwade, A new denoising filter for brain MR images, In Eighth Indian Conference on Computer Vision Graphics and Image Processing (ICVGIP), 2012.